ABSTRACT

JONES, JESSE PHILIP. The Quasidiffusion Method For Solving Radiation Transport Problems On Arbitrary Quadrilateral Meshes In 2D $r-z$ Geometry. (Under the direction of Dmitriy Y. Anistratov.)

In this work we develop a Quasidiffusion (QD) method for solving the radiation transport equation in 2D $r-z$ geometry on adaptive-like meshes of arbitrary quadrilaterals. Radiation transport on grids of this type in $r-z$ geometry has applications in astrophysics, inertial confinement fusion, reactor design, and high energy density physics. These fields are characterized by their complex multi-physics problems. In multi-physics settings it is common to have computational meshes dictated by physical phenomena other than radiation transport, such as hydrodynamics where body fitted meshes, Adaptive Mesh Refinement (AMR), and spatial meshes that change in time are to be expected. The research presented here seeks to directly treat these kinds of complicated meshes arising in multiphysics problems.

In order to create a QD method for use on such meshes in $r-z$ a new discretization is developed and presented here for the Low-Order Quasidiffusion (LOQD) equations based on a 2nd order cell centered difference scheme for the P_1 equations. Two different extensions of the LOQD discretization to adaptive-like grids are considered. A thorough analysis of the new LOQD discretization is performed and confirms that for the meshes considered the method converges with 2nd order behavior when a 2nd order transport discretization is used. Results are presented for the QD method using two different transport discretizations.

The Quasidiffusion Method For Solving Radiation Transport Problems On Arbitrary Quadrilateral Meshes In 2D $r - z$ Geometry

by
Jesse Philip Jones

A dissertation submitted to the Graduate Faculty of
North Carolina State University
in partial fulfillment of the
requirements for the Degree of
Doctor of Philosophy

Nuclear Engineering

Raleigh, North Carolina

2019

APPROVED BY:

Yousry Y. Azmy	Carl T. Kelley
David J. Kropaczek	Dmitriy Y. Anistratov Chair of Advisory Committee

DEDICATION

I dedicate this to my family and to the love of my life Megan Smith.

ACKNOWLEDGEMENTS

I first want to thank Dr. Dmitriy Y. Anistratov not only for the immense amount of guidance he has given me over the years but also for the inspiration he has given me to achieve all that I have done. A sincere thank you is also due to the entire faculty of the Nuclear Engineering Department at North Carolina State University and some members of the Department of Mathematics such as Dr. Tim Kelley and Dr. Ilse Ipsen. Without all of you I wouldn't be the scientist I am today, nor would any of the opportunities that are open to me now have ever been possible.

This work was supported in part by the Nuclear Enegery University Program (NEUP) of the U.S. Department of Energy and by the Graduate Fellowship in Nuclear Engineering (GFINE) of the U.S Nuclear Regulatory Commission (NRC).

TABLE OF CONTENTS

LIST OF TABLES

LIST OF FIGURES

Chapter 1

Introduction

1.1 General Overview

Since its inception in 1872 [1] the Boltzmann transport equation has been as helpful and influential as it has been fickle. To this day many people seek better, faster, and cheaper ways to solve it and its derivatives for a myriad of reasons. These reasons, or really applications, range from neutron transport in nuclear reactors [2], to neutrino transport within a supernova [3], to light propagation in the burgeoning video game industry [4]. For some of these applications extreme accuracy is necessary, for others, extreme speed and efficiency. All of these different fields with their diverse needs and requirements share something in common, however, they all tackle the problem of solving models for a set of physical phenomena that is staggering in complexity. Some models seek to do away with parts of the underlying physics and get away with not treating them thus rendering a cheaper problem to solve for a given situation. Other models incorporate these physics and often require very smart solution methods, and or clever modes of implementation, and even still may need immense computing power. Great strides have been made on all fronts over the years. Computers are more powerful now than ever and show no sign of stopping. New methods are devised all the time that use better and better schemes to acquire more accurate solutions of transport problems and to do it faster than before. Not to mention, existing methods are constantly being reformulated to increase efficiency and parallelism in their implementation. The goal of this research is to continue this trend by developing a new and better deterministic method for solving the transport equation for a certain class of problems.

1.2 Problems of Interest

One particular application of the transport equation, radiative transfer, involves the modeling of photon behavior and interaction with a medium and the tracking of the internal energy of that medium. This, in and of itself, is a complicated and multifaceted prospect, however, it is often further complicated in practice by other physics. Many practical problems in the world of radiative transfer have not only photonic physics but also hydrodynamics involved. Examples exist in astrophysics, fusion research, high energy density physics (HEDP), etc. In such multiphysics settings computational grids are often determined by these other physical phenomena as in the case of coupled radiative transfer and hydrodynamics. Grids resulting from hydrodynamics can be extremely complex and can change from time step to time step due to the evolution of a problem. As a consequence the radiative transfer equations must either be solved on these complex and essentially arbitrary grids or interpolation/projection and prolongation operators must be used to allow for the different physical phenomena to be modeled on different grids. Interpolation of solutions between grids is not necessarily desirable as it introduces additional approximations and computational expense depending on the complexity of the projection/prolongation being done. Radiation transport in such complex multiphysics settings is what this research is focused on treating directly, on grids determined by other physics models, thus obviating the need for interpolation between grids.

The type of meshes considered here are adaptive-like arbitrary quadrilateral grids. Figure 1.1 depicts a simple example of the our grids of interest. Adaptivity in grid creation is becoming commonplace in modern computational physics. Adaptive refinement of meshes allows for increased accuracy where needed without the expense of refining the entire mesh. This is especially useful in hydrodynamic simulations as body fitted meshes are common and refinement of meshes around material heterogeneities and wavefronts (shocks) can be extremely beneficial accuracy and stability wise.

A large number of problems in the aforementioned fields of astrophysics, HEDP, fusion research, and even in reactor physics exhibit an important attribute, rotational symmetry. A few examples being supernovae, inertial confinement fusion, and some molten salt reactor design concepts. In any case of symmetry, rotational symmetry included, choices in modeling and coordinate system can convey a large reduction in problem complexity and computational cost. For instance, one would probably not simulate radiation transport through a wall in full 3D and would instead opt for modeling the problem in 1D slab

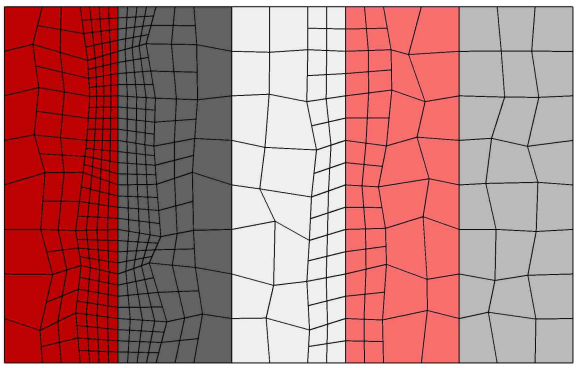

Figure 1.1: Representative mesh of interest with different colors representing different materials/source intensities

geometry. The same is true for rotationally symmetric problems with 2D $r-z$ geometry allowing for simpler modeling with fewer independent variables and unknowns compared to modeling in another coordinate system, i.e. 3D Cartesian geometry. The preponderance of problems of interest with rotational symmetry and $r-z$ geometry's ability to model them with improved efficiency is what motivated this research to be on method development for $r-z$ geometry.

1.3 The Radiation Transport Equation

The radiation transport equation is itself a derivative of the Boltzmann Equation,

$$\frac{\partial f}{\partial t} + \boldsymbol{v} \cdot \boldsymbol{\nabla} f + \boldsymbol{\nabla}_{\boldsymbol{P}} \cdot (\boldsymbol{F} f) = \left[\frac{\partial f}{\partial t}\right]_{coll}, \tag{1.1}$$

where $f\, d\boldsymbol{r}\, d\boldsymbol{v}$ is the number of particles in a differential spatial element $d\boldsymbol{r}$ about the point $\boldsymbol{r}$ having velocities within the differential velocity volume $d\boldsymbol{v}$ about velocity $\boldsymbol{v}$ at time t, $\boldsymbol{\nabla}_r$ is the gradient in space, $\boldsymbol{\nabla}_{\boldsymbol{P}}$ is the momentum gradient, $\boldsymbol{F}$ is applied external forces, and $\left[\frac{\partial f}{\partial t}\right]_{coll}$ is a term which accounts for any interactions between particles [5]. The Boltzmann Equation was originally formulated as part of research into the kinetic theory of gases for describing non-equilibrium thermodynamic systems [5, 6]. However, the equation is quite general and was found to be able to describe the physical behavior of a myriad of phenomena. The specific definition of the terms of the Boltzmann Equation depend on the physical phenomenon being described.

For modeling neutral particle transport, such as for neutrons or photons, the force term in the Boltzmann Equation can be dropped. This is possible as the force term encompasses things such as gravitational interactions and electromagnetic forces which need not be considered for our problems of interest. Additionally the collisional term can be simplified and more easily defined as interactions between the population of interest and the surrounding medium if neutron-neutron and or photon-photon interactions are negligible making the transport equation linear in nature. This is the case in most practical applications such as those we are interested in, however, there are physical systems where this does not hold true. Taking these points into account and defining the angular flux,

$$\psi \equiv vf, \tag{1.2}$$

allows for the basic formulation of the transport equation for neutral particles [6],

$$\frac{1}{v}\frac{\partial}{\partial t}\psi(\boldsymbol{r},\boldsymbol{\Omega},E,t) + \boldsymbol{\Omega}\cdot\boldsymbol{\nabla}\psi(\boldsymbol{r},\boldsymbol{\Omega},E,t) + \sigma_t(\boldsymbol{r},E,t)\psi(\boldsymbol{r},\boldsymbol{\Omega},E,t) = Q(\boldsymbol{r},\boldsymbol{\Omega},E,t). \tag{1.3}$$

Formally $\psi\, d\boldsymbol{r}\, d\boldsymbol{\Omega}\, dE\, dt$ is the total path length traveled by all particles traveling in $d\boldsymbol{r}$ about point $\boldsymbol{r}$ in the differential solid angle $d\boldsymbol{\Omega}$ about direction $\boldsymbol{\Omega}$ with energy residing in dE about E. ψ may be interpreted as the particle path length rate density. Note that the direction of travel $\boldsymbol{\Omega} = \frac{\boldsymbol{v}}{v}$. The total macroscopic cross section in Eqn. (1.3), $\sigma_t(\boldsymbol{r},E,t)$, is the expected number of interactions per path length traveled by particles with energy E at the point $\boldsymbol{r}$ at time t. The total cross section includes all collision interactions with the most basic division of collisional interactions being absorption and scattering meaning

$$\sigma_t(\boldsymbol{r},E,t) = \sigma_a(\boldsymbol{r},E,t) + \sigma_s(\boldsymbol{r},E,t). \tag{1.4}$$

Finally, the term $Q(\boldsymbol{r},\boldsymbol{\Omega},E,t)$ is actually a conglomeration of all terms which contribute to particle production within the differential phase space $d\boldsymbol{r}\, d\boldsymbol{\Omega}\, dE\, dt$. Note that both $Q(\boldsymbol{r},\boldsymbol{\Omega},E,t)$ and the total interaction term, $\sigma_t(\boldsymbol{r},E,t)\psi(\boldsymbol{r},\boldsymbol{\Omega},E,t)$, are obtained by derivation from the collision term,

$$\left[\frac{\partial f}{\partial t}\right]_{coll} \rightarrow\ Q(\boldsymbol{r},\boldsymbol{\Omega},E,t) - \sigma_t(\boldsymbol{r},E,t)\psi(\boldsymbol{r},\boldsymbol{\Omega},E,t). \tag{1.5}$$

In order to actually apply and solve Eqn. (1.3) one must fully define the source term $Q(\boldsymbol{r},\boldsymbol{\Omega},E,t)$. In general for neutral particles this source term is taken to be

$$Q = q_s + q_f + q_{ex}, \tag{1.6}$$

where q_s is the contribution from scattering, q_f is the contribution from fission, and q_{ex} is the contribution from some external source distribution of particles [6]. For non-multiplying media where the fission cross section equals zero, $\sigma_f(\boldsymbol{r}, E, t) = 0$, and for photon transport the contribution from fission doesn't exist, $q_f = 0$. This work focuses on such systems thus we will assume this is the case here. Take note that the introduction of fission into the methods developed here is straight forward. The scattering contribution appears for both neutrons and photons and is fairly complex in form. Any given neutral particle traveling in direction $\boldsymbol{\Omega}$ with energy E upon scattering will change direction and energy to something different, $\boldsymbol{\Omega}'$ and E'. The likelihood that a particle has a scattering interaction is governed by its total scattering cross section $\sigma_s(\boldsymbol{r}, E, t)$. The new energy and direction of heading of the scattered particle will then follow some distribution. This distribution and the scattering cross section are often combined into the differential scattering cross section [6],

$$\sigma_s(\boldsymbol{r}, E \to E', \boldsymbol{\Omega} \cdot \boldsymbol{\Omega}', t) = \sigma_s(\boldsymbol{r}, E, t) p(E \to E', \boldsymbol{\Omega} \cdot \boldsymbol{\Omega}'). \tag{1.7}$$

p is a probability distribution function describing the probability that a particle heading in $\boldsymbol{\Omega}$ with energy E upon scattering will be heading in direction $\boldsymbol{\Omega}'$ with energy E'. This representation of the differential scattering cross section assumes isotropy of the scattering medium. It is the differential scattering cross section with the consideration that all particles within $d^3\boldsymbol{r}$ with any energy and direction of heading may be able to scatter into $d\boldsymbol{\Omega}\, dE$ at time t that defines the scattering source:

$$q_s = \int_0^\infty \int_{4\pi} \sigma_s(\boldsymbol{r}, E' \to E, \boldsymbol{\Omega}' \cdot \boldsymbol{\Omega}, t) \psi(\boldsymbol{r}, \boldsymbol{\Omega}', E, t) d\boldsymbol{\Omega}' dE'. \tag{1.8}$$

The external radiation source contribution, q_{ex} can be any of a number of sources. For example, for neutrons q_{ex} may be defined by radioactive decay of unstable radioisotopes resulting in neutron production. For photons q_{ex} could also be defined by radioactive decay, however, for a wide range of problems in radiative transfer it is governed by Planck's law,

$$B_\nu(\nu, T) = \frac{2h\nu^3}{c^2} \frac{1}{e^{\frac{h\nu}{k_B T}} - 1}, \tag{1.9}$$

where ν is the frequency of radiation emitted, T is the temperature, h is the Planck constant, k_B is Boltzmann's constant, and c is the speed of light [7]. Planck's law describes the emission of electromagnetic radiation from black bodies in thermodynamic equilibrium with their surroundings at a given temperature T. Black bodies are objects that absorb all incoming radiation, and emit their own thermal radiation. To retain generality we will not yet restrict the external source as far as angle of emission instead letting it be given by

$$q_{ex} = q(\boldsymbol{r}, \boldsymbol{\Omega}, E, t). \tag{1.10}$$

Thus the radiation transport equation with a fleshed out source term becomes

$$\frac{1}{v}\frac{\partial}{\partial t}\psi(\boldsymbol{r}, \boldsymbol{\Omega}, E, t) + \boldsymbol{\Omega} \cdot \boldsymbol{\nabla}\psi(\boldsymbol{r}, \boldsymbol{\Omega}, E, t) + \sigma_t(\boldsymbol{r}, E, t)\psi(\boldsymbol{r}, \boldsymbol{\Omega}, E, t) = \int_0^\infty \int_{4\pi} \sigma_s(\boldsymbol{r}, E' \to E, \boldsymbol{\Omega}' \cdot \boldsymbol{\Omega}, t)\psi(\boldsymbol{r}, \boldsymbol{\Omega}', E, t) d\boldsymbol{\Omega}' dE' + q(\boldsymbol{r}, \boldsymbol{\Omega}, E, t), \tag{1.11}$$

with boundary conditions

$$\psi(\boldsymbol{r}, \boldsymbol{\Omega}, E, t) = \psi^{in}(\boldsymbol{r}, \boldsymbol{\Omega}, E, t), \quad \text{for} \quad \boldsymbol{n} \cdot \boldsymbol{\Omega} < 0, \ \boldsymbol{r} \in \partial D, \tag{1.12}$$

and the initial condition

$$\psi(\boldsymbol{r}, \boldsymbol{\Omega}, E, 0) = \psi^{(0)}(\boldsymbol{r}, \boldsymbol{\Omega}, E). \tag{1.13}$$

In reality this form of the transport equation is quite general and can be easily modified to treat sources such as fission by changing the definition of $q(\boldsymbol{r}, \boldsymbol{\Omega}, E, t)$. Changing the form of $q(\boldsymbol{r}, \boldsymbol{\Omega}, E, t)$ to account for sources such as fission does not change the fundamental structure of the transport equation and thus has limited impact on discretization and solution techniques developed for the transport equation [6].

It is helpful to look at the transport equation recast into operator form,

$$L\psi = S\psi + q, \tag{1.14}$$

where L represents the time derivative, streaming term, and total interaction term and S represents the scattering and external source term. L can be thought of as a loss operator while S can be thought of as a source operator. Due to the integro-differential form of the operators and the dependence of both sides of the equation on ψ requires iterative solution of the transport equation. This can be done in many ways, however, in its simplest form

we have:

$$\psi^s = L^{-1}(S\psi^{s-1} + q). \tag{1.15}$$

Eqn. (1.15) represents a single iterative solve of the transport equation, often called a sweep where s is the sweep or iteration number. A primary difficulty of solving radiation transport problems is the inversion of the loss operator, L, which is easier said than done. For some special cases the transport equation, Eqn. (1.11) has obtainable analytic solutions, however, for most problems of interest it must be discretized and solved with numerical methods and often approximations are made for some terms. Discretization of the transport equation is quite involved as the fully general form defined by Eqn. (1.11) is a 7 dimensional equation in space, angle, energy, and time.

The first independent variable we will consider for discretization is energy. A standard deterministic method for discretization of the transport equation in energy is the multi-group approach [6]. In this approach the energy spectrum is divided up into a number, N_g, of subintervals often called groups with group number denoted by g. It is customary in neutronics to let $g = 1$ be the highest energy group, while for photons the opposite is true with $g = N_g$ being the highest energy. The multigroup transport equations are obtained by integrating Eqn. (1.11) over the energy intervals $E_{g-1} - E_g$ and defining group collapsed quantities:

$$\psi_g(\boldsymbol{r}, \boldsymbol{\Omega}, t) = \int_{E_g}^{E_{g-1}} \psi(\boldsymbol{r}, \boldsymbol{\Omega}, E, t) dE, \tag{1.16}$$

$$\frac{1}{v_g} = \frac{\int_{E_g}^{E_{g-1}} f_s(\boldsymbol{r}, E, t) \frac{1}{v} dE}{\int_{E_g}^{E_{g-1}} f_s(\boldsymbol{r}, E, t) dE}, \tag{1.17}$$

$$\sigma_{t_g}(\boldsymbol{r}, t) = \frac{\int_{E_g}^{E_{g-1}} f_s(\boldsymbol{r}, E, t) \sigma_t(\boldsymbol{r}, E, t) dE}{\int_{E_g}^{E_{g-1}} f_s(\boldsymbol{r}, E, t) dE}, \tag{1.18}$$

$$\sigma_{s_{gg'}}(\boldsymbol{r}, \boldsymbol{\Omega}' \cdot \boldsymbol{\Omega}) = \frac{\int_{E_g}^{E_{g-1}} \int_{E_{g'}}^{E_{g'-1}} f_s(\boldsymbol{r}, E', t) \sigma_s(\boldsymbol{r}, E' \to E, \boldsymbol{\Omega}' \cdot \boldsymbol{\Omega}) dE' dE}{\int_{E_{g'}}^{E_{g'-1}} f_s(\boldsymbol{r}, E', t) dE'}, \tag{1.19}$$

and,

$$q(\boldsymbol{r}, \boldsymbol{\Omega}, t) = \int_{E_g}^{E_{g-1}} q(\boldsymbol{r}, \boldsymbol{\Omega}, E, t) dE. \tag{1.20}$$

The function $f_s(\boldsymbol{r}, E, t)$ is known as an energy shape or spectral weight function [6].

$f_s(\boldsymbol{r}, E, t)$ acts as a weighting function in the generation of mutligroup cross sections and is meant to take into account the energy distribution of particles at a given point in space and time. Obviously, the exact energy distribution of particles will not be known a priori for a given problem, thus the specific definition of $f_s(\boldsymbol{r}, E, t)$ and the precise calculation of multigroup cross sections is a non-trivial problem. Generation of multigroup cross sections is indeed an area of ongoing research. Performing the integration over energy of the transport equation and substituting in Eqns. (1.16) - (1.20) yields

$$\frac{1}{v_g}\frac{\partial}{\partial t}\psi_g(\boldsymbol{r}, \boldsymbol{\Omega}, t) + \boldsymbol{\Omega} \cdot \boldsymbol{\nabla}\psi_g(\boldsymbol{r}, \boldsymbol{\Omega}, t) + \sigma_{t_g}(\boldsymbol{r}, t)\psi_g(\boldsymbol{r}, \boldsymbol{\Omega}, t) = \sum_{g=1}^{N_g} \int_{4\pi} \sigma_{s_{gg'}}(\boldsymbol{r}, \boldsymbol{\Omega}' \cdot \boldsymbol{\Omega}, t)\psi_g(\boldsymbol{r}, \boldsymbol{\Omega}', t)d\boldsymbol{\Omega}' + q_g(\boldsymbol{r}, \boldsymbol{\Omega}, t), \quad (1.21)$$

with boundary conditions

$$\psi_g(\boldsymbol{r}, \boldsymbol{\Omega}, t) = \psi_g^{in}(\boldsymbol{r}, \boldsymbol{\Omega}, t), \quad \text{for} \quad \boldsymbol{n} \cdot \boldsymbol{\Omega} < 0, \ \boldsymbol{r} \in \partial D, \quad (1.22)$$

and the initial condition

$$\psi_g(\boldsymbol{r}, \boldsymbol{\Omega}, 0) = \psi_g^{(0)}(\boldsymbol{r}, \boldsymbol{\Omega}). \quad (1.23)$$

A further simplification can be made by integrating Eqn. (1.11) over all energies, or equivalently summing Eqn. (1.21) over all groups [6]. This results in the one-group transport equation, also known as one-speed and sometimes the grey transport equation. Solving the one-speed transport equation is nearly identical to solving an individual group equation of the multigroup equations with real differences only appearing on the right hand side. Many solution and discretization methods for the transport equation are developed for the one-speed transport equation due to the ease of extension to multigroup problems. We do the same in this work, only considering one-group problems. The one-group transport equation is given by

$$\frac{1}{v}\frac{\partial}{\partial t}\psi(\boldsymbol{r}, \boldsymbol{\Omega}, t) + \boldsymbol{\Omega} \cdot \boldsymbol{\nabla}\psi(\boldsymbol{r}, \boldsymbol{\Omega}, t) + \sigma_t(\boldsymbol{r}, t)\psi(\boldsymbol{r}, \boldsymbol{\Omega}, t) = \int_{4\pi} \sigma_s(\boldsymbol{r}, \boldsymbol{\Omega}' \cdot \boldsymbol{\Omega}, t)\psi(\boldsymbol{r}, \boldsymbol{\Omega}', t)d\boldsymbol{\Omega}' + q(\boldsymbol{r}, \boldsymbol{\Omega}, t), \quad (1.24)$$

with boundary conditions

$$\psi(\boldsymbol{r}, \boldsymbol{\Omega}, t) = \psi^{in}(\boldsymbol{r}, \boldsymbol{\Omega}, t), \quad \text{for} \quad \boldsymbol{n} \cdot \boldsymbol{\Omega} < 0, \ \boldsymbol{r} \in \partial D, \tag{1.25}$$

and the initial condition

$$\psi(\boldsymbol{r}, \boldsymbol{\Omega}, 0) = \psi^{(0)}(\boldsymbol{r}, \boldsymbol{\Omega}). \tag{1.26}$$

At this point it is convenient to look at the treatment of the scattering term for practical problems. For methods that are continuous in angle, such as Monte Carlo methods, little more needs to be done to the scattering term seen in Eqn. (1.24). For deterministic transport methods, however, the usual treatment for the scattering source is to expand the scattering cross section in Legendre polynomials in terms of the scattering angle, $\mu = \boldsymbol{\Omega}' \cdot \boldsymbol{\Omega}$, [6],

$$\sigma_s(\boldsymbol{r}, \boldsymbol{\Omega}' \cdot \boldsymbol{\Omega}, t) = \sum_{l=0}^{\infty} \frac{2l+1}{4\pi} P_l(\boldsymbol{\Omega}' \cdot \boldsymbol{\Omega}) \sigma_{s_l}(\boldsymbol{r}, t), \tag{1.27}$$

where

$$\sigma_{s_l}(\boldsymbol{r}, t) = \frac{1}{2} \int_{-1}^{1} P_l(\mu) \sigma_s(\boldsymbol{r}, \mu, t) d\mu. \tag{1.28}$$

In practice the expansion in Eqn. (1.27) is truncated at some point. Keeping only the leading order term, $l = 0$, approximates the scattering as purely isotropic, i.e. scattering from any angle to any other angle is equally likely. This is the approximation we make here. Extending to anisotropy of the scattering source is fairly straight forward for the discretization and solution methods developed in this work [8, 9]. Substituting the expansion in and truncating all but the leading term transforms the one-group scattering source term as follows:

$$\int_{4\pi} \sigma_s(\boldsymbol{r}, \boldsymbol{\Omega}' \cdot \boldsymbol{\Omega}, t) \psi(\boldsymbol{r}, \boldsymbol{\Omega}', t) d\boldsymbol{\Omega}' \approx \frac{\sigma_{s_0}(\boldsymbol{r}, t)}{4\pi} \int_{4\pi} \psi(\boldsymbol{r}, \boldsymbol{\Omega}', t) d\boldsymbol{\Omega}' = \frac{\sigma_{s_0}(\boldsymbol{r}, t)}{4\pi} \phi(\boldsymbol{r}, t), \tag{1.29}$$

where we have used the definition of the scalar flux,

$$\phi(\boldsymbol{r}, t) = \int_{4\pi} \psi(\boldsymbol{r}, \boldsymbol{\Omega}', t) d\boldsymbol{\Omega}'. \tag{1.30}$$

For many practical problems external sources are indeed isotropic, so we will now restrict it to

$$q(\boldsymbol{r}, \boldsymbol{\Omega}, t) = \frac{1}{4\pi} q(\boldsymbol{r}, t). \tag{1.31}$$

Hereafter we will drop the zero subscript on the 0th Legendre moment of the scattering cross section as from now on scattering is taken to be isotropic.

The next dimension we will focus on is angle. A widely used angular discretization method in the deterministic transport methods field is discrete ordinates [6]. The discrete ordinates approximation entails defining a set of discrete angles, $\boldsymbol{\Omega}_m$, at which the transport equation is to be solved. The set of angles chosen often follows some quadrature rule. Angular integrals are then approximated by quadrature sums of the quantities in question. This leads to a set of M equations where M is the order of the quadrature set used to define the set of discrete angles. Following this approach for one-group problems with isotropic scattering we get

$$\frac{1}{v}\frac{\partial}{\partial t}\psi_m(\boldsymbol{r}, t) + \boldsymbol{\Omega}_m \cdot \boldsymbol{\nabla}\psi_m(\boldsymbol{r}, t) + \sigma_t(\boldsymbol{r}, t)\psi_m(\boldsymbol{r}, t) = \frac{1}{4\pi}(\sigma_s(\boldsymbol{r}, t)\phi(\boldsymbol{r}, t) + q(\boldsymbol{r}, t)), \tag{1.32}$$

with boundary conditions

$$\psi_m(\boldsymbol{r}, t) = \psi_m^{in}(\boldsymbol{r}, t), \quad \text{for} \quad \boldsymbol{n} \cdot \boldsymbol{\Omega}_m < 0, \ \boldsymbol{r} \in \partial D, \tag{1.33}$$

and the initial condition

$$\psi_m(\boldsymbol{r}, 0) = \psi_m^{(0)}(\boldsymbol{r}). \tag{1.34}$$

The scalar flux is then obtained by the quadrature sum

$$\phi(\boldsymbol{r}, t) \approx \sum_{m=1}^{M} w_m \psi_m(\boldsymbol{r}, t), \tag{1.35}$$

where w_m are the quadrature weights.

The second to last dimension we will focus on is time. There are a variety of methods for discretizing the transport equation in time. For example, one family of methods involve using a differencing scheme to approximate the time derivative and defines the remaining terms of the equation at some point in time [10]. The simplest methods in this family are the 1st order explicit forward Euler method and the 1st order implicit backwards Euler method. The forward Euler, or simply Euler, method approximates the time derivative with a forward difference and evaluates the remaining terms of the

transport equation at the previous time step. This allows the solution on the next time step to be solved for quite simply in terms of the previous time step. The drawback here is conditional stability that often restricts the time step size to be impractically small requiring many steps to be taken to solve a given problem. On the other hand, implicit backward Euler also uses a forward difference for the time derivative, but evaluates the remaining terms at the next, unknown, time step. Backwards Euler is unconditionally stable, though still 1st order in terms of accuracy. Other higher order methods exist such as the Crank-Nicolson method, sometimes referred to as time Diamond differencing for the transport equation. The Crank-Nicolson method is second order accurate, hence it can produce oscillatory solutions for larger time step sizes.

For the sake of demonstration we will take a closer look at the first order unconditionally stable backward Euler method. Following this scheme the transport equation becomes

$$\frac{1}{v}\frac{\psi_m^{j+1}(\boldsymbol{r})-\psi_m^j(\boldsymbol{r})}{\Delta t^j}+\boldsymbol{\Omega}_m\cdot\boldsymbol{\nabla}\psi_m^{j+1}(\boldsymbol{r})+\sigma_t^{j+1}(\boldsymbol{r})\psi_m^{j+1}(\boldsymbol{r})= \frac{1}{4\pi}(\sigma_s^{j+1}(\boldsymbol{r})\phi^{j+1}(\boldsymbol{r})+q^{j+1}(\boldsymbol{r})), \quad (1.36)$$

with boundary conditions

$$\psi_m^j(\boldsymbol{r})=\psi_m^{in^j}(\boldsymbol{r}), \quad \text{for} \quad \text{all } j,\ \boldsymbol{n}\cdot\boldsymbol{\Omega}_m<0,\ \boldsymbol{r}\in\partial D, \quad (1.37)$$

and with initial condition

$$\psi_m^0(\boldsymbol{r})=\psi_m^{(0)}(\boldsymbol{r}), \quad (1.38)$$

where j is the index of time t^j, Δt^j is the time step size on step j, and $\psi_m^j=\psi_m(\boldsymbol{r},t^j)$. Inversion of the loss operator, the left hand side, of Eqn. (1.36) is not immediately straight forward without some manipulation of the equation. It is possible to rearrange the equation by placing the t^j term in the time finite difference on the right hand side and defining a modified total cross section on the left hand side:

$$\tilde{\sigma}_t^{j+1}(\boldsymbol{r})=\sigma_t^{j+1}(\boldsymbol{r})+\frac{1}{v\Delta t^{j+1}}. \quad (1.39)$$

Doing this changes Eqn. (1.36) to

$$\boldsymbol{\Omega}_m\cdot\boldsymbol{\nabla}\psi_m^{j+1}(\boldsymbol{r})+\tilde{\sigma}_t^{j+1}(\boldsymbol{r})\psi_m^{j+1}(\boldsymbol{r})=\frac{\psi_m^j(\boldsymbol{r})}{v\Delta t^j}+\frac{1}{4\pi}(\sigma_s^j(\boldsymbol{r})\phi^{j+1}(\boldsymbol{r})+q^{j+1}(\boldsymbol{r})). \quad (1.40)$$

For steady state problems where there is no evolution of the solution of a problem in time, the time derivative simply goes to zero. This turns the transport equation into

$$\boldsymbol{\Omega}_m \cdot \boldsymbol{\nabla}\psi_m(\boldsymbol{r}) + \sigma_t(\boldsymbol{r})\psi_m(\boldsymbol{r}) = \frac{1}{4\pi}(\sigma_s(\boldsymbol{r})\phi(\boldsymbol{r}) + q(\boldsymbol{r})). \tag{1.41}$$

Notice that the form of the steady state transport equation, Eqn. (1.41) is nearly identical to that of the reformulated time discretized time dependent transport equation, Eqn. (1.40). The only difference is the lack of $\frac{\psi_m^j(\boldsymbol{r})}{v\Delta t^j}$ on the right hand side, which acts like a fixed anisotropic source on any given time step. This fact means that spatial discretization and solution methods developed for the steady state transport equation can often be easily extended to the time dependent equation. For this work we consider only the steady state transport equation.

Last, but certainly not least, the spatial dimensions of the transport equation must be discretized. Up until now we have been focusing on the transport equation in general geometry. Eqn. (1.41) and earlier equations presented here are valid for any coordinate system. Before discretizing the transport equation in physical space one must decide on a certain coordinate system, or geometry, in which they wish to define the equation. The choice of coordinate system should take into account the geometric shape and material structure of the physical system(s) to be modeled, especially any symmetries the problem(s) may have. As pointed out earlier a coordinate system that takes advantage of features of the problem such as symmetry, domain shape, material distribution, etc. can help lower the complexity of the equations to be solved. Whatever coordinate system is chosen defines the independent spatial variables and the form of the gradient and divergence operators. The form of the gradient/divergence operators changes the form of the streaming term on the left hand side of the transport equation. For simplicity let us drop the angular direction index m and the explicit spatial dependence on $\boldsymbol{r}$. In Cartesian geometry the independent spatial variables are x, y, and z, and streaming term in the transport equation becomes

$$\boldsymbol{\Omega} \cdot \boldsymbol{\nabla}\psi = \boldsymbol{\nabla} \cdot \boldsymbol{\Omega}\psi = \frac{\partial}{\partial x}\Big(\Omega_x\psi\Big) + \frac{\partial}{\partial y}\Big(\Omega_y\psi\Big) + \frac{\partial}{\partial z}\Big(\Omega_z\psi\Big), \tag{1.42}$$

where

$$\Omega_x = \sin\theta\cos\gamma, \quad \Omega_y = \sin\theta\sin\gamma, \quad \Omega_z = \cos\theta. \tag{1.43}$$

If a given problem has a solution that is independent of a certain spatial variable, for example z, then the derivative term associated with that spatial variable will go to zero. This yields 2D $x-y$ geometry. This is often done as an approximation for physical systems such as nuclear reactors where the axial material distribution and solution are fairly homogeneous causing leakage effects in the z direction to be small, while the material distribution and solution in the $x-y$ plane at a given height is quite heterogeneous and leakage effects are large. This same principle holds for a second dimension, for example y, yielding 1D slab geometry. For other geometries the spatial variables and gradient/divergence operators change.

In this work we are interested in 2D cylindrical $r-z$ geometry. In $r-z$ geometry the spatial variables are r and z, obviously, and also the azimuthal angle γ. The streaming term in the transport equation for $r-z$ becomes

$$\boldsymbol{\Omega}\cdot\boldsymbol{\nabla}\psi = \boldsymbol{\nabla}\cdot\boldsymbol{\Omega}\psi = \frac{1}{r}\frac{\partial}{\partial r}\Big(r\Omega_r\psi\Big) + \frac{\partial}{\partial z}\Big(\Omega_z\psi\Big) + \frac{\partial}{\partial\gamma}\Big(\frac{1}{r}\Omega_\gamma\psi\Big), \tag{1.44}$$

where

$$\Omega_r = \sin\theta\cos\gamma, \quad \Omega_z = \cos\theta, \quad \Omega_\gamma = -\sin\theta\sin\gamma. \tag{1.45}$$

Immediately a few things become apparent when comparing the Cartesian streaming term to the $r-z$ streaming term. First, we say 2D $r-z$, however, there are three independent variables and three derivative terms in the $r-z$ divergence operator and thereby the streaming term. 2D Cartesian would only have two independent spatial variables and two derivative terms in its divergence operator and streaming term. This happens due to the azimuthal angle, γ, being an independent spatial variable in $r-z$ geometry. Characteristic lines following a direction of radiation travel in $r-z$ geometry move in three dimensional space, namely r, z, and γ. The angular derivative term, $\frac{\partial}{\partial\gamma}\Big(\frac{1}{r}\Omega_\gamma\psi\Big)$, describes the redistribution of particles in the azimuthal angle just as the r and z spatial derivatives describe the redistribution of particles in $r-z$ space. Secondly we see that the form of the r derivative term is fundamentally different then say the x derivative in Cartesian geometry. That is because streaming of particles in the r direction is fundamentally different than the x direction in Cartesian geometry. The difference is that in Cartesian geometry any two adjacent differential volumes can be considered identical, in curvilinear geometry this is not the case in the r direction. Looking at two adjacent differential volumes in r in curvilinear geometry, the two will be at different radii and therefore

have different geometry. These differences, especially the azimuthal redistribution term, pose challenges to discretization of the transport equation in curvilinear coordinates. A detailed explanation of discretization of the transport equation in $r-z$ will be reserved for later sections where we introduce specific methods.

The formal statement of the equation that we wish to solve on our grids of interest is the one group, steady state, discrete ordinate radiation transport equation with isotropic scattering in $r-z$ geometry,

$$\frac{1}{r}\frac{\partial}{\partial r}\Big(r\Omega_r\psi\Big)+\frac{\partial}{\partial z}\Big(\Omega_z\psi\Big)+\frac{\partial}{\partial\gamma}\Big(\frac{1}{r}\Omega_\gamma\psi\Big)+\sigma_t\psi=\frac{1}{4\pi}(\sigma_s\phi+q), \tag{1.46}$$

with boundary conditions,

$$\psi=\psi^{in},\quad \text{for}\quad \boldsymbol{n}\cdot\boldsymbol{\Omega}<0,\ r,z\in\partial D. \tag{1.47}$$

It is this equation, Eqn. (1.46), that we seek to find a better solution method for compared to what has been previously developed [11–21]. Solving this "basic" transport equation is, in reality, where most of the difficulty lies in solving radiation transport problems. As pointed out following each step of our discretization and simplification of the original general form of the transport equation, Eqn. (1.11), treatment of multigroup or time dependent problems is extremely similar to dealing with (1.46).

1.4 Proposed Methodology

The methodology put forth in this work to solve radiation transport problems of interest on complex grids in $r-z$ geometry is to use the Quasidiffusion (QD) Method. The QD method is a highly efficient method for solving radiation transport problems [9, 22]. Not only does the QD method exhibit rapid iterative convergence, it also enables one to reduce the dimensionality of transport problems and opens up possibilities for improvement of coupling with multiphysics equations [15, 23]. This reduction of dimensionality of the problem comes in the form of a collapse in angle. The system of equations of the QD method consists of the high-order transport equation and the low-order QD (LOQD) equations for the 0th and 1st angular moments of the transport equation. These high and low-order equations are then solved in an iterative framework where the high-order solution is used to generate factors that act as coefficients in the low-order equations.

The solution of the low-order equations is used to update integral flux based source terms thereby speeding up convergence of the overall solution. This iterative framework transfers work from the expensive high-order equations to the cheaper low-order equations resulting in fewer transport iterations.

The fast iterative convergence that is the hallmark of the QD method is due to the definition of the factors used in the low-order acceleration scheme. These factors, known as the QD or Eddington factors [24], are only weakly dependent on the high-order solution for a given problem. This weak dependence leads to rapid convergence of the factors causing rapid convergence of the solution to a problem as a whole.

Another extremely attractive feature of the QD method is that it demonstrates stable convergence when independent discretizations are used for the high-order and low-order equations. Many acceleration schemes require consistency or at the very least degrade performance wise with inconsistency between the high and low-oder discretizations within a two-level method framework. The problem with requiring consistency between high-order and low-order equations is that a certain discretization may work wonders for one equation set and wreak havoc upon the other. For example, certain discontinuous finite element discretizations of the transport equation are both accurate and relatively cheap to solve, while the corresponding consistent discretization of the P_1 equations results in a difficult to solve set of equations [25]. These difficulties may be that a consistent discretization has considerably more unknowns and or the resulting problem is poorly conditioned compared to a similar inconsistent discretization. This and the aforementioned features of the QD method make it well suited for solving the transport equation in a wide variety of applications, especially so in the type of problems we consider.

In this work we develop a method for solving radiation transport problems on adaptive-like arbitrary quadrilateral grids in $r-z$ geometry using the Quasidiffusion method. Doing this required the development of a new and robust discretization for the LOQD equations as well as careful consideration of how best to discretize the transport equation.

1.5 Dissertation Overview

The main results of the work done in this dissertation are the development of the aforementioned new discretization of the LOQD equations in 2D $r-z$ geometry and the formulation of QD methods based on this new discretization with two different high-order

transport discretizations. The developed discretization method for the LOQD equations and resulting QD methods give solutions and are shown to converge on adaptive-like, randomized, quadrilateral meshes. Two different treatments for hanging nodes, extending the LOQD discretization to adaptive-like grids are presented. One is based on work done previously [26, 27], and a new highly general approach that allows for straight forward extension to polygonal grids.

The results of this research have been presented by the candidate at the following venues:

- The International Conference on Mathematics and Computational Methods Applied to Nuclear Science and Engineering, M&C 2017, in Jeju, Korea, April 16-20, 2017,
- The International Conference on Mathematics and Computational Methods Applied to Nuclear Science and Engineering, M&C 2019, in Portland, OR, August 25-29, 2019, and
- Scientific Seminar to the Reactor and Nuclear Systems Division at Oak Ridge National Laboratory in Oak Ridge, TN, May 02, 2019.

Results were published in the proceedings of M&C 2017 and M&C 2019 [28, 29].

The remainder of this dissertation is organized as follows. Chapter 2 explores the status of the problem, detailing a number of common high-order transport equation discretizations and transport solutions methods. Chapter 2 also gives a brief history of QD method development with a focus on recent developments on our grids of interest and $r-z$ geometry. Chapter 3 presents the formulation of the LOQD equations and QD method in $r-z$ geometry, the derivation of the new LOQD discretization including extension to adaptive-like grids, and the derivation of the transport discretization methods we used to formulate the QD method. In Chapter 4 we describe the methodology used to analyze the LOQD discretization and resulting QD method and perform that analysis presenting a myriad of results. Finally in Chapter 5 we draw final conclusions and discuss possible future work.

Chapter 2

Status of The Problem

2.1 Transport Discretizations

Much can be written about the deterministic methods that have been developed for discretizing and solving the transport equation in $r-z$ geometry, as many have been developed for this purpose even for use on arbitrary grids. Stochastic methods have of course also been developed for use in curvilinear geometry, however, we will limit our discussion to deterministic methods. Common among discretization methods is the definition of a computational grid or mesh made up of subintervals upon which discretized equations, problem properties, and sources are defined. These discretized equations are then solved using some technique, almost invariably involving some sort of sweep. The term "sweep" meaning the sequential solution of the discrete transport equations defined on a computational grid. Sweeps come about because of the hyperbolic nature of the differential operator of the transport equation. Hyperbolic equations such as transport, in the absence of integral terms such as scattering, are one directionally dependent as opposed to elliptic equations where the solution everywhere always affects the solution everywhere else.

One class of methods for discretizing the transport equation in $r-z$ are characteristic methods [17, 21]. As with any characteristic method, methods of this type use the hyperbolic nature of the transport equation to transform it into a differential equation defined along characteristics. This is done by a change of variables from the independent spatial variables of the used coordinate system to characteristic length, the distance traveled of particles along a track, along which the solution may be obtained. Characteristic

methods come in many variants. The Method Of Long characteristics (MOLC) involves characteristic lines that travel through the entire domain of a problem uninterrupted where intersections with cells of the original computational grid become 1D-like cells of the characteristics [21, 30]. MOLC involves the solution of many 1D-like transport problems, one for each characteristic, and the integration of the resultant angular fluxes to get needed grid functions such as the scalar flux. The Method Of Short characteristics (MOSC) is another variant where characteristics are only tracked through a single computational grid cell [31–33]. This then involves the approximation of the incoming angular flux of a given characteristic on a cell face. Different approximations exist for this, each resulting in a different discretization method. Unique to characteristic methods in $r-z$ geometry is the fact that characteristics are actually curves in the $r-z$ plane. This caveat introduces an additional layer of difficulty to characteristic methods as tracking curves and finding intersections with the surfaces of computational grid cells can become nontrivial.

Finite volume (FV) [16] and finite difference (FD) [12] methods are also popular for discretizing the transport equation in $r-z$. These methods treat the transport equation just as their names imply. Finite volume methods involve the integration of the transport equation over an individual control volume so as to approximate the equation [13]. Finite difference methods replace the derivative terms with difference formulas. Diamond Differencing (DD) is a well known finite difference scheme.

In addition to these other methods there are a number of finite element methods (FEM) for discretizing the transport equation in $r-z$ [20] that use the Galerkin FEM approach to discretize spatially [18]. In general, FEM methods involve defining trial or basis functions that the primary unknowns of a problem are expanded in using expansion coefficients. The equation of interest is multiplied by the basis functions and integrated over space to obtain a system of discrete equations for the expansion coefficients. In these methods it is commonly seen that the angular derivative term is treated with a difference formula, and the spatial derivatives are what are dealt with using the actual FEM approach [20]. FEM methods allow for arbitrary spatial convergence order by way of the basis functions chosen. A higher order set of polynomial basis functions will result in a higher order set of discretized equations. Within the family of FEM methods two large subcategories exist, continuous and discontinuous finite element approaches. Put simply, continuous FEM (CFEM) methods enforce continuity at cell boundaries usually resulting in fewer unknowns than for discontinuous FEM (DFEM) methods which

carry multiple unknowns located around cell boundaries allowing for a discontinuous representation of the solution. DFEM methods usually involve definition of coupling conditions at cell interfaces to relate the two such as upwinding [20]. Allowing the solution to be discontinuous at cell boundaries usually results in DFEM approaches having an advantage over CFEM approaches accuracy wise.

A further group of discretization methods is sub-cell/corner balance methods in which particle conservation is enforced on sub-cells defined about the vertexes of the original computational mesh within each cell [34,35]. The angular derivative is dealt with similarly to FEM discretizations with a difference formula. Within this family of methods two stand out, the Simple Corner Balance (SCB) and Upstream Corner Balance (UCB) methods. Both have discrete balance equations defined on corner based sub-cells. The difference between the two is in the sub-cell to sub-cell particle transfer. SCB uses an average between two adjacent cells to define the angular flux on that face, and UCB uses a sub-cell local differencing scheme to extrapolate the flux on a face. The SCB scheme behaves similarly to Linear Discontinuous Finite Element Method (LDFEM or just LD) discretizations, with the two being equivalent in 1D slab geometry [34].

Each of these groups of methods have advantages and disadvantages associated with them, and these advantages and disadvantages govern how suitable a given discretization is for use on certain problems and for use within the QD method. Among the advantages and disadvantages of each is whether or not the method has a flux dip near $r = 0$ as is common with discrete ordinate approaches in curvilinear geometry, what is the spatial accuracy of the scheme, does the method exhibit nonmonotonicity especially near material heterogeneities, does it attain the diffusion limit, and of course whether the method is conservative. How each of these then play into use as part of the QD method is an entirely different story, one which will be expounded upon later.

The spatial accuracy of each of these classes of schemes is in truth variable, with each scheme allowing for either higher or lower order accuracy treatment. For FEM schemes higher or lower order polynomials can be chosen as basis functions. For FD methods different difference formulas can be used. The MOSC scheme involves approximation of incoming radiation on the faces of a cell. Interpolation is usually done here and the order of that interpolation can be higher or lower order yielding higher or lower order discretizations as a result. In any of these families of methods the representation of the source term can be defined differently, e.g. flat sources, linear sources, higher

order polynomials, etc. Any change made here renders a different method with different accuracy and spatial convergence properties, but care must be taken. Generally with higher accuracy comes higher computational cost, and higher order discretizations tend to be more nonmonotonic. Godunov's theorem tells us that any linear scheme over 1st order cannot be expected to give strictly monotonic solutions. Thus the choice of order can become a balancing act of ensuring maximum accuracy per unit cost computationally.

Nonmonotonicity of a scheme, though nonphysical in nature, is not an inherently negative effect by itself. Given a radiation transport problem with a large material discontinuity a 1st order method might give a solution that is monotonic but far from the true solution. On the same problem a 2nd order method would likely give an oscillatory solution around the discontinuity, but that solution would likely be significantly closer in some sense to the true solution due to the higher convergence order of the method. That being said, however, nonmonotonicity can lead to other problems at least for certain solution methods such as QD. This plays into the aforementioned balancing act of spatial order, really making it a three way struggle.

"Attaining the diffusion limit" refers to the property of a transport discretization that as a given problem approaches diffusion dominance, higher scattering ratio and being far from boundaries, the discretized transport equation approaches a valid discretization of the diffusion equation [36–38]. It is also generally taken to mean that as a problem approaches diffusion dominance the scalar flux solution resulting from the discretized transport equation approaches the solution of the diffusion equation. A transport discretization that does not attain the diffusion limit will not obtain the correct solution for diffusion dominated problems, or diffusion dominated regions of a problem. In the problems that we consider it is absolutely possible to at least have regions of a problem where this occurs. In general any discretization of the transport equation cannot be automatically guaranteed to limit to a valid discretization of the diffusion equation. This is seen in some commonly used discretizations of the transport equation such as characteristic methods on certain meshes [37]. However, there are many common FEM, FD/FV, and characteristic schemes that do attain the diffusion limit without any special considerations.

The so called "flux dip" problem seen for many discrete ordinates methods is a nonphysical effect that occurs in the vicinity of $r = 0$ where the scalar flux is artificially lower than it should be. The reason for this dip was shown to be a failure of the chosen transport discretization method to accurately approximate the diffusion equation at $r = 0$

in the diffusion limit [39]. Note that by definition of the transport problem in $r-z$ the angular flux is isotropic in the azimuthal angle, γ. Therefore at any point along the rotational axis, $r=0$, where the scalar flux has a derivative of zero in the z direction the angular flux will be perfectly isotropic. At such a point the diffusion equation is exact, thus the need for the discretization used for the transport equation to reduce to a proper discretization of the diffusion equation. Characteristic methods exhibit this problem as well as many FEM, FD/FV, and corner balance methods without proper treatment of the angular flux in azimuthal angle. It was found that using weighted Diamond Differencing in the azimuthal angle in FEM, FD/FV, and corner balance schemes can eliminate this dip [39].

A method being conservative or nonconservative is straight forward both in meaning and in implication. It is obviously undesirable for a method to not conserve particles, or for any method to not conserve anything for that matter. However, when being used within the framework of some solution methods such as QD the story is not so simple, as the low-order problem can be used to enforce conservation of particles. This will be discussed more later.

An important item of research in this work was to determine what transport discretization(s) would perform satisfactorily within the QD method in $r-z$ geometry and how to implement them. As can be seen there are a lot of factors to consider in this respect, and some of those factors end up not as they appear at first glance when used with certain solution methods such as QD. We make no claim to have found the "best" transport discretization to use, however, we did strive to demonstrate the performance of the developed method with significantly different transport methods, and much can be inferred from the work here as to what discretizations would be better than others.

2.2 Solution Methods

2.2.1 Common Solution/Acceleration Methods

Perhaps even more diverse than the field of transport discretization methods is the field of solution methods that have been developed. There are an abundance of them in fact, with development being spurred by the need and desire to simulate ever more complex problems with ever increasing accuracy. Source iterations (SI), representing the simplest and most straight forward approach, is the classic solution method for the transport

equation. SI for solution of the transport equation consists of doing a sweep with a fixed right hand side (source) and then updating that source using the new angular flux solution. This process is repeated until the solution converges. For some problems SI works just fine and converges quickly, however, for many problems it does not. For instance, any problem with a large scattering ratio, $c = \frac{\sigma_s}{\sigma_t}$, will likely be difficult to solve using SI alone.

The ever increasing need for efficiency and accuracy necessitates the ever more efficient solution methods, i.e. for modern problems something better than simple SI is required. The QD method falls into a category of two-level acceleration methods which has a number of extremely popular methods in both production level implementations as well as in research settings [40]. Common solution methods that can be categorized as two-level methods include but are certainly not limited to diffusion synthetic acceleration (DSA) [41], weighted alpha (WA) methods [42], nonlinear diffusion acceleration (NDA) [43], and coarse mesh finite differencing (CMFD) [44]. In reality each of these methods has blossomed into entire families of related methods in recent years as work has been done to improve them. What is discussed here focuses mainly on the classic versions of each as covering every variation of each method would be quite the daunting task. All of these solution/acceleration methods seek to do two things, one, to transfer solution work from the highly dimensional high-order transport equation to lower dimensionality low-order equations, and two, to speed up iterative convergence. Some of these methods do this through taking certain angular moments of the transport equation such as QD and WA methods. Others do this by formulating and solving low-order equations with different closures such as NDA and DSA where the diffusion equation or generalized P_1 equations are solved to correct or speed up convergence. CMFD takes this a step further by solving a low-order diffusion problem on a coarser spatial grid than is seen in the high-order transport problem. Every one of these methods has its strengths and weaknesses making them more or less suited to a given problem.

DSA is also known as a preconditioning scheme [41, 45]. It is derived by first defining equations for linear corrections of the angular flux solution of the transport equation by taking the difference between the original transport equation and a "half step" equation defined by a source iteration (transport sweep). These equations for corrections have the same complexity as the original transport equation and thus are approximated using diffusion, hence being called Diffusion Synthetic Acceleration. Transport Synthetic Acceleration (TSA) is derived by the same procedure, however, it uses a transport model

to approximate the equations for corrections. The transport model used obviously needs to be simpler or cheaper than the original to benefit computationally. The solution of a problem using DSA has on any given iteration a transport sweep and a diffusion equation solve. The solution of the low-order diffusion problem is used to correct the scalar flux thus accelerating convergence of the problem. DSA takes advantage of the fact that transport sweeps, or source iterations, tend to damp error modes with stronger angular dependence while corrections based on the diffusion equation tend to damp error modes with weak angular dependence [45]. This allows DSA to give significant speed up as compared to unaccelerated transport sweeps for a wide range of problems. The disadvantages of DSA come into play with discretization. Consistent discretization of the transport equation and low-order diffusion correction equations result in unconditional stability and consistent acceleration over all optical thicknesses of a problem [45, 46]. Optical thickness being the total cross section times cell width, $\tau = h\sigma_t$. As was said in the proposed methodology section of this work, requiring consistency between the high-order and low-order equations can be highly undesirable as one discretization may work wonders for transport and be terrible either accuracy wise or computational expense wise for the low-order equation or vice versa [25]. Discretizing the high-order and low-order equations in DSA inconsistently can lead to conditional stability, with divergent iterations for optically thick problems for some choices of discretization. For any inconsistent choice of discretization for DSA there will at least be a degradation of accelerative ability of the method with increasing optical thickness of a problem [45]. For well behaved problems this situation may never arise, however, this disadvantage can become crippling in coupled time dependent radiative transfer hydrodynamics simulations. In radiative transfer problems very low-energy groups can have a total cross section several orders of magnitude greater than high-energy groups. That means for these groups whatever mesh is being used will likely have very optically thick cells and DSA will fail or at least slow down. Hence for our problems of interest DSA is not a satisfactory option.

NDA is somewhat akin to DSA in that it uses the generalized P_1 equations as the low-order set of equations, however, it has key differences in form and function. The set of equations for NDA is not formulated in terms of corrections as in DSA and instead consists of a particle balance equation and a modified 1st moment equation also known as a generalized Fick's Law both in terms of flux and current. The generalization done is the addition of a compensation term to the 1st moment equation forcing the 1st moment

equation to be satisfied by the transport solution upon convergence [43, 47]. The solution procedure using NDA starts on each iteration with a transport sweep, the transport solution is used to generate the compensation term, and then the low-order equations are solved to get an updated scalar flux solution. This procedure can be rearranged to start with a diffusion solve in order to get a good initial iterate. In general, NDA requires consistent discretization between the high-order transport and low-order P_1 equations for unconditional stability. Obviously, this last point is undesirable for our purposes.

CMFD is very closely related to NDA as its low-order equations are the balance equation and the same generalized Fick's law, however, CMFD solves the low-order equations on a different, coarser grid than transport and uses aspects of homogenization [44]. For CMFD a coarse grid is defined, usually grouping cells of the fine transport grid that have some relation such as all the cells of a fuel pin in reactor physics problems, and homogenization is done to get angular flux averaged compensation terms, cross sections, and diffusion coefficients. The solution procedure is the same as with NDA with the exception of the additional data needed for the low-order equations and the correction of the scalar flux is done multiplicatively instead of by replacement using the low-order solution,

$$\phi_i^{s+1} = \phi_i^{s+1/2} \frac{\phi_j^{s+1}}{\sum_{i \in j} \phi_i^{s+1/2}} \quad \text{for all } i \in j. \tag{2.1}$$

Here i is the index of a fine mesh cell and j is the index of a coarse mesh cell. CMFD gives a large reduction in dimensionality as it is a collapse not only over angle but also space. Classic CMFD is only conditionally stable [48], with instability seen for larger material property discontinuities (high heterogeneity) and large optical thicknesses. With increasing optical thickness CMFD gives degraded performance and a higher likelihood of instability. Thus CMFD suffers from the same or similar problems as DSA with inconsistent discretization. As was said, for our problems of interest large material discontinuities and possibly huge optical thicknesses can be expected.

WA methods, similar to these other methods, consists of the high-order transport equation and a set of low-order equations. In 1D slab geometry the low-order equations in WA methods are derived by multiplying the transport equation by the weight $|\mu|^\alpha, \alpha \geq 0$ and integrating over the ranges $-1 \leq \mu \leq 0$ and $0 \leq \mu \leq 1$ [45]. Defining the nonlinear functionals

$$A_{\pm} = (\alpha+1)\frac{\int_0^{\pm 1} |\mu|^{\alpha+1}\psi \; d\mu}{\int_0^{\pm 1} \psi \; d\mu} \quad \text{and} \quad B_{\pm} = (\alpha+1)\frac{\int_0^{\pm 1} |\mu|^{\alpha}\psi \; d\mu}{\int_0^{\pm 1} \psi \; d\mu} \tag{2.2}$$

allows for the formulation of the low-order equations,

$$\pm \frac{d}{dx}\left(A_{\pm}\psi_{\pm}\right) + \sigma_t B_{\pm}\psi_{\pm} = \frac{\sigma_s}{2}\phi + \frac{q}{2}. \tag{2.3}$$

Where

$$\psi_{\pm} = \pm \int_0^{\pm 1} \psi \; d\mu, \quad \text{and} \quad \phi = \psi_+ + \psi_-. \tag{2.4}$$

Different choices of the parameter α result in a different method with different properties. For the choice of $\alpha \approx 0.366$ the WA method behaves very much like DSA and transport synthetic acceleration using a 2 point Gaussian quadrature set (S_2SA) [45]. Classic choices of α are $\alpha = 0$ and $\alpha = 1$ yielding the First Flux (FF) method and Second Flux (SF) method respectively. When spatial discretization comes into play the FF and SF methods both tend to perform poorly in diffusion dominated regimes as their discretized low-order equations do not limit to discretizations of the diffusion equation, i.e. they do not attain the diffusion limit [49]. The choice of $\alpha \approx 0.366$ yields discretized low-order equations that do limit to that of the diffusion equation, hence the method behaving similarly to DSA. However, even this choice of parameter doesn't do well to resolve boundary layers within problems such as interfaces between highly diffusive and non-diffusive regions [49].

In contrast to these common solution/acceleration techniques QD, belonging to a family of methods known as nonlinear projective iterative (NPI) methods, does not suffer from inherent stability issues. The QD method does not require consistent discretization of the high-order and low-order equations, large optical thicknesses do not effect it in any meaningful way, it performs well in highly diffusive regimes, and it affords a reduction in dimensionality and fast convergence. This means that for problems involving coupled radiative hydrodynamics QD can be used without stability issues and can be expected to perform well even while using inconsistent discretizations for the high and low-order equations. It is important to point out that these other solution methods are not without their applications. Quite the contrary, there are many problems that lie well within the bounds of where DSA, NDA, CMFD, and WA methods give excellent performance and stability. Many problems in reactor physics fit in this category, hence why these methods are popular in that field.

2.2.2 The Quasidiffusion Method: A Brief History

The QD method has existed for many years originally being developed by Vladimir Gol'din in the 1960s [9]. In Vladimir Gol'din's 1964 paper he outlined the QD method in general geometry proving its equivalence to the high-order transport equation and gave results for it in 1D spherical geometry [9]. He also showed that QD worked for problems with general anisotropic scattering. Development and application of the QD method continued throughout the 1970's with generalization of the boundary conditions by Gol'din and Chetverushkin, Ref. [50], and results being presented for other geometries such as 2D Cartesian by Gol'din [51]. Since these early years the QD method has been applied to a number of different problems in different geometries and in differing formulations. For instance, Gol'din along with a number of colleagues demonstrated the QD method applied to thermal radiative transfer problems [52, 53]. Unfortunately, a full account of all publications, applications, extensions, and the developmental history of QD is beyond the scope of this work. A good starting place for the interested reader on the subject is Marvin Adams' and Edward Larsen's review of Fast Iterative Methods [22].

Its important to note that Gol'din originally developed the QD method as a solution method, not as an acceleration method. Pure acceleration methods, such as consistently discretized DSA, give the exact same solution as solving the unaccelerated discretized high-order transport equation just with hopefully fewer iterations. In general QD does not reproduce the exact same solution as the discretized high-order equation alone as the solution tends to be affected to some extent by the chosen LOQD discretization. However, as Gol'din showed in his original paper the QD system of equations is equivalent to the original transport equation, therefore the solution obtained using QD is still a valid transport solution [9]. QD can be formulated as a pure acceleration method by choosing consistent high and low-order equation discretizations, and in fact this was done by Troshchiev in the late 1960s [54]. Doing so yields exactly the same solution as the chosen discretized, unaccelerated high-order transport equation.

A QD method and discretizations of the LOQD equations have actually been developed for use in $r-z$ geometry [15, 19]. In, Refs. [15, 19], the LOQD equations were discretized using a FV approach where the 0th angular moment of the transport equation is integrated over a cell and the 1st moment equation is integrated over half cells to obtain an equation for each face of a quadrilateral. Monotonicity of the scheme is achieved by diagonalizing the Eddington tensor by way of a coordinate rotation. However, these methods were

originally only demonstrated on structured grids [15,19]. It was shown later that the $x-y$ analogue of that discretization for the LOQD equations does not converge upon refinement of arbitrary (randomized) grids for Cartesian geometry [55]. This gives us a strong reason to believe that the same is true for these methods when applied to $r-z$ geometry as well. $r-z$ geometry and curvilinear coordinate systems in general do not tend to alleviate inherent stability or convergence problems that exist in other geometries. In fact with the angular redistribution term in the transport equation stability and convergence problems of discretizations can be made worse in $r-z$ as opposed to Cartesian. This lack of a known stable, convergent discretization of the LOQD equations on arbitrary grids in $r-z$ was a major motivating factor for this work.

Recently, a discretization method for the LOQD equations on arbitrary quadrilateral, adaptive-like grids in Cartesian $x-y$ geometry was developed [27]. This new discretization uses the approximation of the gradient used to discretize the P_1 equations on arbitrary polyhedral meshes in 3D Cartesian, Ref. [56], to derive approximations for the tensor divergence terms in the LOQD equations [27]. The LOQD discretization developed based on this was shown to converge with 2nd order behavior upon spatial refinement for grids of this type in certain norms [27]. The work in $x-y$ geometry done in Ref. [27] is the foundation of the work done here in $r-z$ geometry, with the discretization and resulting method developed in this work being its $r-z$ analogue. The discretization outlined in [56] is an obvious choice for also basing the discretization of tensor divergence terms in the LOQD equations in $r-z$ since it was shown to be satisfactory for the LOQD equations in $x-y$ [27], and Ref. [56] mentions a possible extension to the P_1 equations in curvilinear coordinates.

Chapter 3

Derivation of LOQD Discretization and Development of QD Method for $r-z$ Geometry

3.1 Introduction

Three major components of the work done here was to first develop a discretization for the LOQD equations that would converge on arbitrary quadrilateral grids in $r-z$, second was to extend that discretization to treat adaptive-like grids, thirdly was to choose a satisfactory transport discretization and formulate the QD method that results from the chosen discretizations. As was accomplished in $x-y$ geometry, [27], it was desired that the new discretization for the LOQD equations in $r-z$ would converge with 2nd order behavior upon spatial refinement. The completion of these tasks had a number of challenges that needed to be overcome. As mentioned earlier, discretization of the transport and LOQD equations in curvilinear geometry is significantly complicated by the form of the divergence operator. This complication comes mainly from the existence of the angular derivative, or angular redistribution term, that appears in addition to the r and z spatial derivatives in the transport equation and the terms this translates into in the LOQD equations. Extension to adaptive-like grids was done in $x-y$ geometry for the LOQD equations in [27], however, what was interesting for this work was to try to improve upon that extension. Finally, choosing a transport discretization to use is not necessarily a straight forward business. There are a number of factors to consider with

even more complication here in $r-z$ compared to $x-y$. To begin the description of the developed work we will start with the formulation and derivation of the QD system of equations.

3.2 Formulation of the LOQD Equations and QD Method in $r-z$ Geometry

The QD method consists of the high-order transport equation and the low-order QD equations closed exactly with the QD, or Eddington, tensor. The LOQD equations are derived for the scalar flux, $\phi = \int_{4\pi} \psi d\mathbf{\Omega}$, and current, $\boldsymbol{J} = \int_{4\pi} \mathbf{\Omega}\psi d\mathbf{\Omega}$, by integrating the transport equation, Eqn. (1.46),

$$\frac{1}{r}\frac{\partial}{\partial r}\Big(r\Omega_r\psi\Big) + \frac{\partial}{\partial z}\Big(\Omega_z\psi\Big) + \frac{\partial}{\partial \gamma}\Big(\frac{1}{r}\Omega_\gamma\psi\Big) + \sigma_t\psi = \frac{1}{4\pi}(\sigma_s\phi + q),$$

over $\mathbf{\Omega}$ with weights 1, Ω_r, and Ω_z. Doing this yields the balance equation and the r and z components of the 1st angular moment equation,

$$\frac{1}{r}\,\frac{\partial(rJ_r)}{\partial r} + \frac{\partial J_z}{\partial z} + \sigma_a\phi = q, \tag{3.1}$$

$$\frac{\partial F_{rr}}{\partial r} + \frac{\partial F_{zr}}{\partial z} + \frac{1}{r}\Big(2F_{rr} + F_{zz} - \phi\Big) + \sigma_t J_r = 0, \tag{3.2}$$

$$\frac{\partial F_{zr}}{\partial r} + \frac{\partial F_{zz}}{\partial z} + \frac{1}{r}F_{zr} + \sigma_t J_z = 0, \tag{3.3}$$

where $\sigma_a = \sigma_t - \sigma_s$, and

$$F_{\alpha\beta} = \int_{4\pi} \Omega_\alpha\Omega_\beta\psi d\mathbf{\Omega}, \quad \alpha,\beta = r,z. \tag{3.4}$$

The QD (aka Eddington) factors are defined as

$$E_{\alpha\beta} = \frac{\int_{4\pi} \Omega_\alpha\Omega_\beta\psi d\mathbf{\Omega}}{\int_{4\pi}\psi d\mathbf{\Omega}}, \quad \alpha,\beta = r,z. \tag{3.5}$$

The QD factors are used to formulate the 1st moment equations for ϕ, J_r, and J_z and close the system of equations.

Using the QD factors along with the definition of the scalar flux, $\phi = \int_{4\pi} \psi d\boldsymbol{\Omega}$, and utilizing the fact that

$$E_{rr} + E_{zz} + E_{\gamma\gamma} = 1 \tag{3.6}$$

we obtain the final continuous form of the 1st moment QD equations [15, 19]

$$\frac{\partial(E_{rr}\phi)}{\partial r} + \frac{\partial(E_{zr}\phi)}{\partial z} + \frac{G}{r}E_{rr}\phi + \sigma_t J_r = 0, \tag{3.7}$$

$$\frac{1}{r}\frac{\partial(rE_{zr}\phi)}{\partial r} + \frac{\partial(E_{zz}\phi)}{\partial z} + \sigma_t J_z = 0, \tag{3.8}$$

where

$$G = 1 + \frac{E_{rr} + E_{zz} - 1}{E_{rr}}. \tag{3.9}$$

The system of equations of the QD method is defined by the high-order equations (1.46) and (1.47) and the low-order equations (3.1), (3.7), and (3.8) with corresponding external boundary conditions [9, 50],

$$\boldsymbol{n} \cdot \boldsymbol{J}|_{r,z\in\partial D} = \left[C(\phi - \phi^{in}) + J^{in}\right]|_{r,z\in\partial D} \quad \text{for} \quad r \neq 0, \tag{3.10a}$$

$$\boldsymbol{n} \cdot \boldsymbol{J}|_{r,z\in\partial D} = 0 \quad \text{for} \quad r = 0, \tag{3.10b}$$

where

$$C = \frac{\int_{\boldsymbol{n}\cdot\boldsymbol{\Omega}>0} \boldsymbol{n}\cdot\boldsymbol{\Omega}\psi d\boldsymbol{\Omega}}{\int_{\boldsymbol{n}\cdot\boldsymbol{\Omega}>0} \psi d\boldsymbol{\Omega}}, \tag{3.11}$$

$$\phi^{in} = \int_{\boldsymbol{n}\cdot\boldsymbol{\Omega}<0} \psi d\boldsymbol{\Omega}, \tag{3.12}$$

$$J^{in} = \int_{\boldsymbol{n}\cdot\boldsymbol{\Omega}<0} \boldsymbol{n}\cdot\boldsymbol{\Omega}\psi d\boldsymbol{\Omega}. \tag{3.13}$$

Note the boundary condition at $r = 0$ is a symmetry condition in $r - z$. Another formulation for (3.10a) is presented in [57],

$$\boldsymbol{n} \cdot \boldsymbol{J}|_{r,z\in\partial D} = \left[B\phi + 2J^{in}\right]|_{r,z\in\partial D} \quad \text{for} \quad r \neq 0, \tag{3.14}$$

where

$$B = \frac{\int_{4\pi} |\boldsymbol{n}\cdot\boldsymbol{\Omega}|\psi d\boldsymbol{\Omega}}{\int_{4\pi} \psi d\boldsymbol{\Omega}}. \tag{3.15}$$

Both boundary condition formulations behave similarly for a wide range of problems, however, they do perform differently for certain specific cases.

The solution of a problem utilizing the QD method involves the solution of the coupled nonlinear system of equations defined by (1.46), (3.1), (3.7), and (3.8). Any solution method suitable for nonlinear equations may be used to solve the QD system of equations, however, for our work we use simple fixed point iteration [9]. Fixed point iteration solves the QD system of equations very rapidly due to the weak dependence of the Eddington factors on the angular flux solution. What this gives is an iterative framework where the transport equation (1.46) is solved to obtain a high-order transport solution which is used to compute the QD factors (3.5) and boundary factors (3.11)-(3.13) and or (3.15). These factors are then used as coefficients of the LOQD equations (3.1), (3.7) and (3.8). The LOQD equations are solved to get a new low-order solution, namely, the 0th and 1st angular moments of the transport solution ϕ and $\boldsymbol{J}$. The solution of the LOQD equations is then used to recompute the right hand side (RHS) of the high-order equation for the next iteration. See algorithm below.

Given: ϕ_o; $\phi = \phi_o$
while *Not Converged* **do**
  Solve Transport Eqn:
  $\boldsymbol{\Omega} \cdot \boldsymbol{\nabla}\psi + \sigma_t\psi = \frac{1}{4\pi}(\sigma_s\phi + q)$
  Generate factors:
  $\overline{\overline{E}} = \frac{\int_{4\pi} \boldsymbol{\Omega}\boldsymbol{\Omega}\psi d\boldsymbol{\Omega}}{\int_{4\pi} \psi d\boldsymbol{\Omega}}$,
  Generate B.C. factors: *Depends on B.C.formulation*
  Solve LOQD Eqns:
  $\boldsymbol{\nabla} \cdot \boldsymbol{J} + \sigma_a\phi = q$
  $\boldsymbol{\nabla} \cdot \left[\overline{\overline{E}}\phi\right] + \sigma_t\boldsymbol{J} = 0$
  Update RHS of transport eq. from QD solution
end

Fixed Point Iteration Scheme of the QD Method

In practice this algorithm is often rearranged placing the solution of the LOQD equations first and defining initial Eddington factors,

$$E_{rr} = E_{zz} = \frac{1}{3} \quad \text{and,} \quad E_{rz} = 0.$$

Doing this starts the solution procedure by solving the P_1 equations to get a good initial iterate.

3.3 Discretization of the LOQD Equations

3.3.1 Reformulation of 1st Moment Equation

A unique feature of the LOQD equations in $r-z$ geometry compared to Cartesian is the existence of the additional non-derivative term involving ϕ in the r component of the 1st moment equation, Eqn. (3.7), namely the term $\frac{G}{r}E_{rr}\phi$. This non-derivative term is similar to drift or convection terms in fluid flow equations. Just as in fluid flow equations this term can pose challenges for discretization especially from a monotonicity stand point. To simplify the derivation of a discretization for the LOQD equations, the r component of the 1st moment equation (3.7) is reformulated in order to eliminate this non-differential term [58–60, 60]. Using the integrating factor method commonly used to solve first order ordinary differential equations it can be combined into the r derivative. We note that in general G is a function of both r and z. A reduced form of Eqn. (3.7) is derived locally within each spatial cell of a given grid using a cell local integrating factor. Consider a spatial cell C_i, where i is the cell index. We define the cell local integrating factor as

$$H_i(r,z) = \exp\left(\int_{r_i^*}^{r} \frac{G(r',z)}{r'}dr'\right), \quad \text{for} \quad r, r_i^*, z \in C_i, \tag{3.16}$$

and multiply Eq. (3.7) by H_i to obtain a semi-continuous, reduced form of the equation [58–60, 60],

$$\frac{\partial(H_i E_{rr}\phi)}{\partial r} + H_i\frac{\partial(E_{zr}\phi)}{\partial z} + H_i\sigma_t J_r = 0. \tag{3.17}$$

It is possible to approximate the integral within the exponential of H_i. In cells that do not border the rotational axis, i.e. all points along all faces of a cell have $r > 0$, H_i is approximated as

$$\int_{r_i^*}^{r} \frac{G(r',z)}{r'}dr' \approx \bar{G}_i \int_{r_i^*}^{r} \frac{1}{r'}dr' = \bar{G}_i \ln\left(\frac{r}{r_i^*}\right), \tag{3.18}$$

where

$$\bar{G}_i = \frac{2\pi}{V_i}\int_{C_i} G(r,z) r dr dz, \tag{3.19}$$

and

$$V_i = 2\pi \int_{C_i} r dr dz. \tag{3.20}$$

Furthermore we approximate $\bar{G}_i$ in the cell C_i as

$$\bar{G}_i = 1 + \frac{\bar{E}_{rr,i} + \bar{E}_{zz,i} - 1}{\bar{E}_{rr,i}}, \tag{3.21}$$

where

$$\bar{E}_{\alpha\alpha,i} = \frac{2\pi}{V_i} \int_{C_i} E_{\alpha\alpha}(r,z) r dr dz. \tag{3.22}$$

$E_{\alpha\alpha,i}$ is obtained from the high-order transport solution. This leads to the approximation of the integrating factor as

$$H_i(r,z) \approx h_i(r) = \left(\frac{r}{r_i^*}\right)^{\bar{G}_i}, \quad \text{for} \quad r,z \in C_i. \tag{3.23}$$

For cells that do border the rotational axis, i.e. cells that have a side lying on $r = 0$, a different approximation of $G(r,z)$ is required. The cell local semi-continuous r component of the 1st moment equation that results from using the approximation defined by Eqn. (3.18) is

$$\frac{\partial(E_{rr}\phi)}{\partial r} + \frac{\partial(E_{zr}\phi)}{\partial z} + \frac{\bar{G}_i}{r} E_{rr}\phi + \sigma_t J_r = 0. \tag{3.24}$$

This equation has a singularity at $r = 0$ as in general $\bar{G}_i \neq 0$. In order to eliminate this singularity two conditions must be satisfied around $r = 0$. First, $G = 0$ at $r = 0$ must be reproduced in discrete form, and second, the rate at which $G \to 0$ must be properly approximated. Both conditions are required to properly resolve the integrating factor around $r = 0$. Note that the continuous r component of the 1st moment equation, Eqn. (3.7), has no singularity at $r = 0$. This is due to the fact that $G \to 0$ faster than r. An approximation that satisfies these conditions is to approximate G as

$$G(r,z) \approx \hat{G}(r) = r^P(g_0 + g_1 r) \quad \text{where} \quad P \geq 2, \tag{3.25}$$

giving

$$H_i(r,z) \approx h_i(r) = \exp\left(\int_{r_i^*}^{r} \frac{r'^P(g_0 + g_1 r')}{r'} dr'\right) =$$
$$\exp\left[-\left(g_0 \frac{r_i^{*P}}{P} + g_1 \frac{r_i^{*P+1}}{P+1}\right)\right] \exp\left(g_0 \frac{r^P}{P} + g_1 \frac{r^{P+1}}{P+1}\right), \quad \text{for} \quad r,z \in C_i. \tag{3.26}$$

g_0 and g_1 are fit coefficients that ensure Eqn. (3.25) reproduces the value of $G(r,z)$ at the cell centroid and the cell face farthest from the rotational axis, it's "right" face. $G=0$ at $r=0$ and the rate at which $G\to 0$ as $r\to 0$ is ensured by the factor r^P. $P=2$ was found to give satisfactory results.

The choice of approximation(s) for the integrating factor have an affect on the properties of the proposed discretization scheme. The variant defined by Eqns. (3.18)-(3.21) and Eqns. (3.25)-(3.26) is just one option. Other approximations of the integrating factor as well as averaging methods for the factor G were tried each yielding similar results for our problems of interest. It is important to note that varying the arbitrary reference point r_i^* has no effect on our chosen approximations, Eqns. (3.18)-(3.21) and Eqns. (3.25)-(3.26), as all terms associated with it cancel away.

Dividing Eqn. (3.17) by $H_i(r,z)$ and replacing it with an appropriate approximation gives the final semi-continuous set of LOQD equations in a spatial cell C_i

$$\frac{1}{r}\frac{\partial(rJ_r)}{\partial r}+\frac{\partial J_z}{\partial z}+\sigma_a\phi=q, \tag{3.27a}$$

$$\frac{1}{h_i}\frac{\partial(h_iE_{rr}\phi)}{\partial r}+\frac{\partial(E_{zr}\phi)}{\partial z}+\sigma_tJ_r=0, \tag{3.27b}$$

$$\frac{1}{r}\frac{\partial(rE_{zr}\phi)}{\partial r}+\frac{\partial(E_{zz}\phi)}{\partial z}+\sigma_tJ_z=0. \tag{3.27c}$$

It is this set of equations that is used going forward with the discretization.

For problems that are diffusion dominated, meaning that the angular flux is linear anisotropic, the LOQD equations reduce to the P_1 equations. Problems that exhibit these properties are said to be diffusive due to a lack of streaming or transport effects, i.e. modeling such systems with the diffusion equation is accurate. Problems where this situation occurs are characterized by high scattering ratios, optically thick domains, and a lack of large material property discontinuities. In problems such as this the Eddington factors become

$$E_{rr}=E_{zz}=\frac{1}{3}, \tag{3.28a}$$

$$E_{zr}=0. \tag{3.28b}$$

These values for the Eddington tensor cause the factor G to equal zero, note that this also causes $H(r,z)=h_i(r)=1$, giving the P_1 equations in $r-z$ geometry,

$$\frac{1}{r}\frac{\partial(rJ_r)}{\partial r} + \frac{\partial J_z}{\partial z} + \sigma_a\phi = q, \tag{3.29a}$$

$$\frac{1}{3}\frac{\partial\phi}{\partial r} + \sigma_t J_r = 0, \tag{3.29b}$$

$$\frac{1}{3}\frac{\partial\phi}{\partial z} + \sigma_t J_z = 0. \tag{3.29c}$$

The fact that the LOQD equation set reduces to the P_1 equations makes it necessary that any good discretization of the LOQD equations must also be a good discretization of the P_1 equations.

3.3.2 Discretization of The Semi-Continuous LOQD Equations

Cast in general form, the LOQD equations are

$$\boldsymbol{\nabla}\cdot\boldsymbol{J} + \sigma_a\phi = q \tag{3.30a}$$

and

$$\boldsymbol{\nabla}\cdot(\mathbb{E}\phi) + \sigma_t\boldsymbol{J} = 0, \tag{3.30b}$$

where $\mathbb{E}$ is the QD (Eddington) tensor. In $r-z$ geometry we have

$$\nabla_r = \frac{1}{r}\frac{\partial}{\partial r}, \quad \nabla_z = \frac{\partial}{\partial z}. \tag{3.31}$$

Equation (3.30b), the 1st moment equation in first-order form, shows that discretization of the LOQD equations must involve the definition of an approximation for tensor divergence. As mentioned earlier, the discretization that we developed for the LOQD equations in $r-z$ is based on a cell-centered finite volume scheme for the P_1 equations on arbitrary polyhedra in 3D and a scheme for the LOQD equations in 2D $x-y$ geometry [27, 28, 56].

We approximate the LOQD equations (3.27) locally in each cell, C_i, with the unknowns being:

1. the cell-average scalar flux $\phi_{i,c}$,
2. the face-average scalar fluxes $\phi_{i,f}$, and
3. the normal components of face-average currents $J_{i,f} = \boldsymbol{n}_{i,f}\cdot\boldsymbol{J}_{i,f}$, where $\boldsymbol{n}_{i,f} = (n^r_{i,f}, n^z_{i,f})$ is the outward normal of face f of cell i.

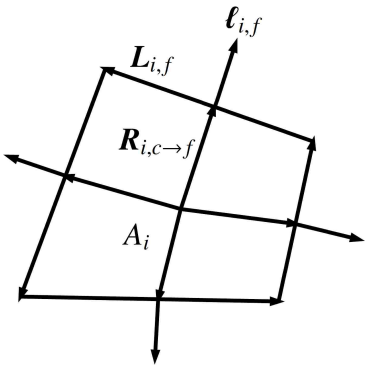

Figure 3.1: Definition of arbitrary cell

We follow a straight forward FV approach for the balance equation, Eqn. (3.27a), integrating it over the volume of a cell C_i to get

$$\sum_{f\in C_i} A_{i,f} J_{i,f} + \sigma_{a,i}\phi_{i,c} V_i = Q_i V_i, \tag{3.32}$$

where $A_{i,f}$ is the rotated facial area and V_i is the rotated cell volume. The cell average scalar flux unknown, $\phi_{i,c}$, is located at the volume centroid of cell C_i, $\boldsymbol{r}_{i,c}$,

$$\boldsymbol{r}_{i,c} = (r_{i,c}, z_{i,c}) = \left(\frac{2\pi}{V_i}\int_{C_i} r^2 dr dz, \frac{2\pi}{V_i}\int_{C_i} rz dr dz\right). \tag{3.33}$$

To begin the discretization of the 1st moment equations we first combine the r and z components and evaluate the resulting equation at $\boldsymbol{r}_{i,f}$,

$$n^r_{i,f}\left(\frac{1}{h_i}\frac{\partial(h_i E_{rr}\phi)}{\partial r} + \frac{\partial(E_{zr}\phi)}{\partial z}\right)\Bigg|_{\boldsymbol{r}_{i,f}} + n^z_{i,f}\left(\frac{1}{r}\frac{\partial(r E_{zr}\phi)}{\partial r} + \frac{\partial(E_{zz}\phi)}{\partial z}\right)\Bigg|_{\boldsymbol{r}_{i,f}} + \sigma_{t,i} J_{i,f} = 0, \tag{3.34}$$

where $\boldsymbol{r}_{i,f}$ corresponds to the point at the center of face f of cell C_i. To derive the discretization of the tensor divergence terms at cell faces in Eqn. (3.34) we apply the cell-face approximation of the gradient of the scalar flux used in the cell-centered P_1 equation discretization proposed in [56]. Note that this approach enabled the derivation of an accurate 2nd-order cell-local discretization of the LOQD equations in 2D Cartesian geometry on adaptive-like arbitrary quadrilateral meshes [27]. The approximation of the

gradient in $r-z$ geometry is given by [56]

$$\boldsymbol{\nabla}\phi_{i,f} = (\phi_{i,f} - \phi_{i,c})\boldsymbol{\xi}_{i,f} + \frac{1}{A_i}\sum_{f' \neq f} \phi_{i,f'}\boldsymbol{\eta}_{i,f',f}, \tag{3.35}$$

where

$$\boldsymbol{\xi}_{i,f} = \frac{\boldsymbol{\ell}_{i,f}}{\boldsymbol{R}_{i,c\to f} \cdot \boldsymbol{\ell}_{i,f}}, \tag{3.36}$$

$$\boldsymbol{\eta}_{i,f',f} = \boldsymbol{\ell}_{i,f'} - \frac{\boldsymbol{R}_{i,c\to f} \cdot \boldsymbol{\ell}_{i,f'}}{\boldsymbol{R}_{i,c\to f} \cdot \boldsymbol{\ell}_{i,f}}\boldsymbol{\ell}_{i,f}, \tag{3.37}$$

$$\boldsymbol{\ell}_{i,f} = \boldsymbol{n}_{i,f}||\boldsymbol{L}_{i,f}||, \tag{3.38}$$

$$A_i = \int_{C_i} drdz, \tag{3.39}$$

$$\boldsymbol{R}_{i,c\to f} = \boldsymbol{r}_{i,c} - \boldsymbol{r}_{i,f}. \tag{3.40}$$

As shown in Figure 3.1, $\boldsymbol{L}_{i,f}$ is the vector that goes between two adjacent corners of a cell. As already defined $\boldsymbol{r}_{i,f}$ and $\boldsymbol{r}_{i,c}$ are the coordinate vectors of the face center and cell centroid respectively. Notice that the approximation of the gradient outlined in [56], Eqn. (3.35), is constructed using a difference formula between the cell face and cell centroid and components of the cell average gradient. We note that this discretization uses area averaging for the cell average gradient

$$\langle \boldsymbol{\nabla}\phi \rangle_i = \frac{1}{A_i}\int_{C_i} \boldsymbol{\nabla}\phi drdz = \frac{1}{A_i}\sum_{f\in C_i} \phi_{i,f}\boldsymbol{\ell}_{i,f}. \tag{3.41}$$

This choice of averaging leads to a second-order approximation of the gradient in $r-z$ and preservation of spherical symmetry as found by our investigation of the discretization. Ref. [61] also points out that use of area averaging aids in the preservation of spherical symmetry. This form of the average gradient is uniform in γ, i.e. it applies throughout a cell's entire rotated volume in 3D.

We apply the discretization of the gradient on a cell face (3.35) to the derivatives in Eqn. (3.34) on a term by term basis as follows:

$$\left\{\frac{\partial g}{\partial r}\right\}_{i,f} = \boldsymbol{e}_r \cdot \{\boldsymbol{\nabla} g\}_{i,f}\,, \quad \text{and} \quad \left\{\frac{\partial g}{\partial z}\right\}_{i,f} = \boldsymbol{e}_z \cdot \{\boldsymbol{\nabla} g\}_{i,f}\,, \tag{3.42}$$

where g is any given scalar function, for example, $rE_{rz}\phi$, $E_{zz}\phi$, etc. As a result we obtain the approximation of the 1st moment equation at cell faces,

$$n^r_{i,f}\left[\frac{1}{h_{i,f}}\left(\Big(h_{i,f}E_{rr,i,f}\phi_{i,f}-h_{i,c}E_{rr,i,c}\phi_{i,c}\Big)\boldsymbol{\xi}_{i,f}\cdot\boldsymbol{e}_r+\frac{1}{A_i}\sum_{f'\neq f}r^{\bar{G}_i}_{i,f'}E_{rr,i,f'}\phi_{i,f'}\boldsymbol{\eta}_{i,f',f}\cdot\boldsymbol{e}_r\right)\right.$$
$$\left.+\Big(E_{rz,i,f}\phi_{i,f}-E_{rz,i,c}\phi_{i,c}\Big)\boldsymbol{\xi}_{i,f}\cdot\boldsymbol{e}_z+\frac{1}{A_i}\sum_{f'\neq f}E_{rz,i,f'}\phi_{i,f'}\boldsymbol{\eta}_{i,f',f}\cdot\boldsymbol{e}_z\right]$$
$$+\,n^z_{i,f}\left[\frac{1}{r_{i,f}}\left(\Big(r_{i,f}E_{rz,i,f}\phi_{i,f}-r_{i,c}E_{rz,i,c}\phi_{i,c}\Big)\boldsymbol{\xi}_{i,f}\cdot\boldsymbol{e}_r+\frac{1}{A_i}\sum_{f'\neq f}r_{i,f'}E_{rz,i,f'}\phi_{i,f'}\boldsymbol{\eta}_{i,f',f}\cdot\boldsymbol{e}_r\right)\right.$$
$$\left.+\Big(E_{zz,i,f}\phi_{i,f}-E_{zz,i,c}\phi_{i,c}\Big)\boldsymbol{\xi}_{i,f}\cdot\boldsymbol{e}_z+\frac{1}{A_i}\sum_{f'\neq f}E_{zz,i,f'}\phi_{i,f'}\boldsymbol{\eta}_{i,f',f}\cdot\boldsymbol{e}_z\right]$$
$$+\,\sigma_{t,i}\boldsymbol{n}_{i,f}\cdot\boldsymbol{J}_{i,f}=0 \quad (3.43)$$

The discrete version of the QD boundary conditions, Eqns. (3.10) and (3.14), become [50]

$$\boldsymbol{n}_{i,f}\cdot\boldsymbol{J}_{i,f}=\big[C_{i,f}(\phi_{i,f}-\phi^{in}_{i,f})+J^{in}_{i,f}\big] \quad \text{for} \quad r_{i,f}\neq 0, \tag{3.44a}$$

and

$$\boldsymbol{n}_{i,f}\cdot\boldsymbol{J}_{i,f}=0 \quad \text{for} \quad r_{i,j}=0, \tag{3.44b}$$

where, $C_{i,f}$, $\phi^{in}_{i,f}$ and, $J^{in}_{i,f}$ are the discrete approximations to their continuous counterparts on face f of cell i. For the alternative boundary condition formulation we get [57],

$$\boldsymbol{n}_{i,f}\cdot\boldsymbol{J}_{i,f}=\big[B_{i,f}\phi_{i,f}+2J^{in}_{i,f}\big] \quad \text{for} \quad r_{i,f}\neq 0. \tag{3.45}$$

where again, $B_{i,f}$ is the discrete approximation to its continuous self. Thus the complete set of discretized LOQD equations in $r-z$ geometry is defined by Eqns. (3.32), (3.43), and either (3.44) or (3.45).

The scheme as defined by Eqns. (3.32), (3.43), and (3.44) gives five equations per cell for interior cells, one balance equation per cell and one 1st moment equation per face. Boundary cells additionally have boundary conditions on external faces. The unknowns on internal faces are continuous and shared between adjoining cells. This allows for the formal definition of conditions on these shared unknowns on simple faces, faces where exactly two cells exist and there are no hanging nodes,

$$||\boldsymbol{L}_{i,f}||\phi_{i,f} = ||\boldsymbol{L}_{i',f'}||\phi_{i',f'} \rightarrow \phi_{i,f} = \phi_{i',f'}, \tag{3.46}$$

$$\boldsymbol{n}_{i,f} \cdot \boldsymbol{J}_{i,f} = -\boldsymbol{n}_{i',f'} \cdot \boldsymbol{J}_{i',f'}. \tag{3.47}$$

This gives nine unknowns associated with each cell, one cell average flux and a face average scalar flux and current for each face. The resulting set of equations, one balance, four 1st moment equations, and four cell boundary/interface conditions can be thought of as a fully cell local finite volume discretization. The matrix that results from this is sparse and non-symmetric. For a logically rectangular $N \times N$ square computational grid this scheme gives $9N^2$ unknowns and equations. The internal continuity conditions defined on faces can be used to eliminate what are essentially duplicate face unknowns, the face average fluxes and currents, reducing the number of unknowns/equations to $5N^2 + 4N$. Both of these systems of equations were investigated in $x - y$ geometry previously [62]. The remaining set of equations consists of a balance equation and a 1st moment equation on each face of a cell.

It was noticed in this work that the internal condition on the current, Eqn. (3.47), in conjunction with the two 1st moment equations defined on internal faces, one from each adjoining cell, makes it possible to eliminate the current defined on cell faces entirely. This leaves only scalar flux values as unknowns. Doing this gives a sparse non-symmetric, matrix with $3N^2 + 2N$ unknowns for an $N \times N$ logically rectangular square grid. It is this smaller set of equations that we use in this work. It is also possible to eliminate the cell average flux [56], however, we have chosen to carry it as a primary unknown. With the elimination of duplicate unknowns on faces as well as face average currents there are only a few logical choices for ordering the unknowns, at least for logically rectangular grids. Here we have chosen to order the unknowns as:

$$\boldsymbol{\phi} = \begin{bmatrix} \phi_c \\ \phi_{c,f=1} \\ \vdots \\ \phi_{c,f=4} \\ \phi_{c'} \\ \phi_{c',f=1} \\ \vdots \end{bmatrix} \tag{3.48}$$

Here the face unknowns are assigned on a "first come first serve" basis, i.e. cell one owns all of its face unknowns with adjacent cells not having ownership of those unknowns. Faces are indexed with counter clockwise wrapping starting from the bottom face.

3.3.3 Extension of LOQD Discretization To Adaptive-Like Grids

The discretization as described up to this point treats logically rectangular grids of arbitrary quadrilaterals. A grid being logically rectangular implies that all quadrilaterals have exactly four neighbors and or external boundaries, one neighbor or boundary across each face. Special treatment is needed in order to treat adaptive-like grids. Adaptive-like grids are characterized by the presence of hanging nodes, or cells having more than one neighbor across a single face. Many transport discretizations have the ability to treat such grids built into them, however, for our case with the LOQD equations we must put in extra effort to define how to treat these cases. To discretize the LOQD equations on such grids we apply two different approaches. The first technique is based on interface continuity conditions of face unknowns [27, 63] similar to what exists for simple interior faces, (3.46) and (3.47). The second method applies a pseudo-polygonal treatment which utilizes the generality of the cell-local discretization scheme for the LOQD equations and the original discretization of the P_1 equations [28, 56].

The first approach is one that has been used successfully before for both the P_1 and the LOQD equations in different geometry [27, 63]. This approach involves introducing interface continuity conditions for faces of a cell that have more than one neighbor across it. Strong continuity of the current and weak continuity of the scalar flux are enforced [27,63],

$$\boldsymbol{n}_{i,f} \cdot \boldsymbol{J}_{i,f} = -\boldsymbol{n}_{i',f'} \cdot \boldsymbol{J}_{i',f'}, \quad \text{for all } i', f' \text{ across face } i, f, \tag{3.49a}$$

$$l_{i,f}\phi_{i,f} = \sum_{i',f'} l_{i',f'}\phi_{i',f'}. \tag{3.49b}$$

Here i is the cell index, f is the index of a face, indexes with " $'$ " denote neighbor indexes, $l_{i,f} = ||\boldsymbol{L}_{i,f}||$ is the length of an individual face, and $\boldsymbol{n}_{i,f}$ is a face normal. Condition (3.49a) enforces particle balance by fixing the value of the current along the interface, and condition (3.49b) enforces continuity of the scalar flux along the face by ensuring the discrete integral of the flux on either side of the complex face is equal. These conditions have the possibly undesirable effect of smearing the solution at these interfaces. Smearing

occurs due to the fixing of the current along the entire interface and from the coarse cell only being directly associated with the average of the flux along the face. Additional unknowns are required to be kept at complex interfaces in this scheme, the coarse cell face unknowns. Figure 3.2a illustrates the interface conditions approach, Eqns. (3.49).

A way to avoid the approximation and additional unknowns introduced with interface conditions, Eqns. (3.49), on the grids we consider is to treat quadrilaterals with multiple neighbors across a face as a polygon with quadrilateral shape. This approach breaks up complex faces into several trivial faces with one neighbor across it. We call this method the pseudo-polygonal approach. Figure 3.2b illustrates the pseudo-polygonal treatment at interfaces. The discretization developed for the LOQD equations in [28] can be applied to arbitrary polyhedral meshes as it is based on a discretization originally designed for arbitrary polyhedra [56]. This allows for direct treatment of adaptive-like meshes by defining additional 1st moment equations for each subinterval on a face with multiple neighbors following the method proposed in [28]. This requires no additional unknowns on interfaces between coarse cells and fine cells and does not smear any grid functions. The advantage of having fewer unknowns at these interfaces between coarse and fine cells scales with the amount of adaptivity of the mesh. This also puts the LOQD discretization method one simple step away from treating arbitrary polygons.

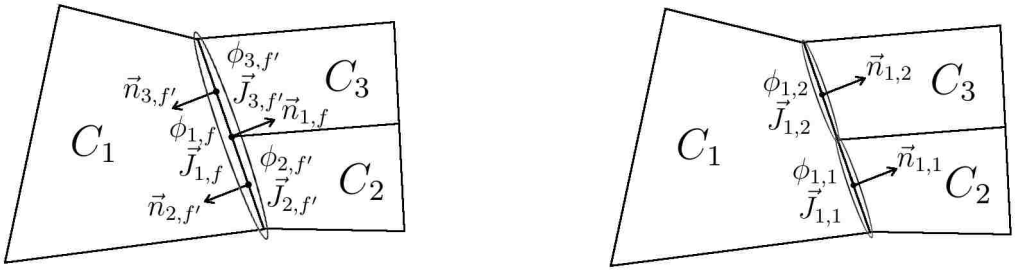

(a) Continuity Conditions (b) Pseudo-Polygonal

Figure 3.2: Adaptive-like Mesh Treatments

The pseudo-polygonal method uses the same set of equations as well as unknown ordering and cell unknown assignment as is used on logically rectangular grids. For the continuity condition approach the same is done for unknown cell assignment and unknown ordering with the only difference being the coarse cell at a complex cell interface

always owns its unknown coarse face flux. The continuity condition approach and pseudo-polygonal method have slightly different coefficient matrix structures due to the extra unknowns and the introduction of Eqns. (3.49) in the continuity condition approach. Note it is still possible to eliminate currents at complex boundaries in the continuity condition approach using the 1st moment equations from each fine face and the coarse face, and this is what we do in practice.

3.4 Transport Discretization Methods

As stated earlier, a major question that had to be answered as part of this research was what discretization method should be used for the transport equation. The short answer is anything since we are using the QD method and any reasonable transport discretization may be applied, however, the long answer is much more involved since it would entail finding what is better or best to use. With the large number of transport discretizations that exist in $r-z$ each with their own unique set of characteristics, determining what is the absolute best transport discretization to couple with the developed LOQD discretization is a daunting task at best. In reality there may not actually be a "best" pairing. Every transport discretization method has advantages and disadvantages; they each have their own features that can make them more or less attractive for use in the QD method and more or less attractive for a certain type of problem. There are a number of factors to take into account in this regard. In the simplest of terms, the better the solution of the high-order problem that is obtained the better the Eddington (QD) factors we will get and in general this will result in a higher quality solution to a problem using QD. The definition of higher quality in the sense of our work is higher accuracy in the obtained average flux throughout a given spatial domain as this translates into more accurate reaction rates, energy deposition, etc.. What complicates things is that a higher-order discretization method that yields higher accuracy angular fluxes may not actually render higher quality Eddington factors, as there is more at play than just discretization order.

The first desire we have of a transport discretization is that the spatial convergence order of the discretization should be equal to that of the discretization method used for the LOQD equations, 2nd order in our case. We emphasize that this is only desirable and not strictly necessary as the QD method can have completely independent discretizations for the high-order and low-order equations. This is desirable because the resulting QD solution

method will be capped at the convergence rate of the lower of the two discretization methods, e.g. if transport is 1st order and the LOQD discretization is 2nd order the resulting method will be 1st order. The same is true if reversed, i.e. if a very high spatial order transport method is used it will not boost the order of convergence of the resulting QD method beyond 2nd order. This would mean that the extra computational expense of a high convergence order transport scheme could be wasted. This is not to say that using a higher convergence order transport discretization would not boost overall accuracy, just the order of convergence. In fact, in the case of using a low convergence order transport discretization it is possible to boost its accuracy by coupling it with a higher convergence order LOQD discretization. This effect is demonstrated in our results. Combining a "cheap" lower convergence order transport discretization with a higher convergence order LOQD discretization is an interesting line of research [8, 27, 58–60, 62, 64].

Another desired quality of the transport discretization is positivity of the flux. As discussed in the introduction some transport methods, for instance diamond differencing and certain FEM discretizations, can result in negative angular fluxes due to the approximations made [20]. Positivity is required to ensure well behaved Eddington factors as they are the ratio of integrals of grid function as given by Eqn. (3.5),

$$E_{\alpha\beta} = \frac{\int_{4\pi} \Omega_\alpha \Omega_\beta \psi d\mathbf{\Omega}}{\int_{4\pi} \psi d\mathbf{\Omega}}, \quad \alpha, \beta = r, z.$$

In Eqn. (3.5) one can see that we have integrals of the angular flux in both the numerator and denominator. If the angular flux is allowed to be negative it becomes possible that integrals over the now alternating sign function can result in zeros, or close to it. If this happens in the denominator the Eddington factors will become unstable. Positivity is ensured for many methods such as characteristic methods and conservative finite volume methods, and for other methods negative flux fixups can nearly always be applied. It is important to note, however, that a generalized QD method that can handle negative solutions has been developed by D. Y. Anistratov [26].

In addition to positivity of the high-order solution it is desired that the high-order transport solution also be monotonic. It is common for high convergence order discretization schemes to result in nonmonotonicity of the discrete solution especially in highly heterogeneous regimes where the solution has steep gradients. Oscillations in the angular flux can translate into oscillations of the Eddington factors themselves. This oscillation of

Eddington factors poses a problem because of how they are used in the LOQD equations. Looking at just the z derivative in the z component of the 1st moment equation,

$$\frac{\partial(E_{zz}\phi)}{\partial z} = \frac{\partial(E_{zz})}{\partial z}\phi + \frac{\partial(\phi)}{\partial z}E_{zz}, \tag{3.50}$$

we see that oscillations will cause changes in sign of the term $\frac{\partial(E_{zz})}{\partial z}\phi$. This can translate into poor modeling of the gradient of the solution in the LOQD equations. Of course, we really discretize the left hand side of (3.50) not the right hand side, this helps with the approximation of this term. Transport discretization schemes that are inherently nonmonotonic may be monotonized by a nonlinear procedure. One monotonization procedure is by simply limiting values that result from high-order, beyond 2nd order, interpolations such that the transport scheme satisfies the maximum principle. Other monotonization procedures involve detecting when and where nonmonotonicity occurs and switching to an inherently monotonic scheme in those regions [65, 66].

There is of course the issue of whether or not the solution obtained by the transport discretization chosen satisfies the diffusion equation when a problem is diffusion dominated, i.e. does the method attain the asymptotic diffusion limit [36]. The QD method can attain the diffusion limit with a transport discretization that does not posses this property [60], thus in general this feature of transport methods is not a concern when used with QD. However, it may be possible that a transport discretization attaining the diffusion limit by itself could be beneficial for the quality of Eddington factors by some means. This is difficult to prove due to the fact that nearly any two transport discretizations that differ with regard to attaining the diffusion limit usually also differ in other ways such as accuracy, oscillations, negativity, etc..

The angular resolution afforded by a transport discretization must also be taken into account. This is not in reference to the resolution of the quadrature set used, as S_n methods often have flexibility in this regard. We are instead referring here to how the transport discretization treats the angular redistribution term seen in (1.46). Many discretizations use a weighted difference for this term, while others, such as characteristic methods, treat it explicitly with particle/characteristic tracking in 3D. There are also simpler treatments such as upwinding in angle. Recall that simpler treatments of this can result in poor solutions in the vicinity of $r = 0$, the so called "flux dip" problem. This problem will result in poor quality Eddington factors near $r = 0$.

In this work two different transport discretizations were used to formulate QD methods to solve problems in $r-z$ on our grids of interest and for testing purposes. The transport discretizations chosen have significantly different properties and can give an idea of how the resulting QD method behaves with a wide range of high-order transport discretizations.

3.4.1 Vertex Based MOSC

The first transport discretization considered is a vertex based method of short characteristics (VBMOSC) which is an $r-z$ analog of more common $x-y$ discretizations [30,67,68]. This method, as with all characteristic methods transforms the transport equation into equations along characteristics. This is done by starting from the nonconservative form of the transport equation in $r-z$,

$$\Omega_r \frac{\partial \psi}{\partial r} + \Omega_z \frac{\partial \psi}{\partial z} + \frac{\Omega_\gamma}{r} \frac{\partial \psi}{\partial \gamma} + \sigma_t \psi = \frac{1}{4\pi}(\sigma_s \phi + q), \tag{3.51}$$

and performing a change of variables from the coordinate system spatial variables to the characteristic length traveled by particles,

$$\psi(r,z) \rightarrow \psi(s). \tag{3.52}$$

Doing this transforms the streaming operator from its original 3D form to a derivative in just the characteristic length:

$$\Omega_r \frac{\partial \psi}{\partial r} + \Omega_z \frac{\partial \psi}{\partial z} + \frac{\Omega_\gamma}{r} \frac{\partial \psi}{\partial \gamma} = \frac{d\psi}{ds}. \tag{3.53}$$

Thus the transport equation becomes a first order ordinary differential equation in only one variable,

$$\frac{d\psi}{ds} + \sigma_t \psi = Q, \tag{3.54}$$

where,

$$Q = \frac{1}{4\pi}(\sigma_s \phi + q). \tag{3.55}$$

The spatially discretized equation for the angular flux following the VBMOSC scheme is derived by analytically solving Eqn. (3.54) on a characteristic through a computational mesh cell:

$$\psi^* = \psi_o e^{-\sigma_{t_i}\Delta s} + \frac{Q_i}{\sigma_{t_i}}\left(1 - e^{-\sigma_{t_i}\Delta s}\right). \tag{3.56}$$

For this vertex based method ψ^* is the angular flux unknown at a vertex, ψ_o is the back traced angular flux incoming on a face, σ_{t_i} is the total cross section in the ith cell, Q_i is the source in the ith cell, and Δs is the track length of the characteristic through the cell. Eqn. (3.56) looks simple, however, in truth it hides much underlying complexity of the method.

Though the discretized transport equation in the VBMOSC scheme might be 1D the transport problem is still fundamentally 3D in $r-z$ geometry. The consequence of this is that in $r-z$ the characteristic tracks reside in three space as each cell is actually a 3D toroidal quadrilateral in r, z and the azimuthal dimension, γ. Figure 3.3 illustrates the

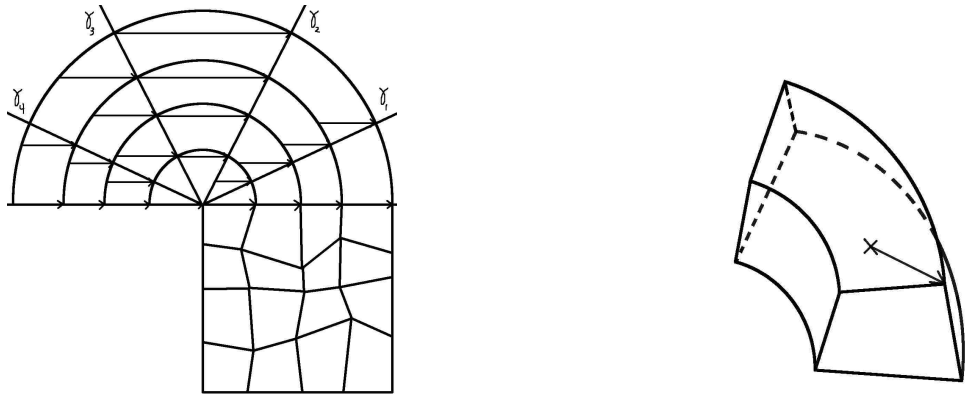

(a) MOSC grid and sweep pattern (b) Cell in transport mesh

Figure 3.3: Grid and 3D Cells of VBMOSC Method

3D cells of the VBMOSC method with a characteristic drawn through the cell as well as the sweep of characteristics done.

As a result of tracking characteristics in 3D within these arbitrary quadrilateral toroids, intersections with curved surfaces must be found. This requires solving a nonlinear set of equations for the intersection points of each characteristic associated with a cell with each face of that cell. This system of equations is derived by taking into account that

$$\frac{d\psi}{ds} = \Omega_r\frac{\partial\psi}{\partial r} + \Omega_z\frac{\partial\psi}{\partial z} + \frac{\Omega_\gamma}{r}\frac{\partial\psi}{\partial\gamma} = \frac{dr}{ds}\frac{\partial\psi}{\partial r} + \frac{dz}{ds}\frac{\partial\psi}{\partial z} + \frac{d\gamma}{ds}\frac{\partial\psi}{\partial\gamma}, \tag{3.57}$$

i.e.

$$\frac{dr}{ds} = \sin\theta\cos\gamma, \tag{3.58}$$

$$\frac{dz}{ds} = \cos\theta, \tag{3.59}$$

and

$$\frac{d\gamma}{ds} = -\frac{\sin\theta\sin\gamma}{r}. \tag{3.60}$$

From these definitions of the derivatives of the spatial variables with respect to the characteristic length one can obtain

$$r\,sin(\gamma) = r_v\,sin(\gamma_m), \tag{3.61}$$

and

$$(z - z_v)tan(\theta_m) = r\,cos(\gamma) - r_v\,cos(\gamma_m), \tag{3.62}$$

where r_v and z_v are the r and z coordinates of a given vertex, θ_m is the polar angle of the characteristic, and γ_m is the azimuthal angle of the characteristic at the vertex. Note that as a particle moves along a characteristic the azimuthal angle changes unless $\gamma_m = 0, \pi$. To complete the set of equations we need an equation that describes the intersected cell face. This can be obtained by taking the dot product of the face vector with the face normal which must equal zero, refer to Figure 3.1,

$$\boldsymbol{n}_{i,f} \cdot \boldsymbol{L}_{i,f} = 0 \tag{3.63}$$

for a given cell face with index i,f. Eqns. (3.61) - (3.63) form a nonlinear system of equations in the three unknown independent spatial variables that define the location of the incoming angular flux on a face, ψ_o. This set of equations can be solved with Newton's method, however, that isn't where the story ends.

Due to the arbitrary shape of cells in our meshes of interest and the curvature of cells in $r - z$ this system of equations can be very stiff (poorly conditioned) and therefore difficult to solve. In order to not introduce undue error due to poor geometry resolution we solve the nonlinear set of equations with the Newton-Armijo method implemented in double precision and use its solution for intersection points as an initial guess to a Newton-Armijo solver implemented in quadruple precision to further refine calculations. It was found that this is necessary in order to determine some intersection points with accuracy near or beyond our desired convergence criteria for solution of the transport

equation. The arbitrary shape and curvature of cells also results in multiple possible face intersection points for a given characteristic. The true intersection point is invariably associated with the shortest track found. Obviously, solving this set of nonlinear equations for every vertex and for every direction in order to resolve the geometry/characteristics is computationally intensive. In contrast, the actual solution procedure of VBMOSC, a sweep evaluating Eqn. (3.56), is fairly straight forward and cheap.

With characteristic-face intersections known, we use bilinear interpolation on faces between vertexes to get incoming angular flux value. The bilinear interpolation must be done on arbitrary quadrilaterals which also adds another layer of complexity. These procedures combined with using flat sources within cells leads to a first order, non-conservative transport discretization method that does not attain the diffusion limit. This discretization in $r-z$ also exhibits the nonphysical dip in the scalar flux near $r=0$ for some problems as described in an earlier section of this work [39]. Obviously this VBMOSC is not what most would consider an ideal transport discretization. However, studying this method, especially for use with QD, has much merit. Characteristic methods are a powerful family of techniques for discretizing and solving hyperbolic problems including the transport equation. MOSC in general is a popular solution technique that has features other discretization methods, such as FD, FV, and FEM, do not possess. It is important to point out that in the QD method the system of equations is defined by the high-order transport equation and the LOQD equations, where the high-order solution is used only to generate factors for the low-order equations. This being the sole purpose of the high-order solution relaxes the requirements on the high-order scheme. For example, as was already pointed out, a non-conservative transport discretization scheme can be used within the QD method and conservation of particles will still be ensured. The requirement on the high-order scheme is to be able to produce a good shape function for averaging the direction cosines, Ω_α and Ω_β. This VBMOSC and indeed MOSC schemes in general are capable of achieving this.

3.4.2 Simple Corner Balance in $r-z$

The second transport discretization considered is the Simple Corner Balance (SCB) scheme [14, 34]. In the SCB scheme a subgrid of corner cells is defined within each cell of the main computational grid with a corner cell placed on each vertex of a cell. Figure 3.4 shows a cell and corresponding corner cell subgrid for a logically rectangular mesh,

where cr is the index of a corner cell, crf is the index of a corner cell face, $\sigma_{x_{cr}}$ are cross sections of the corner cell, Q_{cr} is the source associated with the corner cell, V_{cr} and A_{cr} are the volume and area of the corner cell respectively, $A_{cr,crf}$ is the rotated area of a corner cell face, $\psi_{n,m,cr}$ is the average angular flux in the corner cell in direction $\mathbf{\Omega}_{n,m}$, and $\psi_{n,m,cr,crf}$ is the average angular flux on face crf of the corner cell in direction $\mathbf{\Omega}_{n,m}$. Here n is the index of the polar angle and m is the index of the azimuthal angle. Note

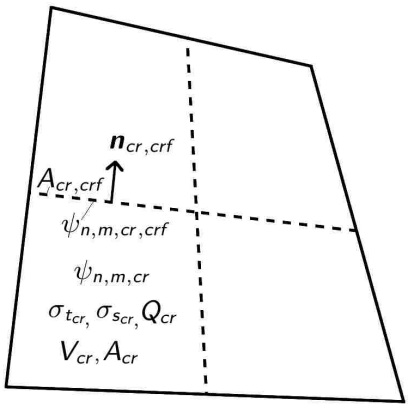

Figure 3.4: SCB Method Cell,

that for the case of hanging nodes, each additional neighbor across a face of a cell will introduce an additional vertex on that face. The SCB scheme handles such meshes by simply defining an additional corner for each additional vertex. The system of equations for the SCB method is defined by detailed balance equations derived for the corner cells of a cell subgrid closed with certain auxiliary conditions.

The discretized detailed balance equations over corner cells in the SCB method are derived by first discretizing the angular redistribution term of Eqn. (1.46) after some slight algebraic manipulation:

$$\frac{\Omega_r}{r}\frac{\partial}{\partial r}\Big(r\psi\Big) + \Omega_z\frac{\partial}{\partial z}\Big(\psi\Big) + \frac{1}{r}\frac{\partial}{\partial \gamma}\Big(\Omega_\gamma\psi\Big) + \sigma_t\psi = \frac{1}{4\pi}(\sigma_s\phi + Q). \tag{3.64}$$

The discretization of the angular redistribution term is done using a weighted central difference about $\mathbf{\Omega}_{n,m}$ over the azimuthal interval w_m of polar angle "level" n,

$$\frac{1}{r}\frac{\partial}{\partial\gamma}\Big(\Omega_\gamma\psi\Big)\Big|_{\theta=\theta_n,\gamma=\gamma_m} \approx \frac{1}{r}\frac{\alpha_{n,m+1/2}\psi_{n,m+1/2,cr}-\alpha_{n,m-1/2}\psi_{n,m-1/2,cr}}{w_m}. \tag{3.65}$$

Substituting this result into the discrete ordinates transport equation gives

$$\frac{\Omega_{r_{n,m}}}{r}\frac{\partial}{\partial r}\Big(r\psi_{n,m}\Big)+\Omega_{z_{n,m}}\frac{\partial}{\partial z}\Big(\psi_{n,m}\Big)+\frac{1}{r}\frac{\alpha_{n,m+1/2}\psi_{n,m+1/2,cr}-\alpha_{n,m-1/2}\psi_{n,m-1/2,cr}}{w_m}+$$
$$\sigma_t\psi_{n,m}=\frac{1}{4\pi}(\sigma_s\phi+Q). \tag{3.66}$$

The weights, $\alpha_{n,m+1/2}$ and $\alpha_{n,m-1/2}$, are derived to yield the correct solution for the case of an infinite homogeneous medium, which results in a uniform isotropic angular flux [6]. Using the more obvious choice of having $\Omega_{\gamma_{n,m+1/2}}$ and $\Omega_{\gamma_{n,m-1/2}}$ instead of the weights in Eqn. (3.65)/(3.66) puts requirements on the quadrature set used that are incompatible with most popular quadrature rules, e.g. Gauss-Legendre [6]. To derive the weights in Eqn. (3.65)/(3.66) one performs the substitution

$$\psi_{n,m}=\frac{\phi}{4\pi} \tag{3.67}$$

in Eqn. (3.66),

$$\frac{\Omega_{r_{n,m}}}{r}\frac{\partial}{\partial r}\Big(r\frac{\phi}{4\pi}\Big)+\Omega_{z_{n,m}}\frac{\partial}{\partial z}\Big(\frac{\phi}{4\pi}\Big)+\frac{1}{r}\frac{\alpha_{n,m+1/2}\frac{\phi}{4\pi}-\alpha_{n,m-1/2}\frac{\phi}{4\pi}}{w_m}+$$
$$\sigma_t\frac{\phi}{4\pi}=\frac{1}{4\pi}(\sigma_s\phi+Q). \tag{3.68}$$

Since ϕ for the case of an infinite homogeneous medium is uniform (constant) the z derivative evaluates to zero, $\frac{\phi}{4\pi}$ can be pulled out of the r derivative which evaluates to 1, and due to the isotropy we can subtract the scattering source from both sides. Simplifying the result gives

$$\left(\frac{\Omega_{r_{n,m}}}{r}+\frac{1}{r}\frac{\alpha_{n,m+1/2}-\alpha_{n,m-1/2}}{w_m}\right)\phi+\sigma_a\phi=Q. \tag{3.69}$$

Note that in an infinite homogeneous problem the scalar flux $\phi=\frac{Q}{\sigma_a}$ thus we get

$$\left(\frac{\Omega_{r_{n,m}}}{r}+\frac{1}{r}\frac{\alpha_{n,m+1/2}-\alpha_{n,m-1/2}}{w_m}\right)\phi=0. \tag{3.70}$$

This result makes sense because we would expect the streaming term for such problems to go to zero, this is simply a statement of that. Eqn. (3.70) can be rearranged into a recursion relation for the weights on a given polar angle "level",

$$\alpha_{n,m+1/2} = \alpha_{n,m-1/2} - \Omega_{r_{n,m}} w_m. \tag{3.71}$$

It can be easily shown that a good choice of starting weight is

$$\alpha_{n,1/2} = 0. \tag{3.72}$$

The rest of the derivation of the discretized detailed balance equation over a corner follows a finite volume approach. Integrating Eqn. (3.66) over the volume of a corner cell,

$$V_{cr} = 2\pi \int\int_{A_{cr}} r dr dz, \tag{3.73}$$

yields

$$\sum_{crf=1}^{4} (\boldsymbol{n}_{cr,crf} \cdot \boldsymbol{\Omega}_{r,z_{n,m}} A_{cr,crf} \psi_{n,m,cr,crf}) + 2\pi A_{cr} \frac{\alpha_{n,m+1/2}\psi_{n,m+1/2,cr} - \alpha_{n,m-1/2}\psi_{n,m-1/2,cr}}{w_m} + \sigma_{t_{cr}} V_{cr} \psi_{n,m,cr} = \frac{V_{cr}}{4\pi}(\sigma_{s_{cr}}\phi_{cr} + Q_{cr}). \tag{3.74}$$

For a given direction this gives a set of four equations per cell, one per corner, on a logically rectangular mesh. However, there are significantly more than four unknowns in a cell as can be seen in Eqn. (3.74). Thus auxiliary relationships are needed to relate unknowns.

Many possible choices can be made regarding auxiliary relationships for the unknowns of Eqn. (3.74), and indeed there are several different schemes that each have unique sets of auxiliary relations for it. The SCB scheme uses pure upwinding at cell boundaries [14, 34],

$$\psi_{n,m,cr,crf} = \begin{cases} \psi_{n,m,cr,crf} & \boldsymbol{n}_{cr,crf} \cdot \boldsymbol{\Omega}_{r,z_{n,m}} > 0 \\ \psi_{n,m,cr',crf'} & \boldsymbol{n}_{cr,crf} \cdot \boldsymbol{\Omega}_{r,z_{n,m}} < 0 \end{cases}, \tag{3.75}$$

the average angular flux between two adjacent corner cells for internal corner cell face unknowns,

$$\psi_{n,m,cr,crf} = \frac{1}{2}(\psi_{n,m,cr} + \psi_{n,m,cr'}), \tag{3.76}$$

and a weighted diamond differencing relationship for the half angle angular fluxes

$$\psi_{n,m,cr} = \tau_{n,m}\psi_{n,m+1/2,cr} + (1-\tau_{n,m})\psi_{n,m-1/2,cr}, \tag{3.77}$$

where

$$\tau_{n,m} = \frac{\Omega_{r_{n,m}} - \Omega_{r_{n,m-1/2}}}{\Omega_{r_{n,m+1/2}} - \Omega_{r_{n,m+1/2}}}. \tag{3.78}$$

The auxiliary relationship for internal corner cell face unknowns, Eqn. (3.76), gives the angular flux a linear distribution within a cell by interpolating between corners for these internal faces. That coupled with the upwinding relation on cell boundaries causes the angular flux unknowns associated with the corner cells, $\psi_{n,m,cr}$, to act very much like unknowns centered right at the corners of a cell, i.e. on the vertexes. The use of the weighted Diamond difference formula to relate the half angle angular fluxes to the integer angle angular fluxes allows SCB to properly reproduce the diffusion solution near $r = 0$ in the diffusion limit and thereby eliminates the so called flux dip problem [39]. Simpler relationships such as step or unweighted Diamond differencing can be used, however, they are susceptible to the flux dip problem near $r = 0$ As was said in the introduction, SCB, with its set of auxiliary conditions, behaves similarly to linear DFEM discretizations with the two being equivalent in 1D slab geometry [34]. After application of the auxiliary conditions in the SCB scheme one gets a set of four coupled linear equations in four unknowns for any given cell and direction. This system of equations, giving such a small coefficient matrix per cell, is easily solved with direct methods such as Gaussian Elimination. In our implementation we use Gaussian Elimination with Complete Pivoting and solve for the angular flux in parallel, parallelized over the polar angle. Parallelization over the azimuthal angle in $r-z$ geometry is nontrivial as the angles are coupled, see Eqn. (3.77).

The SCB scheme is a 2nd order accurate, conservative transport discretization that attains the diffusion limit and does not exhibit the so called flux dip problem near $r = 0$. These properties make SCB an attractive option for use with our new discretization of the LOQD equations in the QD method. One downside to note is that SCB can give nonmonotonic angular flux solutions for certain problems and grids.

Chapter 4

Analysis of Discretization Scheme And Resulting QD Method

4.1 Analysis Methodology

Analysis of any numerical method is of the utmost importance as without it there would be little to no basis for using or applying it to any problem. The method we have developed is no different, and thus we conducted a rigorous analysis of it to determine its behavior when applied to problems of interest. The main point of interest in our study of the proposed method is whether it converges on the type of grids we consider as this represents a major scientific contribution of this work. The second item that is focused on is convergence rate. 2nd order convergence behavior in space is expected due to the choices made in the derivation of the LOQD discretization and confirmation of that rate is needed. We do this analysis using a number of techniques on a number of problems. It is also important to validate the proposed method in transport effect heavy problems as well as diffusion dominated problems where the LOQD equations limit to the P_1 equations. To determine whether or not the method converges upon refinement and to measure what rate it converges with we use classic convergence studies comparing the differences between successive solutions, convergence studies using the Method of Manufactured Solutions (MMS), and comparison between discrete solutions to problems with known analytic solutions.

MMS is a procedure where an exact solution to a problem is chosen and a right hand side or source is defined such that the exact solution of the continuous form of the

equations in question will yield the chosen solution with the defined right hand side. A discrete system of equations derived to approximate the continuous equations may then be analyzed by supplying the manufactured source as the right hand side of the discrete problem. As the grid that the discrete equations are solved on is refined it is desired that the numerical solution will converge to the specified exact solution. This procedure allows for the comparison of the discrete solution to a chosen analytic solution providing a rigorous study of the behavior of a method. Comparing directly to an analytic solution facilitates the study of convergence behavior in several norms. For our purposes, MMS problems are formulated by substituting the chosen analytic solutions and factors into Eqns. (3.1) and (3.27b) to define MMS sources,

$$Q^* = \frac{1}{r}\frac{\partial(rJ_r^*)}{\partial r} + \frac{\partial(J_z^*)}{\partial z} + \sigma_a\phi^* - q \tag{4.1}$$

and

$$Q_{r_i}^* = \frac{1}{r^{\hat{G}_i}}\frac{\partial(r^{\hat{G}_i}E_{rr}^*\phi^*)}{\partial r} + \frac{\partial(E_{rz}^*\phi^*)}{\partial z} + \sigma_t J_r^* \tag{4.2}$$

where

$$J_r^* = \frac{1}{\sigma_t}\frac{\partial(E_{rr}^*\phi^*)}{\partial r} + \frac{\partial(E_{zr}^*\phi^*)}{\partial z} + \frac{G^*}{r}E_{rr}^*(r,z)\phi^*, \tag{4.3}$$

$$J_z^* = \frac{1}{\sigma_t}\frac{1}{r}\frac{\partial(rE_{zr}^*\phi^*)}{\partial r} + \frac{\partial(E_{zz}^*\phi^*)}{\partial z}, \tag{4.4}$$

$$\hat{G}_i = \frac{2\pi}{V_i}\int_{A_i} rG^* dr dz, \quad G^* = 1 + \frac{E_{rr}^* + E_{zz}^* - 1}{E_{rr}^*} \tag{4.5}$$

Q^* and $Q_{r_i}^*$ replace the right hand side of eqns. (3.27) and (3.27b) respectively. These new right hand sides are averaged exactly upon discretization. Vacuum boundary conditions for MMS problems are given by the following equations also averaged exactly when discretized:

$$\boldsymbol{n}_{i,f}\cdot\boldsymbol{J} = \frac{1}{2}\phi + Q_{b_{i,f}}^*, \tag{4.6}$$

and

$$Q_{b_{i,f}}^* = \boldsymbol{n}_{i,f}\cdot\boldsymbol{J}^* - \frac{1}{2}\phi^*. \tag{4.7}$$

Throughout the tests presented in this work we use a randomization algorithm in the construction of spatial grids in order to create grids of arbitrary quadrilaterals. The procedure is applied to interior grid points, non-boundary points, before any adaptive-like

refinement is done. The randomization is done by choosing two uniformly distributed random numbers, $\xi \in [0, 2\pi]$ used to determine the direction a grid point will be moved and $\rho \in [0, \rho_{max}]$ used to determine how far to move that point. The grid point is then moved by

$$\tilde{r} = r + \rho\ cos(\xi), \quad \tilde{z} = z + \rho\ sin(\xi). \tag{4.8}$$

The maximum ρ, ρ_{max}, that we allow for is 0.35 due to concave cells becoming possible at $\rho > \frac{1}{2\sqrt{2}} \approx 0.353553$ [64]. Concave cells are undesirable for a number of reasons, and can always be eliminated by re-meshing, especially when adaptive refinement can be used. Unless otherwise specified all grids considered were generated using $\rho_{max} = 0.35$.

In the tests presented here we use two distinct methods of grid refinement. We have what one might call a "worst case scenario" grid refinement method where a sequence of refined grids is actually a set of randomly generated grids that each have a finer average cell spacing than the last. Each grid in such a sequence is generated completely independently from any other grid. Figure 4.1 gives an example of this type of grid refinement. The other grid refinement method used is more along the lines of the classic mode of operation for grid refinement where a sequence of refined grids are true refinements of previous grids. In this method we often start with a randomized grid of some structure and proceed to cut each cell in half along their mid line for each refinement. Figure 4.2 depicts this type of refinement. For all convergence studies done each successive grid refinement is by a factor of 2 regardless of refinement method.

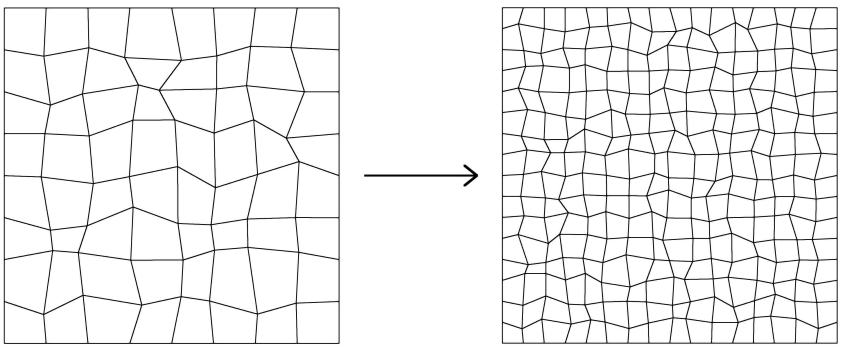

Figure 4.1: "Worst case scenario" grid refinement.

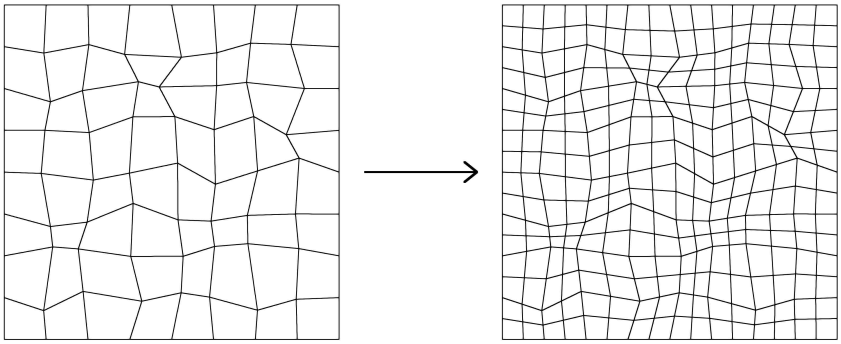

Figure 4.2: Classic grid refinement.

Preconditioned BiCGSTAB is used to invert the LOQD matrix equations. BiCGSTAB is a reasonable choice for solution of the LOQD equations in $r-z$ as it was shown to outperform GMRES and perform similarly to TFQMR for the LOQD equations in $x-y$ using an ILUD preconditioner [62]. The preconditioner used in this work is Red-Black SOR where the cell balance equations are red and the cell face equations, the 1st moment equations, are black. Looking at the equations themselves, the balance equation is diagonally dominant while the face equations are not. This lead us to choose SOR extrapolation parameters such that over-relaxation of the red cell average equations and under-relaxation of the black face equations is performed, which gives fast convergence of the BiCGSTAB algorithm. 3-5 Red-Black SOR iterations were found to give fast convergence on a wide range of problems. The stopping criteria for the BiCGSTAB algorithm is taken to be $\varepsilon_{LO} = 10^{-14}$.

A true convergence criteria in the ∞ norm was used for the iterative solution of the transport equation for both the QD method and source iteration method [9],

$$||\boldsymbol{\phi}^s - \boldsymbol{\phi}^{s-1}||_\infty < \left(\frac{1}{\rho_\infty^s} - 1\right)\varepsilon, \tag{4.9}$$

where s is the iteration index, $\boldsymbol{\phi}^s$ is the vector of flux values on iteration s, ε is a small parameter taken to be $\varepsilon = 10^{-10}$, and the rate of convergence, ρ_∞^s, is estimated on each iteration by

$$\rho_\infty^s \approx \frac{||\boldsymbol{\phi}^s - \boldsymbol{\phi}^{s-1}||_\infty}{||\boldsymbol{\phi}^{s-1} - \boldsymbol{\phi}^{s-2}||_\infty}. \tag{4.10}$$

We acknowledge that $\varepsilon = 10^{-10}$ is a very tight convergence criterion. This was used to ensure that any iterative errors would be reduced to well below what would affect the convergence study results.

4.2 Results and Analysis for The LOQD Discretization

The discretization method developed for the LOQD equations in $r-z$ is completely new and thus requires thorough analysis of its properties. It is important to study the discretization by itself independent of the effects of being coupled with the high-order transport equation in the QD method. Also important is the analysis of the discretization in the case of diffusion dominated regimes which causes the LOQD equations to limit to the P_1 equations. The tests we present in this section were formulated to evaluate the performance of the developed scheme when applied to the LOQD as well as P_1 equations with prescribed analytic factors. The use of prescribed analytic factors allows for the analysis of the low-order discretization without the use of a high-order solution. The tests were selected to analyze the convergence of the method on logically rectangular orthogonal, randomized, and arbitrary adaptive-like grids. The MMS studies using prescribed factors can also be thought of as an analysis of the discretization applied to a more general class of elliptic problems that are not defined by a particle transport problem.

All grid refinement studies in this section were done with the "worst case scenario" type grid refinement. This is done for two reasons. The first is that that this type of refinement showcases the newly developed LOQD discretization's ability to handle highly arbitrary grids and converge regardless of grid sequence. The second reason is that for the analysis of the low-order equations we either have trivial Eddington factors, as is the case with diffusion, or analytically specified factors such as in MMS tests. This translates into much less chaotic convergence rates as the Eddington factors are exact and are not dependent on a transport equation discretization's convergence properties.

4.2.1 Test 1: Diffusion With Linear Solution In z

The first test we present is for the discretization applied to the P_1 diffusion equations on a single level grid (no adaptive refinement). The proposed method is of second order, and as a result we expect exact treatment of problems with linear solutions. This test is meant to show that the method reproduces linear solutions on randomized grids. The domain of this test is $r \in [0,1]$, $z \in [0,1]$. For this problem there is no distributed source, and the cross sections are taken to be $\sigma_t = \sigma_s = 1$ [69]. The left boundary is on the rotational axis and hence

$$\boldsymbol{n} \cdot \boldsymbol{J}|_{r=0} = 0, \quad \text{for} \quad z \in [0,1]. \tag{4.11a}$$

The right boundary is taken to be reflective,

$$\boldsymbol{n} \cdot \boldsymbol{J}|_{r=1} = 0, \quad \text{for} \quad z \in [0,1]. \tag{4.11b}$$

The condition at the top is defined to be a Marshak vacuum boundary,

$$\boldsymbol{n} \cdot \boldsymbol{J}|_{z=1} = \frac{1}{2}\phi, \quad \text{for} \quad r \in [0,1]. \tag{4.11c}$$

The bottom boundary with incoming radiation is given by

$$\boldsymbol{n} \cdot \boldsymbol{J}|_{z=0} = \frac{1}{2}\phi + 1, \quad \text{for} \quad r \in [0,1]. \tag{4.11d}$$

The solution of this diffusion problem is linear in z.

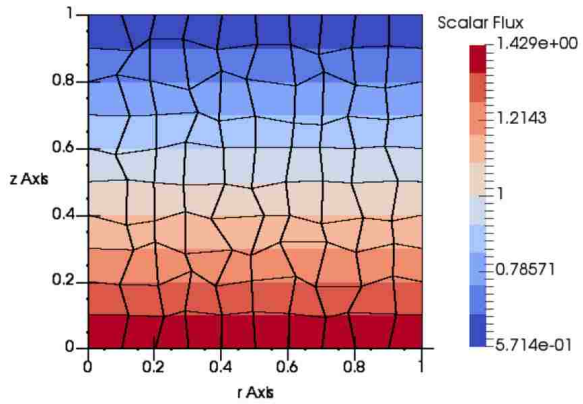

Figure 4.3: Isoline graph with computational mesh.

Figure 4.3 shows the result as well as the computational grid used for the problem. We chose to use a coarse color map for the solution to act as an isoline plot to highlight the linear solution the proposed scheme obtains throughout the domain. The magnitude as well as the slope matches the analytic solution with high accuracy even for this coarse mesh. The norm of the difference between the numerical solution and analytic solution is

on the order of the convergence criterion used for solving the equations:

$$||\phi - \phi^*||_2 = 2.7219 \times 10^{-14}. \tag{4.12}$$

This confirms that the method exactly reproduces linear solutions on randomized grids in $r - z$.

4.2.2 Test 2: Convergence Study for Proposed Scheme Applied to The P_1 Equations On Single Level Meshes

The second set of results is a grid refinement convergence study of the method when applied to the P_1 equations on single level grids. For this test case we ran a problem with a series of grids each refined by a factor of two. We use Aitken extrapolation to generate a reference based on the solutions computed specifically on the sequence of orthogonal grids. This reference was then used to determine the convergence order of the scheme on the orthogonal as well as the randomized grids.

Being a diffusion problem, the diagonal of the QD (Eddington) tensor is set to one third, and the off diagonal terms become zero (E_{rr}=E_{zz}=$\frac{1}{3}$, E_{zr}=0) as pointed out earlier. The domain of the problem is 1.0 cm $\times$ 1.0 cm. The medium is homogeneous with cross sections $\sigma_t = \sigma_a = 1.0$, and a uniform external source $q = 1.0$. The boundary conditions are vacuum at every side of the problem domain defined by the Marshak BCs, see Eqn. (4.11c). Table 4.1 shows the discrete integral of the scalar flux over the problem domain $\Phi = \int_D \phi(r,z) r dr dz \approx \sum_i \phi_i V_i$ and the estimated order of convergence P for each grid used found by comparison with the reference. Figure 4.4 gives these same measured convergence rates in graphical form. The subscripts on Φ and P indicate the maximum perturbation, ρ_{max}, of the vertexes used for generating the grid, as a range of randomizations is considered in this test. These results show that the method does converge with second-order for the P_1 equations on randomized grids regardless of the level of randomization.

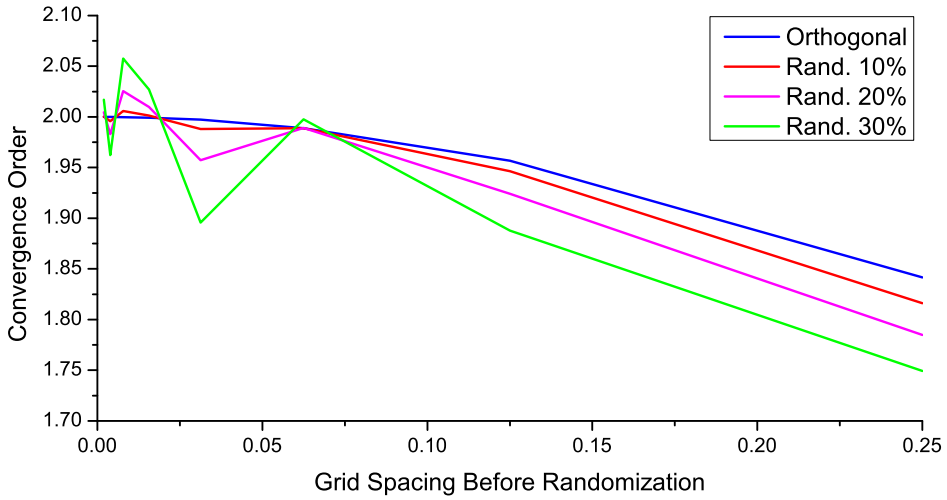

Figure 4.4: Order of spatial convergence (P) for the diffusion problem in Test 2.

Table 4.1: Convergence study of proposed scheme applied to the diffusion equation.

Grid	Φ_{ortho}	P_{ortho}	$\Phi_{10\%}$	$P_{10\%}$	$\Phi_{20\%}$	$P_{20\%}$	$\Phi_{30\%}$	$P_{30\%}$
2×2	1.278075	-	1.277001	-	1.275963	-	1.274953	-
4×4	1.236202	1.841716	1.236187	1.816122	1.236240	1.784914	1.236345	1.749356
8×8	1.224173	1.956789	1.224200	1.946467	1.224279	1.924215	1.224417	1.887710
16×16	1.221051	1.988968	1.221058	1.988892	1.221078	1.989076	1.221106	1.997645
32×32	1.220263	1.997238	1.220267	1.988105	1.220277	1.957413	1.220297	1.895649
64×64	1.220065	1.999311	1.220067	2.001336	1.220069	2.009691	1.220073	2.027179
128×128	1.220016	1.999827	1.220016	2.005964	1.220017	2.025359	1.220017	2.057445
256×256	1.220004	1.999948	1.220004	1.995849	1.220004	1.982960	1.220004	1.962297
512×512	1.220001	1.999899	1.220001	2.000253	1.220001	2.004501	1.220001	2.016958
Reference	1.21999991	-	-	-	-	-	-	-

4.2.3 Test 3: Two Region Diffusion Problem

This test is a diffusion problem devised to demonstrate the convergence of the solution obtained by the scheme on successively refined randomized grids throughout space. The test consists of a homogeneous medium with cross sections $\sigma_t = 1.0, \sigma_s = 0.5$. The domain of the problem is $r \in [0, 5], z \in [0, 3]$. The left half of the domain has a unit distributed source, while the right side has no source. This test has two individual cases that both have randomized sub domains separated by orthogonal lines of cell faces. The first test has only a straight vertical line of faces at the problem midpoint, $r = 2.5$, refer to Figure 4.5. The second test is identical except that an additional horizontal line of straight faces is added at the problem midpoint, namely $z = 1.5$. The results for this test are cross

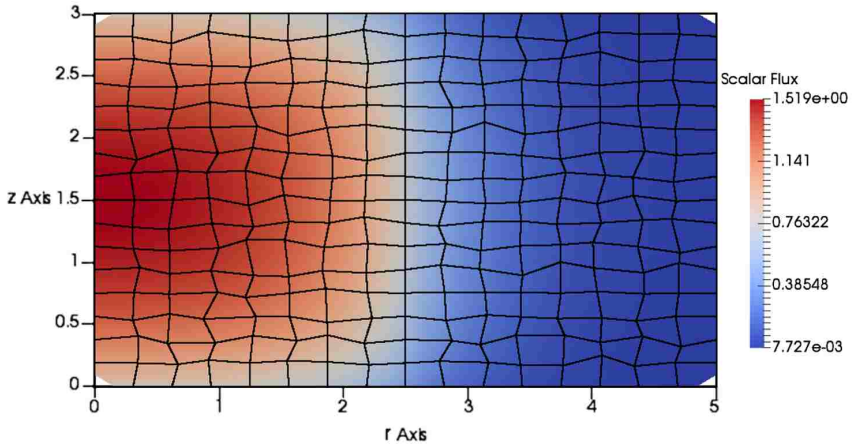

Figure 4.5: Scalar flux solution on two region randomized grid.

sectional slices of the solution running through the non-randomized cell edges for both cases. This allows for demonstration of the point wise behavior of the solution as the grid is refined. We give the solution for both cases on five grids as indicated in Figures 4.6 and 4.7. These results show that upon refinement the solution on randomized grids converges to the solution obtained on a fine orthogonal grid point wise for diffusion problems.

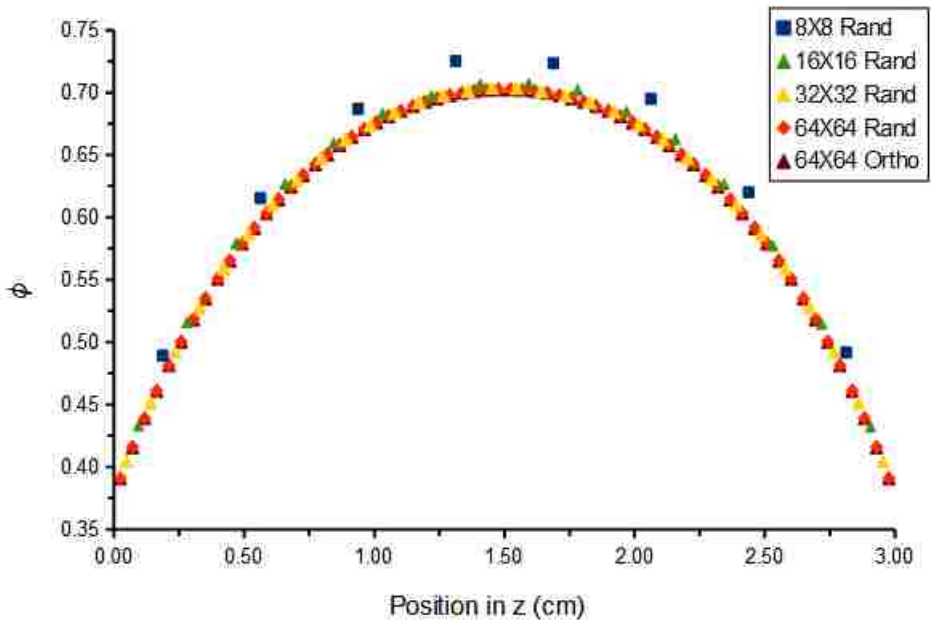

Figure 4.6: Test 3, case 1: $\phi(2.5, z)$.

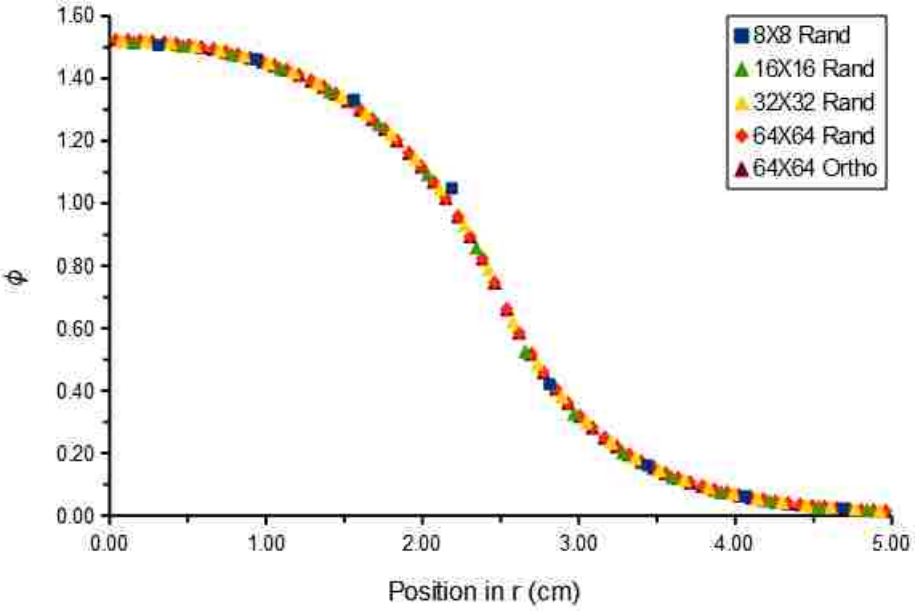

Figure 4.7: Test 3, case 2: $\phi(r, 1.5)$.

4.2.4 Test 4: Convergence Study for the Proposed Scheme Applied to the P_1 equations on Multilevel Meshes Using MMS

The final test for pure diffusion problems demonstrates the method's ability to treat problems of this kind on arbitrary meshes with hanging nodes, i.e. adaptively refined meshes. For this test MMS was used to determine the convergence rates and errors on each grid. As before the test is a homogeneous 1.0 cm $\times$ 1.0 cm medium with cross sections $\sigma_t = \sigma_a = 1.0$. The mesh is 3 levels with the right third being refined by a factor of 4, the center third being refined by a factor of 2 and the left third not being refined, refer to Figure 4.8.

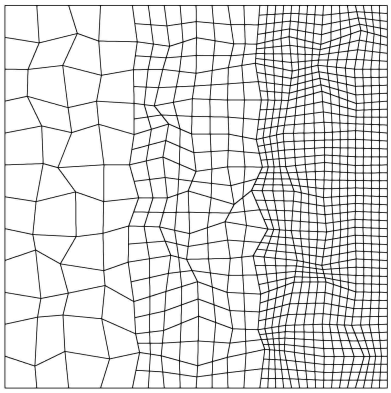

Figure 4.8: 3 Level Mesh (Original Coarse Randomized mesh: 12 $\times$ 12).

All meshes for this test were generated with a coarse randomized grid and then refinement was done. The maximum randomization parameter was taken to be $\rho_{max} = 0.35$ for all grids in this test. The chosen analytic solution for the scalar flux is given by

$$\phi^*(r,z) = cos\left(\frac{\pi r}{2R_{ext}}\right) cos\left(\frac{\pi(z-\frac{H}{2})}{H_{ext}}\right), \tag{4.13}$$

where $R_{ext} = 1.2$ and $H_{ext} = 1.4$ are a chosen extrapolated radius and height respectively and H is the domain height. Eddington factors are of course that of diffusion, $E_{rr} = E_{zz} = \frac{1}{3}$ and $E_{rz} = 0$.

The results for this test using the continuity condition extension to adaptive-like meshes is given in Table 4.2 and the results for the pseudo-polygonal approach are given in Table 4.3. In the tables $h \approx 0.01$ is the mesh spacing of the unrefined region of the finest grid before randomization, Φ is the integral of the scalar flux over the domain, L is the leakage across the top right quarter of the domain, $||\boldsymbol{\varepsilon}_\phi||_{L_2}$ and $||\boldsymbol{\varepsilon}_J||_{L_2}$ are the L_2 norm of the error in the cell average scalar flux and the face average current normalized by volume and area respectively found by comparing to the analytic solution, and P_x is the convergence rate in the related norm found by taking the ratio of successive norms of the differences between the discrete and analytic solution. The results show that the solution for the scalar flux from both treatments for hanging nodes converge with second order on adaptive-like grids for the P_1 equations. The solution for the face average current for both methods behaves with roughly 1st order convergence, this is consistent with what is seen in 2D Cartesian Geometry for this discretization when used for the LOQD equations [27]. The continuity condition approach gives slightly less error for the cell average scalar flux while the pseudo-polygonal method gives slightly less error for the face average current. The lower error in the face average current using the pseudo-polygonal approach can be explained by the lack of smearing of the current on complex faces.

Table 4.2: MMS convergence study of continuity conditions on a 3-level grid for diffusion.

Grid	Φ	L	$\|\|\boldsymbol{\varepsilon}_\phi\|\|_{L_2}$	$\|\|\boldsymbol{\varepsilon}_J\|\|_{L_2}$	$P_{\|\|\boldsymbol{\varepsilon}_\phi\|\|_{L_2}}$	$P_{\|\|\boldsymbol{\varepsilon}_J\|\|_{L_2}}$
$16h$	1.5429347	1.8822583	3.193E-03	2.960E-03	-	-
$8h$	1.5412284	1.8822450	1.004E-03	1.198E-03	1.669	1.305
$4h$	1.5407690	1.8822721	2.275E-04	4.444E-04	2.142	1.431
$2h$	1.5406689	1.8822647	6.118E-05	1.818E-04	1.895	1.289
h	1.5406423	1.8822656	1.532E-05	7.563E-05	1.997	1.266
Analytic	1.5406326	1.8822644	-	-	-	-

Table 4.3: MMS convergence study of pseudo-polygonal treatment on a 3-level grid for diffusion.

Grid	Φ	L	$\|\|\boldsymbol{\varepsilon}_\phi\|\|_{L_2}$	$\|\|\boldsymbol{\varepsilon}_J\|\|_{L_2}$	$P_{\|\|\boldsymbol{\varepsilon}_\phi\|\|_{L_2}}$	$P_{\|\|\boldsymbol{\varepsilon}_J\|\|_{L_2}}$
$16h$	1.5434331	1.8824078	3.328E-03	2.174E-03	-	-
$8h$	1.5413543	1.8822323	1.035E-03	8.095E-04	1.685	1.425
$4h$	1.5408027	1.8822717	2.371E-04	3.111E-04	2.126	1.379
$2h$	1.5406779	1.8822644	6.393E-05	1.363E-04	1.891	1.191
h	1.5406443	1.8822654	1.601E-05	6.505E-05	1.997	1.067
Analytic	1.5406326	1.8822644	-	-	-	-

4.2.5 Test 5: Convergence Study for the Proposed Scheme Applied to the LOQD Equations on Single Level Meshes Using MMS

Next we look at how the newly developed discretization method performs when used for the LOQD equations. This test uses MMS similarly to Test 4 (Sec. 4.2.4) with the addition of analytically prescribed Eddington factors. The domain of the test problem is 1.0 cm $\times$ 1.0 cm with homogeneous cross sections throughout, $\sigma_t = 1.0, \sigma_a = 0.5$, and $\sigma_s = 0.5$. The chosen analytic solution is the same as Test 4, Eqn. (4.13). The analytic Eddington factors for this test are taken to be

$$E^*_{rr}(r,z) = \frac{1}{3} + r^2(z - 0.5H)^2, \tag{4.14a}$$

$$E^*_{zz}(r,z) = \frac{1}{3} + r^2(z - 0.5H)^2, \tag{4.14b}$$

$$E^*_{zr}(r,z) = r^2(z - 0.5H). \tag{4.14c}$$

A range of maximum randomization parameters, ρ_{max}, were used for this study.

In addition to comparison with the analytic solution with L_2 norms of the error in this MMS test we also look at the integral of the scalar flux across the domain, just as in other tests. Here we can compare to the integral of the analytic scalar flux directly. Figure 4.9 shows the convergence rate of the total scalar flux for different ρ_{max} choices

found by taking successive ratios of the difference between discrete and analytic solutions,

$$\left| \sum_i (\phi_{i,c} V_i) - \int_D \phi^*(r,z) r dr dz \right|. \tag{4.15}$$

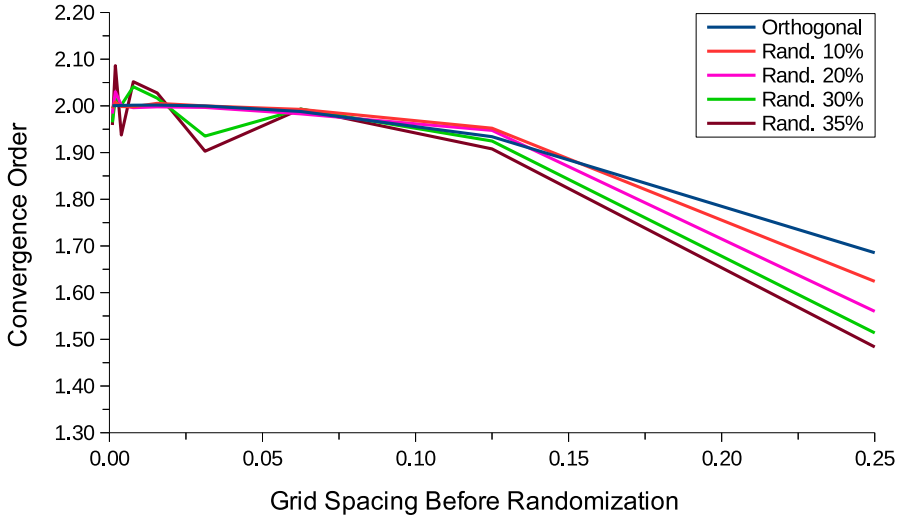

Figure 4.9: Order of convergence of total scalar flux in Test 5.

Table 4.4 contains a subset of the results for this test, showing the results for the finest 5 grids with the largest randomization parameter $\rho = 0.35$. $h \approx 9.8 \times 10^{-4}$ is the grid spacing on the finest grid before randomization. The definition of the quantities given in Table 4.4 are the same as those in Tables 4.2 and 4.3 from the previous test. As with the diffusion equations, this discretization when applied to the LOQD equations gives 2nd order convergence for the scalar flux and 1st order convergence for the face average current. Note that both the flux integral and L_2 norm measures show 2nd order convergence for the scalar flux.

Table 4.4: MMS convergence study of discretization method on a single level grid for the LOQD equations.

Grid	Φ	L	$\|\|\varepsilon_\phi\|\|_{L_2}$	$\|\|\varepsilon_J\|\|_{L_2}$	$P_{\|\|\varepsilon_\phi\|\|_{L_2}}$	$P_{\|\|\varepsilon_J\|\|_{L_2}}$
$16h$	1.5408962	1.3554909	1.671E-04	6.425E-04	2.027	0.983
$8h$	1.5407004	1.3555202	4.285E-05	3.291E-04	1.963	0.965
$4h$	1.5406497	1.3555246	1.089E-05	1.696E-04	1.976	0.956
$2h$	1.5406369	1.3555266	2.733E-06	8.519E-05	1.995	0.993
h	1.5406336	1.3555270	6.541E-07	4.275E-05	2.063	0.995
Analytic	1.5406326	1.3555271	-	-	-	-

4.2.6 Test 6: Convergence Study for the Proposed Scheme Applied to the LOQD Equations on Multilevel Meshes Using MMS

Just as with previous tests this test utilizes MMS to measure error and convergence rates of quantities of interest. The domain of this test is 1cm $\times$ 1cm with homogeneous cross sections $\sigma_t = 1.0, \sigma_a = 0.5$, and $\sigma_s = 0.5$. The chosen analytic solution is again the same as Test 4, Eqn. (4.13) and the analytic Eddington factors are the same as Test 5, Eqns. (4.14). The meshes used for this test are the same as Test 4, 3 levels with the right third being refined by a factor of 4, the center third being refined by a factor of 2 and the left third not being refined, refer to Figure 4.8. Tables 4.5 and 4.6 contain the results of this test for the continuity conditions and pseudo-polygonal method respectively, where $h \approx 0.01$. We again see 2nd order convergence in space for the scalar flux and near 1st order convergence for the face average current for both methods. We also see that for this test the pseudo-polygonal method is slightly more accurate than the continuity condition approach. These results confirm that the discretization method achieves the expected convergence rate for the scalar flux on our target grids for the intended equations, the LOQD equations.

Table 4.5: MMS convergence study of continuity conditions on a 3-level grid.

Grid	Φ	L	$\|\|\varepsilon_\phi\|\|_{L_2}$	$\|\|\varepsilon_J\|\|_{L_2}$	$P_{\|\|\varepsilon_\phi\|\|_{L_2}}$	$P_{\|\|\varepsilon_J\|\|_{L_2}}$
$16h$	1.5468966	1.3561145	4.317E-03	3.632E-03	-	-
$8h$	1.5422983	1.3556983	1.379E-03	1.723E-03	1.646	1.076
$4h$	1.5410130	1.3555571	3.201E-04	6.245E-04	2.108	1.464
$2h$	1.5407355	1.3555390	8.028E-05	2.634E-04	1.995	1.245
h	1.5406581	1.3555302	2.010E-05	1.219E-04	1.998	1.111
Analytic	1.5406326	1.3555271	-	-	-	-

Table 4.6: MMS convergence study of pseudo-polygonal treatment on a 3-level grid.

Grid	Φ	L	$\|\|\varepsilon_\phi\|\|_{L_2}$	$\|\|\varepsilon_J\|\|_{L_2}$	$P_{\|\|\varepsilon_\phi\|\|_{L_2}}$	$P_{\|\|\varepsilon_J\|\|_{L_2}}$
$16h$	1.5466303	1.3564540	4.267E-03	4.057E-03	-	-
$8h$	1.5421921	1.3557353	1.339E-03	1.691E-03	1.672	1.263
$4h$	1.5409956	1.3555672	3.125E-04	6.287E-04	2.099	1.427
$2h$	1.5407300	1.3555416	7.749E-05	2.549E-04	2.012	1.302
h	1.5406566	1.3555308	1.946E-05	1.188E-04	1.994	1.101
Analytic	1.5406326	1.3555271	-	-	-	-

4.2.7 Analysis of Matrices of the Discretized LOQD Equations

As explained in Section 3.3.2 the set of discretized LOQD equations that we have developed for an $N \times N$ logically rectangular grid of cells yields a system of $3N^2 + 2N$ equations, or $3M + 2\sqrt{M}$ if M is the total number of cells. The system of equations is non-symmetric, and not necessarily positive definite. This necessitates that a solution method be used that can handle such matrices, e.g. GMRES, BiCGSTAB, etc.. To analyze the structure

and conditioning of the discretized LOQD equations matrix we define a basic two region problem with a 1cm × 1cm domain, homogeneous cross sections $\sigma_t = 1.0, \sigma_a = 0.5$, and $\sigma_s = 0.5$, distributed source on the left half, no source on the right half, and vacuum boundary conditions. Figure 4.10 depicts the matrix structures of the LOQD equations with converged QD factors for this problem without adaptive refinement and with adaptive refinement using the two treatments for it. The transport method used was SCB. The meshes used for generating the matrices are shown in Figure 4.11.

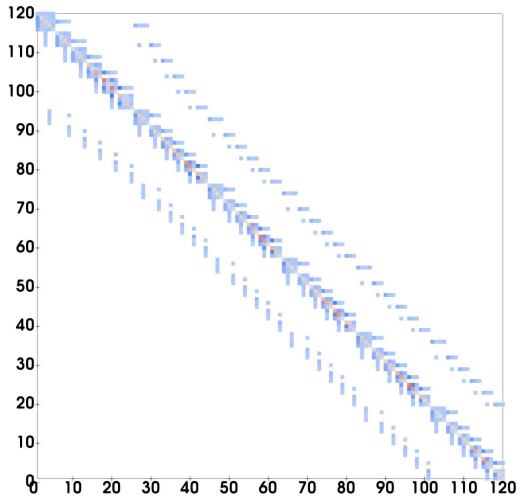

(a) Matrix of Unrefined Problem

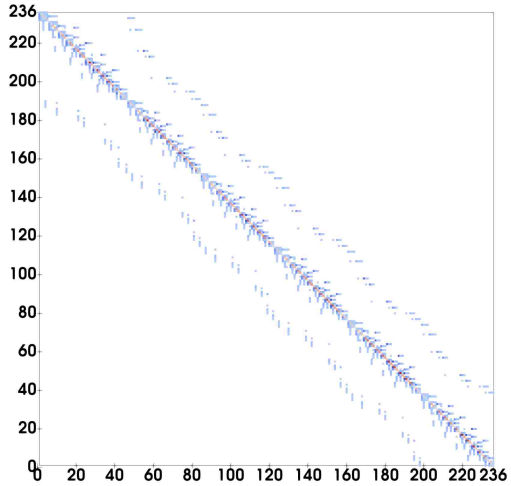

(b) Matrix of Refined Problem with Pseudo-Polygonal

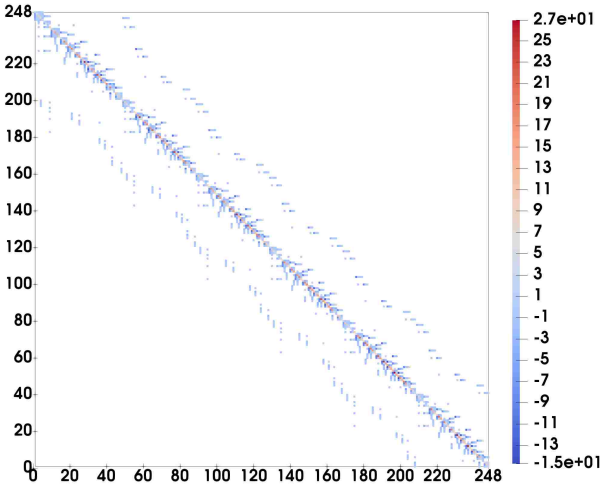

(c) Matrix of Refined Problem with Continuity Conditions

Figure 4.10: Matrix Structures

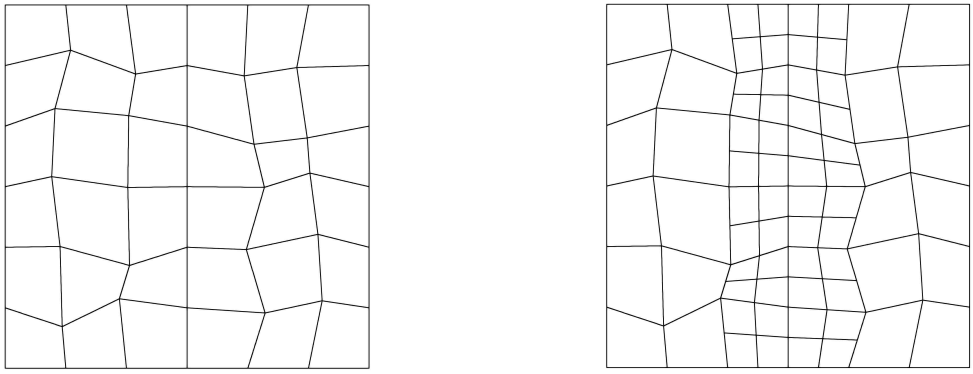

(a) Unrefined Mesh (b) Adaptively Refined Mesh

Figure 4.11: Meshes Used for Matrix Analysis

An important quantity when analyzing matrix problems is the condition number defined as

$$K(A) = ||A||_2||A^{-1}||_2. \tag{4.16}$$

The condition number is a measure of how sensitive a matrix is to input error and it gives an idea of the difficulty for inverting that matrix. It can be expected that a matrix with a higher condition number will take more iterations to invert than one with a lower condition number when using an iterative technique such as GMRES or BiCGSTAB. To get an idea of the magnitude of condition numbers we can expect from the LOQD system of equations we will do a similar study to what is seen in [62] by performing a series of refinements of our sample problem. Here we do true successive refinements of the grids shown in Figure 4.11 each by a factor of 2. Figure 4.12 shows the condition numbers versus number of unknowns/grid spacing for the LOQD equations for the non-adaptive mesh and adaptive meshes. This study shows that in general the condition numbers for the developed LOQD scheme scale with $O(h^{-3})$ where h is an average measure of grid spacing in a single dimension, and that the condition number for non-adaptive and adaptive grids with either treatment behaves fairly similarly. After performing an immense number of tests with different grids, material properties, and source distributions we have seen a trend that the pseudo-polygonal method always yields condition numbers that are no worse than the continuity condition method. In some cases the pseudo-polygonal method yields significantly better condition numbers. It is difficult to see at the scale of Figure 4.12, however, the pseudo-polygonal method consistently gives at least slightly better

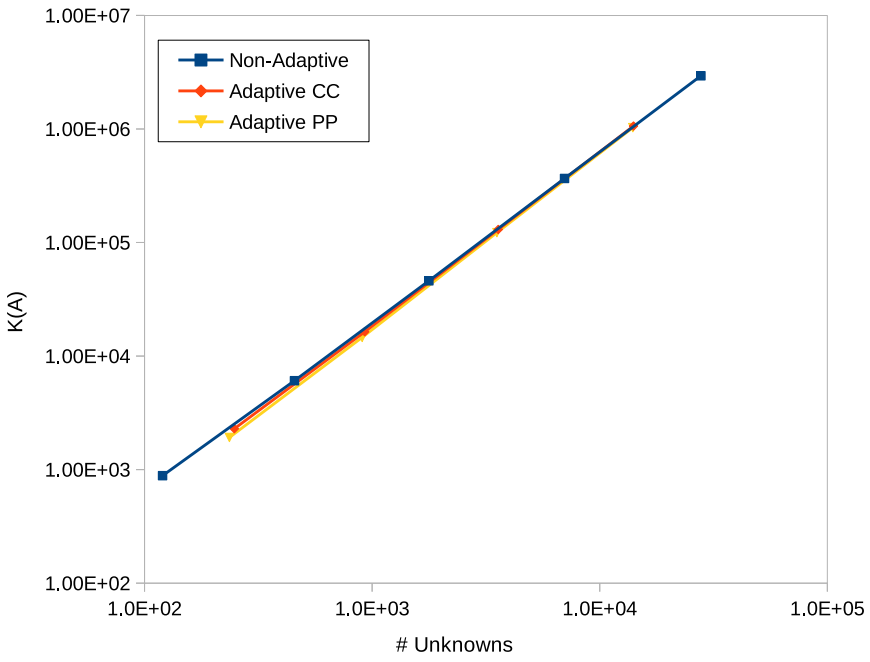

Figure 4.12: Condition Number Study

condition numbers than the continuity conditions for the sample problem here. Table 4.7 gives the number of unknowns for each matrix as well as the corresponding condition numbers for the grids in Figure 4.11.

Table 4.7: Properties of LOQD Matrices for Sample Problem

	N	$K(A)$
No Refinement	120	8.8446E+02
Pseudo-Poly.	236	1.9203E+03
Cont. Cond.	248	2.2911E+03

As one can see in Table 4.7 the continuity condition approach gives a condition number that is 19.3% higher than the pseudo-polygonal method for the same grid. This difference cannot be accounted for purely by the difference in the numbers of unknowns as with this minimal amount of adaptivity they are quite close in that regard.

4.3 Results and Analysis for the QD Method for Transport Problems in $r-z$ Geometry

We now shift our focus to the performance of the QD method in $r-z$ geometry based on the newly developed LOQD equation discretization. The performance of the overall QD method is of course dependent on the quality of the Eddington factors supplied to the low-order equations and hence the transport discretization chosen. We analyze the QD method with two different transport discretizations with significantly different properties, as described earlier SCB and VBMOSC.

In this section all grid refinement studies were performed using the classic approach to grid refinement. This is done as opposed to the "worst case scenario" refinement method so as to obtain reliably measurable convergence rates. Note that the QD method is a nonlinear method, and convergence of the solution relies not only on the convergence of the high-order equations and subsequently the QD factors, but also the low-order set of equations, the LOQD equations. This can translate into chaotic convergence rates on certain grid sequences when the grids under consideration are not extremely fine, hence our choice to use a better behaved refinement here.

Throughout the results presented here a simple Gauss-Legendre product quadrature set was used for the angular mesh for transport. Gauss-Legendre quadrature sets are used for both the polar and azimuthal angles. The mesh is made up of polar "levels", i.e. angles, each with a corresponding azimuthal quadrature discretization. The number of azimuthal angles per polar "level" per octant is given by the formula

$$N_{az}(p) = N_{az_{max}} - INT\left(\frac{N_{az_{max}} - N_{az_{min}}}{N_p - 1}(N_p - p)\right). \tag{4.17}$$

Where $N_{az_{max}}$ is the chosen maximum number of azimuthal angles per polar level corresponding to the polar level closest to $\theta = \frac{\pi}{2}$, $N_{az_{min}}$ is the chosen minimum number of azimuthal angles per polar level corresponding to the polar level closest to $\theta = 0$, N_p is the polar quadrature set order, and p is the index of the current polar level. Note that for $r-z$ geometry the discretized transport equation is defined on the angular interval $\theta \in [0, \pi]$ and $\gamma \in [0, \pi]$. Unless otherwise stated all results were generated with $N_p = 8$, $N_{az_{max}} = 8$, and $N_{az_{min}} = 2$ which is convenient to denote as set $8 \times (2, 8)$.

4.3.1 Test 1: Convergence Study of The QD Method with SCB and VBMOSC on Single Level Meshes

We start our analysis of the newly developed QD method similarly to the LOQD discretization alone with a simple single level mesh on a simple problem, 1.0 cm $\times$ 1.0 cm with constant homogeneous cross sections and source, $\sigma_t = 1.0$, $\sigma_a = 0.5$, $\sigma_s = 0.5$, and $q = 1.0$. External boundary conditions are vacuum. The initial grid for this study was a 16 $\times$ 16 randomized grid, with subsequent grids being classical refinements of previous grids. Tables 4.8 and 4.9 show the convergence study results where $h \approx 0.00195$. The definitions of Φ and L are the same as in previous sections, P_Φ and P_L are convergence rates of those measures. Note that the convergence rates here are calculated by taking the ratio of successive differences of the discrete solution.

Table 4.8: Results of Single Level Convergence Study of SCB and VBMOSC

	SCB				VBMOSC			
Grid	Φ	L	P_Φ	P_L	Φ	L	P_Φ	P_L
$32h$	1.712565	0.972578	-	-	1.595515	0.909024	-	-
$16h$	1.713211	0.972070	-	-	1.666453	0.940379	-	-
$8h$	1.713603	0.971886	0.72245	1.47138	1.696744	0.954284	1.22765	1.17313
$4h$	1.713756	0.971830	1.34984	1.69983	1.710651	0.961133	1.12305	1.02150
$2h$	1.713809	0.971814	1.55337	1.83406	1.717398	0.964803	1.04353	0.90025
h	1.713825	0.971810	1.66717	1.84916	1.720738	0.966714	1.01432	0.94179

Here we see that VBMOSC behaves exactly as expected with very stable 1st order convergence. VBMOSC being only 1st order starts out with a poor solution as compared to SCB. SCB approaches 2nd order but our results here do not go quite far enough to fully approach asymptotic behavior for it. Refering to Table 4.9, the QD method using either transport discretization converges more chaotically than simple SI. This is to be expected due to the QD system of equations being nonlinear and the convergence of the solution being dependent on the convergence of the low-order equations and the

Table 4.9: Results of Single Level Convergence Study of QD-SCB and QD-VBMOSC

	QD-SCB				QD-VBMOSC			
Grid	Φ	L	P_Φ	P_L	Φ	L	P_Φ	P_L
$32h$	1.720665	0.970140	-	-	1.714741	0.967516	-	-
$16h$	1.714791	0.971712	-	-	1.713290	0.970440	-	-
$8h$	1.713851	0.971874	2.64495	3.28113	1.713481	0.971714	2.92116	1.19863
$4h$	1.713821	0.971823	4.92671	1.66252	1.713610	0.972370	0.57407	0.95833
$2h$	1.713871	0.971781	-0.70570	0.30838	1.713574	0.972748	1.82641	0.79405
h	1.713896	0.971767	0.98351	1.48716	1.713528	0.972954	-0.33631	0.87245
Avg.	-	-	1.96237	1.68480	-	-	1.24633	0.95587

high-order equation/Eddington factors. Taking the average of the measured convergence rates reveals that the QD method using SCB and VBMOSC converges with 2nd and 1st order respectively. The QD method using VBMOSC converges with 1st order in space due to the QD factors stemming from VBMOSC converging with 1st order behavior. However, using the SCB solution on the finest grid as a reference we see a large jump in accuracy of both the flux and corner leakage for QD-VBMOSC compared to VBMOSC alone. This indicates that the higher convergence order discretization of the LOQD equations used in the QD method boosted the accuracy of VBMOSC. This follows from the Eddington factors only being weakly dependent upon the high-order transport solution. This is an important result as it demonstrates the possibility of obtaining accurate radiation transport solutions while using cheaper high-order discretizations.

4.3.2 Test 2: Two Region Transport Problem

This test is meant to show the convergence behavior of the developed QD method, and that of the two transport discretizations used, throughout space. This test is similar to Test 3 in the previous section, however, here there is exactly one case using grids with non-randomized straight lines of cells running vertically and horizontally through the midpoint of the problem. Figure 4.13 depicts the initial coarse 8×8 cell grid used in this problem. As indicated in Figure 4.13 the domain of the problem is $r \in [0, 5], z \in [0, 3]$. Cross sections are homogeneous with $\sigma_t = 1.0, \sigma_s = 0.5$. The left half of the domain has

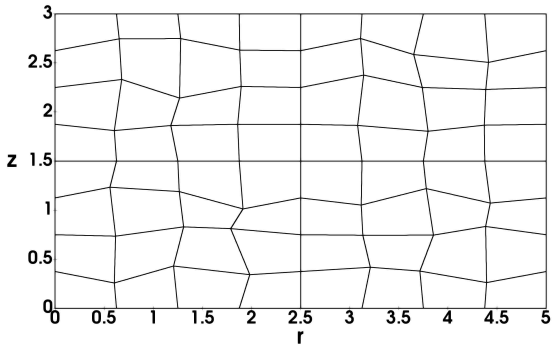

Figure 4.13: Coarse Grid For Two Region Transport Problem

a unit distributed source, while the right side has no source. Boundary condition are vacuum except for the rotational boundary at $r = 0$.

First we will compare how the transport methods and corresponding QD method perform accuracy wise on a coarse grid. Figures 4.14 and 4.15 show the r and z cross sections of the scalar flux along the lines of straight cell faces using the coarse 8×8 grid shown in Figure 4.13. The reference was generated using SCB on a 216×216 grid of orthogonal cells. Tables 4.10 and 4.15 give the 1 and 2 norms of the differences between the solutions and the reference for both solution cross sections.

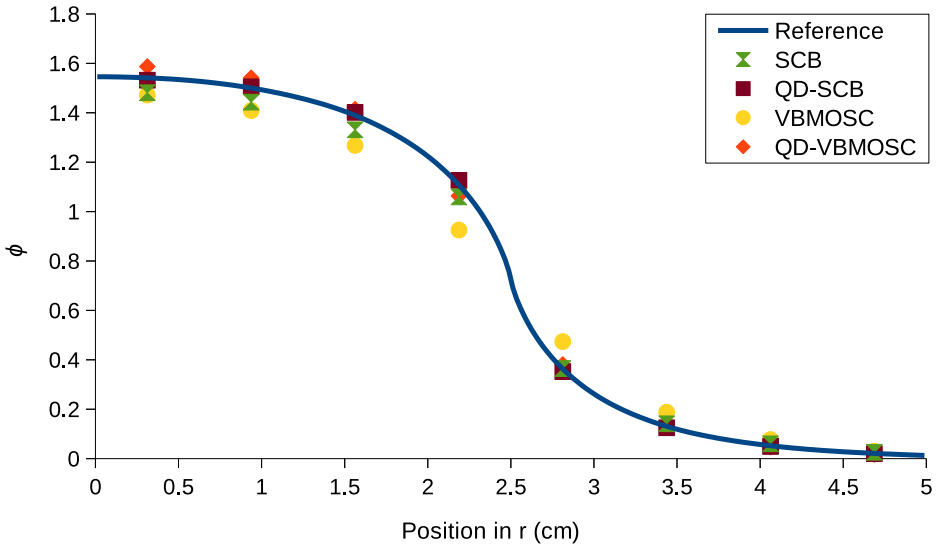

Figure 4.14: $\phi(r, 1.5)$ for Different Transport Schemes

Table 4.10: Norms of Differences Between $\phi(r, 1.5cm)$ from Different Methods and Reference

Norm	VBMOSC	QD-VBMOSC	SCB	QD-SCB
1-Norm	0.66694	0.18451	0.24689	0.06621
2-Norm	0.27837	0.08190	0.11296	0.02787

For the cross section in r, Figure 4.14, it is obvious that VBMOSC alone gives the least accurate solution especially around the boundary between the source and no source regions. QD-VBMOSC does a significantly better job than VBMOSC essentially everywhere and especially at the boundary between the two regions and on the right where there is no source. SCB alone does quite well, however, QD-SCB is seen to outperform it throughout the left half of the domain. The measures given in Table 4.10 confirm and quantify these visual findings and reveals that for this cross section of the solution QD-VBMOSC actually outperforms SCB alone. This is a significant result.

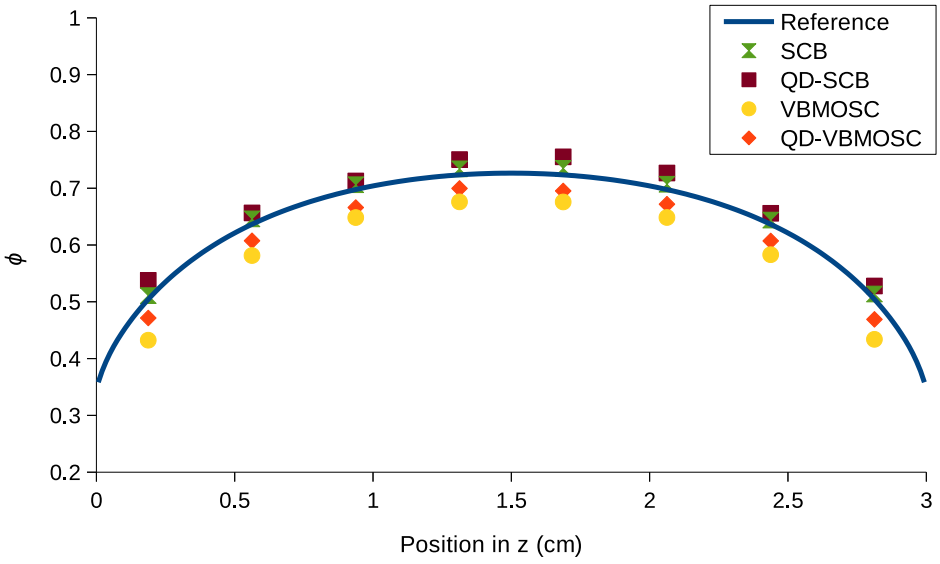

Figure 4.15: $\phi(2.5, z)$ for Different Transport Schemes

Table 4.11: Norms of Differences Between $\phi(2.5cm, z)$ from Different Methods and Reference

Norm	VBMOSC	QD-VBMOSC	SCB	QD-SCB
1-Norm	0.44468	0.23600	0.07262	0.19919
2-Norm	0.15943	0.08401	0.02602	0.07250

The z cross section of the solutions and reference, taken at the boundary between source regions, tells a somewhat different story than the r cut. Obviously VBMOSC by itself gives the poorest solution, and QD-VBMOSC is seen to be a significant improvement over VBMOSC alone. However, for this cross section we see that SCB by itself is the closest to the reference, with QD-SCB actually having more error than SCB alone. In comparing the SCB based methods to VBMOSC based methods we see that solutions using SCB are closer to the reference.

Next we look at the convergence of each method upon refinement of the grid. The convergence study of each method starts with the coarse 8×8 grid shown in Figure 4.13 and proceeds with two classical grid refinements. Figures 4.16 - 4.19 show the convergence of the r cross section and Figures 4.20 - 4.23 show the convergence of the z cross section.

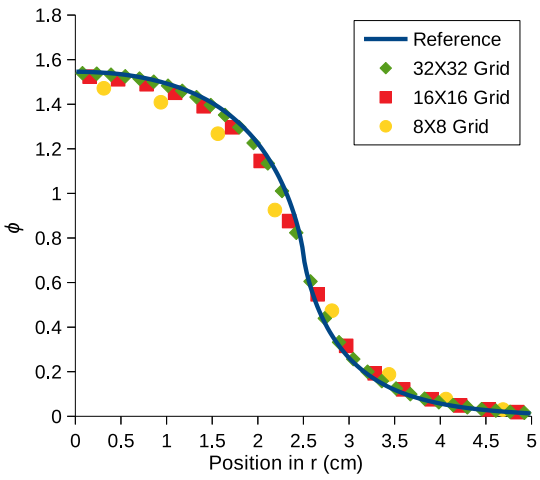

Figure 4.16: Convergence of VBMOSC r Cross Section

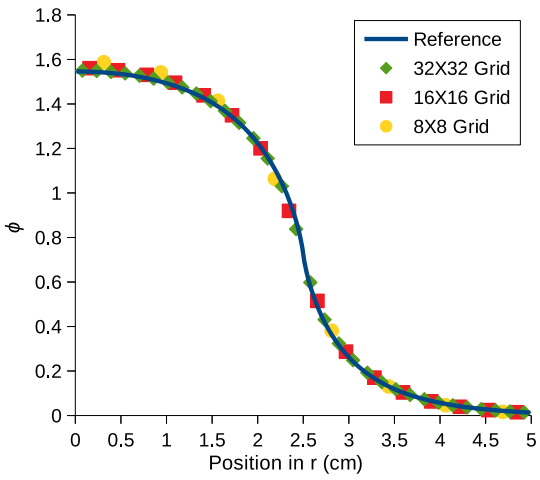

Figure 4.17: Convergence of QD-VBMOSC r Cross Section

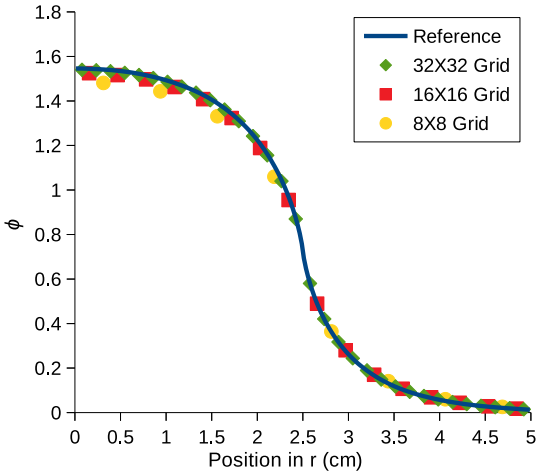

Figure 4.18: Convergence of SCB r Cross Section

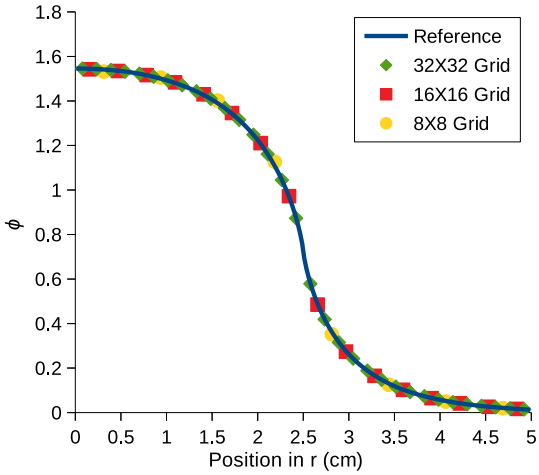

Figure 4.19: Convergence of QD-SCB r Cross Section

The r cross section results shows that each method converges as would be suggested by their orders of convergence, other than perhaps QD-SCB which at this scale looks almost exact even on the first grid. The important thing to point out here is that the developed QD method using both transport discretizations converges to a fine solution on an orthogonal grid upon grid refinement.

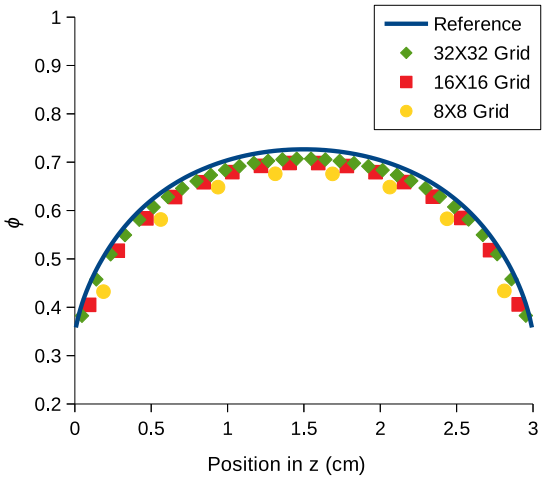

Figure 4.20: Convergence of VBMOSC z Cross Section

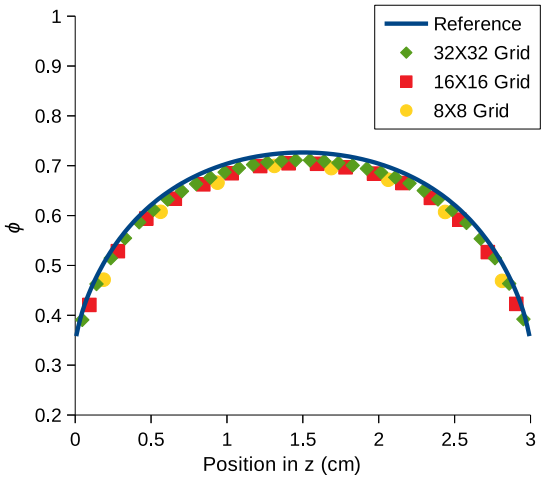

Figure 4.21: Convergence of QD-VBMOSC z Cross Section

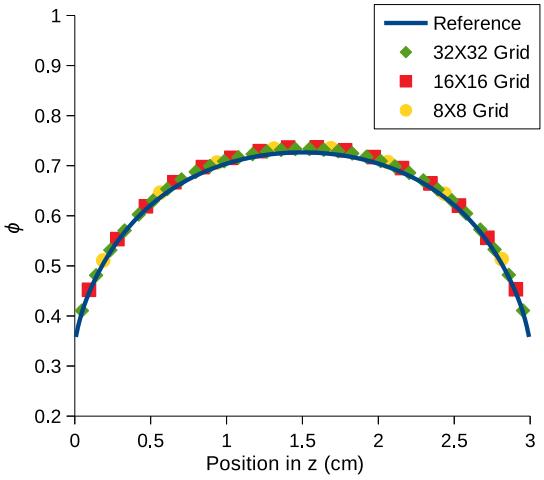

Figure 4.22: Convergence of SCB z Cross Section

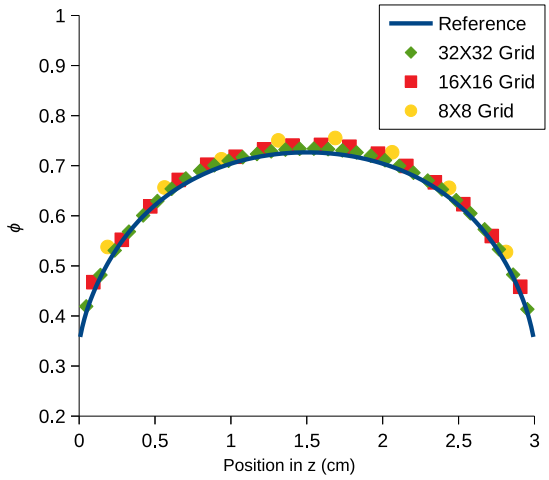

Figure 4.23: Convergence of QD-SCB z Cross Section

In the z direction cross section results we see again that the developed QD method converges upon refinement toward the reference solution. The benefit of using VBMOSC within QD as opposed to by itself is also seen here with the solutions of QD-VBMOSC being closer to the reference for all grids. What is interesting to note here is that upon comparing QD-SCB to SCB it appears that the solutions are approaching each other on finer grids. That is, they are not just approaching the reference, but in fact are approaching the same solution on a given grid. The solutions of SCB and QD-SCB are nearly indiscernible on the 32×32 grid at this scale while their distance from the reference is still easily seen. This is opposed to the significant difference seen between the two on the initial 8×8 grid. This could indicate that the QD-SCB scheme has some higher order error terms, higher than 2nd order, with significant magnitude on coarse grids that SCB alone does not have. The error terms we refer to here are the spatial truncation error terms associated with the discretizations used, i.e. the truncation error found by performing Taylor series expansions of differencing schemes [10, 70]. This would explain why the difference between the SCB and QD-SCB solutions disappears for finer grids as error terms with order higher than $O(h^2)$ will obviously shrink faster than the leading $O(h^2)$ term.

4.3.3 Test 3: Convergence Study of the QD Method with SCB and VBMOSC on Multilevel Meshes

In this study we use the same test problem used in previous sections, 1.0 cm $\times$ 1.0 cm with constant homogeneous cross sections and source, $\sigma_t = 1.0$, $\sigma_a = 0.5$, $\sigma_s = 0.5$, and $q = 1.0$. External boundary conditions are vacuum. The initial grid is formed by randomizing a coarse 6×6 grid of cells and refining the right third by a factor of 4 and the center third by a factor of 2, the same initial grid as other multilevel tests in previous sections. Subsequent grid refinements for this test are true refinements of the previous grid each by a factor of 2 over the entire domain, i.e. the classic approach. Results for SCB and VBMOSC by themselves and the results for the QD method using SCB and VBMOSC with the new LOQD discretization using both extensions to multilevel grids are given in Tables 4.12 - 4.14 where $h \approx 0.01$. Note that the convergence rates here are calculated by taking the ratio of successive differences of the discrete solution.

The results we see for this set of multilevel meshes are very similar to that of the single level mesh. SCB and VBMOSC by themselves both behave as expected with 2nd and 1st order convergence behavior respectively. Just as with the single level mesh the QD method using VBMOSC is 1st order in space due to the QD factors coming from VBMOSC converging with 1st order behavior, and a similar jump in accuracy is seen for the QD-VBMOSC method compared to VBMOSC by itself. Very little difference is seen for QD-VBMOSC with the two treatments for adaptive-like grids. QD-SCB with both cell coupling methods converges with at least 2nd order, though obviously not as uniformly as SCB alone. We can see that the pseudo-polygonal method for QD-SCB begins to approach the fine mesh solution faster than the continuity conditions after the second grid despite what the indicated convergence rates show.

Table 4.12: Results of Multilevel Convergence Study of SCB and VBMOSC

	SCB				VBMOSC			
Grid	Φ	L	P_Φ	P_L	Φ	L	P_Φ	P_L
$16h$	1.71524	0.97232	-	-	1.66016	0.94271	-	-
$8h$	1.71424	0.97199	-	-	1.69499	0.95573	-	-
$4h$	1.71394	0.97187	1.74296	1.39439	1.71048	0.96223	1.16855	1.00355
$2h$	1.71386	0.97182	1.91870	1.57386	1.71757	0.96548	1.12844	0.99751
h	1.71384	0.97181	1.99339	1.84522	1.72090	0.96710	1.08896	1.01073

Table 4.13: Results of Multilevel Convergence Study of QD-SCB and QD-VBMOSC with Pseudo-Polygonal Treatment

	QD-SCB Pseudo-Polygonal				QD-VBMOSC Pseudo-Polygonal			
Grid	Φ	L	P_Φ	P_L	Φ	L	P_Φ	P_L
$16h$	1.71679	0.97266	-	-	1.71132	0.97118	-	-
$8h$	1.71445	0.97203	-	-	1.71239	0.97196	-	-
$4h$	1.71393	0.97183	2.16947	1.67633	1.71298	0.97249	0.88872	0.56335
$2h$	1.71386	0.97177	2.81901	1.80492	1.71325	0.97281	1.11084	0.69576
h	1.71387	0.97176	2.60795	2.18190	1.71336	0.97299	1.24483	0.86375

Table 4.14: Results of Multilevel Convergence Study of QD-SCB and QD-VBMOSC with Continuity Conditions

	QD-SCB Continuity Conditions				QD-VBMOSC Continuity Conditions			
Grid	Φ	L	P_Φ	P_L	Φ	L	P_Φ	P_L
$16h$	1.715565	0.97239	-	-	1.71108	0.97124	-	-
$8h$	1.714218	0.97196	-	-	1.71235	0.97200	-	-
$4h$	1.713949	0.97182	2.32367	1.55232	1.71297	0.97250	1.04858	0.60201
$2h$	1.713911	0.97177	2.80908	1.75789	1.71324	0.97282	1.15597	0.66650
h	1.713908	0.97176	3.65748	1.98127	1.71336	0.97299	1.25673	0.83755

4.3.4 Test 4: Convergence Study of the QD Method with SCB and VBMOSC on Multilevel Meshes for a Heterogeneous Problem

This test adds another layer of complexity, material heterogeneity. Figure 4.24 shows the geometry and coarsest grid used in the convergence study here. The red region has cross sections $\sigma_t = 2.0$, $\sigma_a = 1.5$, $\sigma_s = 0.5$, and source $q = 1.0$, and the gray region has cross sections $\sigma_t = 1.0$, $\sigma_a = 0.1$, $\sigma_s = 0.9$, and has no external source. This test resembles a cylindrical source placed in water. The scalar flux solution on the finest grid using SCB is shown in Figure 4.25.

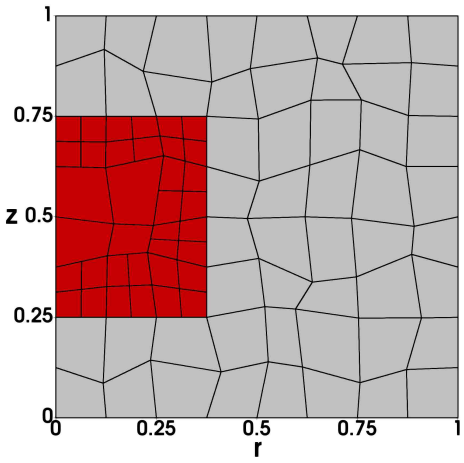

Figure 4.24: Geometry and Coarsest Grid of Test 4

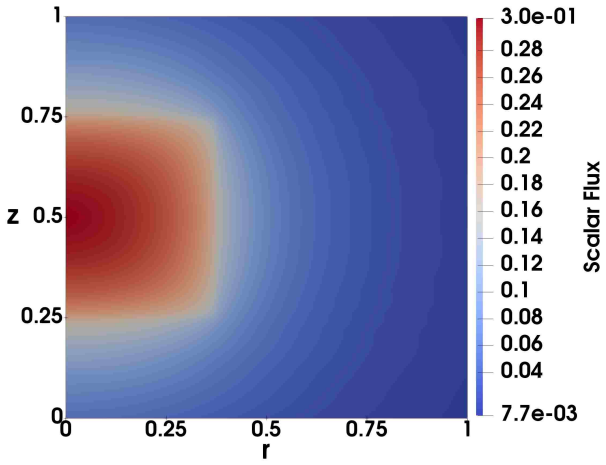

Figure 4.25: Scalar Flux on Finest Grid

Its easy to see from Tables 4.15 - 4.17 that these results are a little more muddled compared to those of simpler problems for VBMOSC based methods. VBMOSC by itself and QD-VBMOSC do not appear to be in a regime of asymptotic approach to the solution on this sequence of grids. Even finer grids were ran to ensure that the solutions from VBMOSC and QD-VBMOSC do in fact converge and it was confirmed that they do at impractically fine grids $h < 9.8 \times 10^{-4}$. Note that h in the Tables here corresponds to the pre-randomized spacing on the finest grid in the un-adaptively refined area with $h \approx 3.90625 \times 10^{-3}$. It does appear that using VBMOSC within the QD method gives an advantage over VBMOSC alone, as we have come to expect from QD, as the QD-VBMOSC solutions are closer to that of SCB on all grids compared to VBMOSC alone. SCB alone and QD-SCB both show stable 2nd order convergence for both LOQD extensions to adaptive-like grids with the continuity conditions slightly outperforming the pseudo-polygonal method.

Table 4.15: Results of Multilevel Convergence Study of SCB and VBMOSC on a Heterogeneous Problem

	SCB				VBMOSC			
Grid	Φ	L	P_Φ	P_L	Φ	L	P_Φ	P_L
$32h$	0.1490555	0.0465034	-	-	0.1550244	0.0510277	-	-
$16h$	0.1502829	0.0464061	-	-	0.1539805	0.0502747	-	-
$8h$	0.1506520	0.0464000	1.7337	3.9951	0.1545546	0.0507317	0.8626	0.7205
$4h$	0.1507475	0.0464043	1.9509	0.5075	0.1554342	0.0512199	-0.6154	-0.0954
$2h$	0.1507705	0.0464056	2.0486	1.6831	0.1561647	0.0515714	0.2679	0.4741
h	0.1507760	0.0464060	2.0900	1.7108	0.1566267	0.0517856	0.6610	0.7145

Table 4.16: Results of Multilevel Convergence Study of QD-SCB and QD-VBMOSC with Pseudo-Polygonal Treatment on a Heterogeneous Problem

	QD-SCB Pseudo-Polygonal				QD-VBMOSC Pseudo-Polygonal			
Grid	Φ	L	P_Φ	P_L	Φ	L	P_Φ	P_L
$32h$	0.1497380	0.0467848	-	-	0.1519933	0.0482986	-	-
$16h$	0.1502495	0.0466930	-	-	0.1516295	0.0476034	-	-
$8h$	0.1504825	0.0467143	1.1346	2.1092	0.1513948	0.0473560	0.6327	1.4899
$4h$	0.1505553	0.0467223	1.6774	1.4089	0.1513604	0.0473187	2.7674	2.7310
$2h$	0.1505756	0.0467247	1.8428	1.7547	0.1513995	0.0473340	-0.1837	1.2868
h	0.1505806	0.0467255	2.0390	1.5716	0.1514423	0.0473565	-0.1279	-0.5585

Table 4.17: Results of Multilevel Convergence Study of QD-SCB and QD-VBMOSC with Continuity Conditions on a Heterogeneous Problem

	QD-SCB Continuity Conditions				QD-VBMOSC Continuity Conditions			
Grid	Φ	L	P_Φ	P_L	Φ	L	P_Φ	P_L
$32h$	0.1497694	0.0467996	-	-	0.1519706	0.0483430	-	-
$16h$	0.1502679	0.0467012	-	-	0.1516216	0.0476110	-	-
$8h$	0.1504907	0.0467177	1.1618	2.5718	0.1513933	0.0473585	0.6126	1.5356
$4h$	0.1505583	0.0467233	1.7219	1.5787	0.1513605	0.0473202	2.7991	2.7208
$2h$	0.1505765	0.0467247	1.8895	1.9268	0.1513997	0.0473346	-0.2572	1.4166
h	0.1505808	0.0467253	2.0728	1.2804	0.1514424	0.0473567	-0.1228	-0.6230

We note that the results in Tables 4.15 - 4.17 show that SCB and QD-SCB are converging to two different solutions for this problem. Our hypothesis for this behavior is a difference in effective angular discretization truncation error for QD-SCB and SCB alone. For a given finite differencing scheme of spatial convergence order p it is possible to represent the difference operator and associated error as [10, 70]

$$\boldsymbol{\nabla} f(x,y) = \boldsymbol{D}_p f(x,y) + \boldsymbol{O}(h_x^p) + \boldsymbol{O}(h_y^p), \tag{4.18}$$

where D_p is the finite difference operator, h_x is the mesh spacing or stencil width in the x direction, and h_y is the mesh spacing or stencil width in the y direction. The truncation error of such a scheme is simply [10, 70]

$$\boldsymbol{E}(h_x,h_y) = \boldsymbol{\nabla} f(x,y) - \boldsymbol{D}_p f(x,y) = \boldsymbol{O}(h_x^p) + \boldsymbol{O}(h_y^p). \tag{4.19}$$

Recall that the divergence operator in curvilinear geometry involves a derivative in angle. In $r-z$ the streaming term in the transport equation is given by Eqn. (1.44):

$$\boldsymbol{\nabla}\cdot\boldsymbol{\Omega}\psi = \frac{1}{r}\frac{\partial}{\partial r}\Big(r\Omega_r\psi\Big) + \frac{\partial}{\partial z}\Big(\Omega_z\psi\Big) + \frac{\partial}{\partial\gamma}\Big(\frac{1}{r}\Omega_\gamma\psi\Big).$$

Therefore the truncation error of a pth spatial order and nth angular order discretization of the transport equation in $r-z$ geometry would be

$$E(h_r, h_z, \Delta\gamma) = \boldsymbol{\nabla} \cdot \boldsymbol{\Omega}\psi(r, z, \boldsymbol{\Omega}) - \boldsymbol{D}_p \cdot \boldsymbol{\Omega}\psi(r, z, \boldsymbol{\Omega}) = O(h_r^p) + O(h_z^p) + O(\Delta\gamma^n), \quad (4.20)$$

where $\Delta\gamma$ is the effective angular spacing. Note we put a different convergence order for the spatial and angular dimensions here as we make no claim they would be the same. If the high-order transport equation and the LOQD equations were discretized consistently we would expect that the truncation error for the high and low-order equations would be identical. However, we are discretizing the high and low-order equations independently. Referring to the sections on SCB and the newly developed LOQD discretization, Sections 3.3 and 3.4.2 respectively, it is obvious that the treatment in $r - z$ space is completely different. What is perhaps more subtle is the fact that the approximation of the equations in γ is also fundamentally different between the two. In SCB the angular derivative is approximated explicitly with a weighted difference with half angle angular fluxes obtained using weighted diamond differencing. In the derivation of the LOQD equations the angular redistribution term is integrated over angle. This integration eliminates it from the balance equation. In the 1st moment equations the redistribution term isn't eliminated, however, we reformulate both the r and z components of the equation combining the 1st moments of the redistribution term into the r derivatives. Those r derivatives are then treated using the developed spatial discretization scheme. What this causes is the $O(\Delta\gamma^n)$ truncation error term to be different for the high and low-order equation discretizations. As one refines only in space, r and z, the spatial truncation errors for both discretizations would shrink to zero, i.e. $O(h_r^p) + O(h_z^p) \to 0$ as $h_r, h_z \to 0$. However, this would leave the two different $O(\Delta\gamma^n)$ terms for the two different discretizations unchanged, causing SCB and QD-SCB to seemingly converge to different solutions.

To test this hypothesis we conducted a convergence study in angle using a fine spatial mesh. Table 4.18 gives the solutions from SCB and QD-SCB using continuity conditions on the finest spatial grid, grid h, for three angular meshes. On such a fine spatial grid we would expect that $O(h_r^p) + O(h_z^p)$ would be small such that

$$O(h_r^p) + O(h_z^p) << O(\Delta\gamma^n), \quad (4.21)$$

for a sufficiently coarse angular quadrature set. Following our hypothesis, upon refinement of the angular mesh we would expect the solutions from the two methods to approach

each other. The results obtained behave in exactly this way giving us reason to believe this hypothesis is correct, see Table 4.18.

Table 4.18: Results for SCB and QD-SCB Upon Angular Refinement

	Φ			L		
Ang. Mesh	SCB	QD-SCB	Diff.	SCB	QD-SCB	Diff
$8 \times (2, 8)$	0.1507760	0.1505808	0.0001951	0.0464060	0.0467253	0.0003193
$16 \times (4, 16)$	0.1506061	0.1505363	0.0000698	0.0464237	0.0465311	0.0001075
$32 \times (8, 32)$	0.1505374	0.1505180	0.0000194	0.0464374	0.0464674	0.0000301

4.3.5 Test 5: Diffusion Limit Study

Here we look at the ability of each transport discretization and the corresponding QD method to obtain a solution in the diffusion limit. The domain is 1.0 cm $\times$ 1.0 cm with constant homogeneous unscaled cross sections and source, $\sigma_t = 1.0$, $\sigma_a = 0.5$, $\sigma_s = 0.5$, and $q = 1.0$. Boundary conditions other than the rotational condition are vacuum. The grid here is a 3 level grid with cells refined by a factor of 4 on the right third of the domain, a factor of 2 in the center third, and not refined on the left, refer to Figure 4.8. Only one grid is used with a spacing of $h = \frac{1}{18}$ in the unrefined region. The grid before "adaptive" refinement is randomized. The diffusion limit study is done by scaling the source and cross sections by a small parameter ϵ:

$$\hat{q} = \epsilon q, \quad \hat{\sigma}_t = \frac{\sigma_t}{\epsilon}, \quad \hat{\sigma}_a = \epsilon \sigma_a, \quad \hat{\sigma}_s = \hat{\sigma}_t - \hat{\sigma}_a. \tag{4.22}$$

The metric used to compare the methods is the integral of the discrete fluxes over the domain, Φ. Theory tells us that SCB attains the diffusion limit, VBMOSC does not, and that regardless of the transport discretization used the QD method will attain it. The results we get here match with theory completely, Table 4.19. The important result here is that neither of the proposed treatments for adaptive-like meshes disturb the ability of the QD method to ensure attaining the diffusion limit.

Table 4.19: Results of Diffusion Limit Study of Different Methods

	Diffusion		SCB	VBMOSC	QD-SCB		QD-VBMOSC	
ϵ	Pseudo-Poly.	Cont. Cond.			Pseudo-Poly.	Cont. Cond.	Pseudo-Poly.	Cont. Cond.
1.0	1.2202E+00	1.2202E+00	1.3343E+00	1.3291E+00	1.3344E+00	1.3344E+00	1.3336E+00	1.3336E+00
0.1	4.5745E-01	4.5749E-01	4.7045E-01	4.3889E-01	4.7137E-01	4.7137E-01	4.7115E-01	4.7089E-01
0.01	3.3781E-01	3.3785E-01	3.3440E-01	8.5194E-02	3.3862E-01	3.3866E-01	3.3948E-01	3.3846E-01

4.3.6 Test 6: Bent Pipe Problem

Up until now the tests presented were purposefully chosen to be ideal or close to ideal cases where analysis of the convergence properties of the methods in question is most feasible. Larger more complex problems with more severe heterogeneities, realistic adaptive refinement, and directionally peaked fluxes can exhibit chaotic convergence behavior or require refinement beyond what a desktop computer is capable of in order to show asymptotic convergence rates. This problem, however, was chosen because of its difficulty. This test is an $r-z$ geometry analog of a common pipeline radiation transport problem. Figure 4.26a details the problem setup along with a representative grid that has a pre-randomization cell width of $h = 0.5cm$ in the non-adaptively refined region. The grid used for calculations is a refinement of Figure 4.26a by a factor of 4. The domain is $8cm \times 16cm$. This test is meant to showcase the method's ability to treat problems with material heterogeneity, directionally peaked angular fluxes, and realistic adaptivity. The results were obtained using the QD method with VBMOSC and SCB using the pseudo-polygonal adaptive-like grid treatment, their respective scalar flux solutions are given in Figures 4.26b and 4.26c. Results for the continuity conditions method are similar. The QD factors generated by solving the problem using the QD method with SCB are given in Figure 4.27. Figures 4.26b and 4.26c show that the QD method obtains reasonable solutions using both transport discretizations with the solutions agreeing closely. Figures 4.27a - 4.27c depict the Eddington factors for the pipeline problem obtained with the converged QD-SCB solution. The large variation in the Eddington factors from one region to another highlights the high level of anisotropy of the angular flux in this problem.

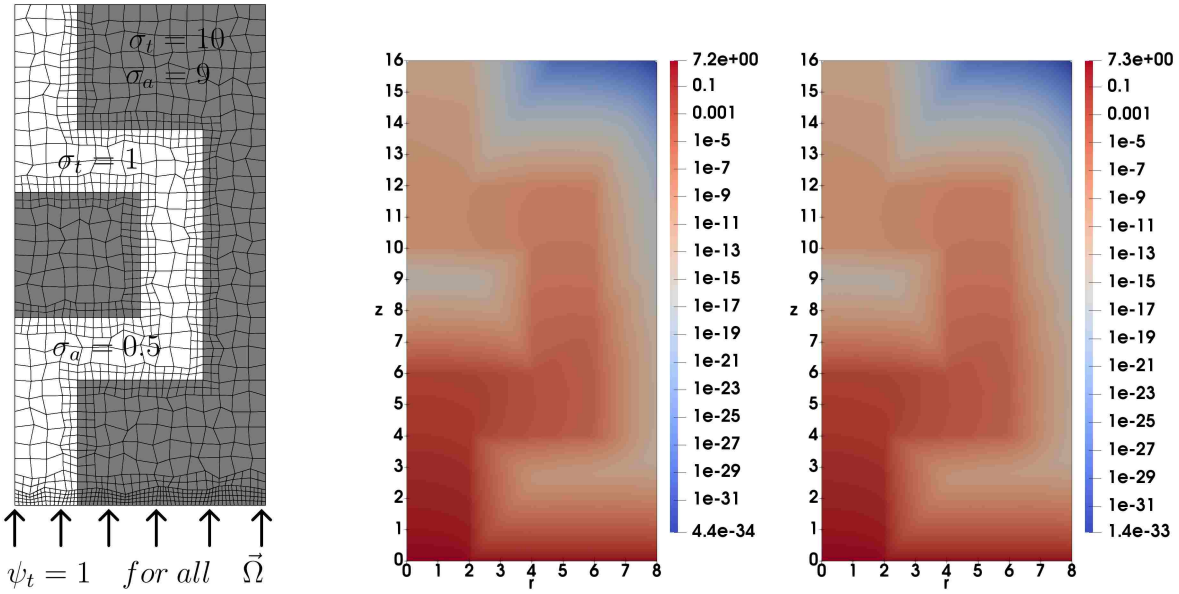

(a) Pipeline Problem Definition

(b) Scalar Flux QD-VBMOSC

(c) Scalar Flux QD-SCB

Figure 4.26: Pipeline Problem Setup and Solutions

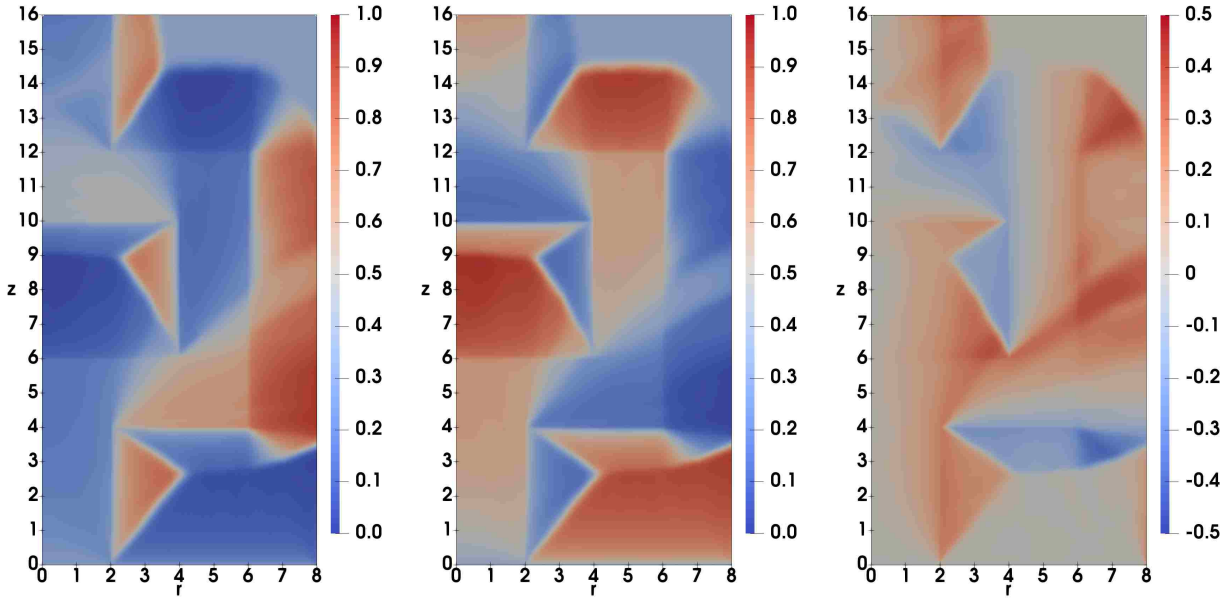

(a) E_{rr}

(b) E_{zz}

(c) E_{rz}

Figure 4.27: QD (Eddington) Factors for Pipe Problem With QD-SCB

4.3.7 Test 7: T-Problem

This is another test chosen for the challenges it poses, and another analogue of a fairly well known problem, the so called T-Problem. Figure 4.28a shows the definition of the problem. The mesh depicted in Figure 4.28a is representative of the one used for calculations, with the utilized mesh being finer by a factor of $\frac{3}{5}$. This is a challenging problem for a number of reasons. Firstly the material properties are highly discontinuous, with adjacent materials having a total cross section different by a factor of 1000. Secondly is the extreme optical thickness of the $\sigma_t = 1000$ region. The mesh we used for computation had a pre-randomization spacing of $h = 0.1$ in non-adaptively refined regions and $h_{AMR} = 0.025$ in the finest adaptively refined area. In the high total cross section region this translates into cells with optical thickness $\tau = h\sigma_t = 100$ and $\tau_{AMR} = h_{AMR}\sigma_t = 25$. Thus for the mesh we used here even the finest cell would still be considered very optically thick. Problems such as this is exactly where acceleration/solution methods other than QD such as inconsistent DSA, NDA, CMFD, etc. can be expected to give at best degraded performance and at worst fail completely. The last difficulty to note is the high scattering ratio of the optically thick regions of the problem, $c = \frac{\sigma_s}{\sigma_t} = 0.9999$. This last point necessitates that some good acceleration/solution method be chosen for this problem.

Again we see that the developed QD method can obtain reasonable solutions for a difficult problem, and that the solutions resulting from QD using different transport discretizations agree quite closely. It is difficult to differentiate between the results for the scalar flux coming from QD-SCB and QD-VBMOSC at the scale shown in Figures 4.28b and 4.28c, however, QD-SCB does in fact do a significantly better job of resolving the gradient of the flux at material boundaries. The Eddington factors for this problem using SCB as the transport discretization are given in Figure 4.29.

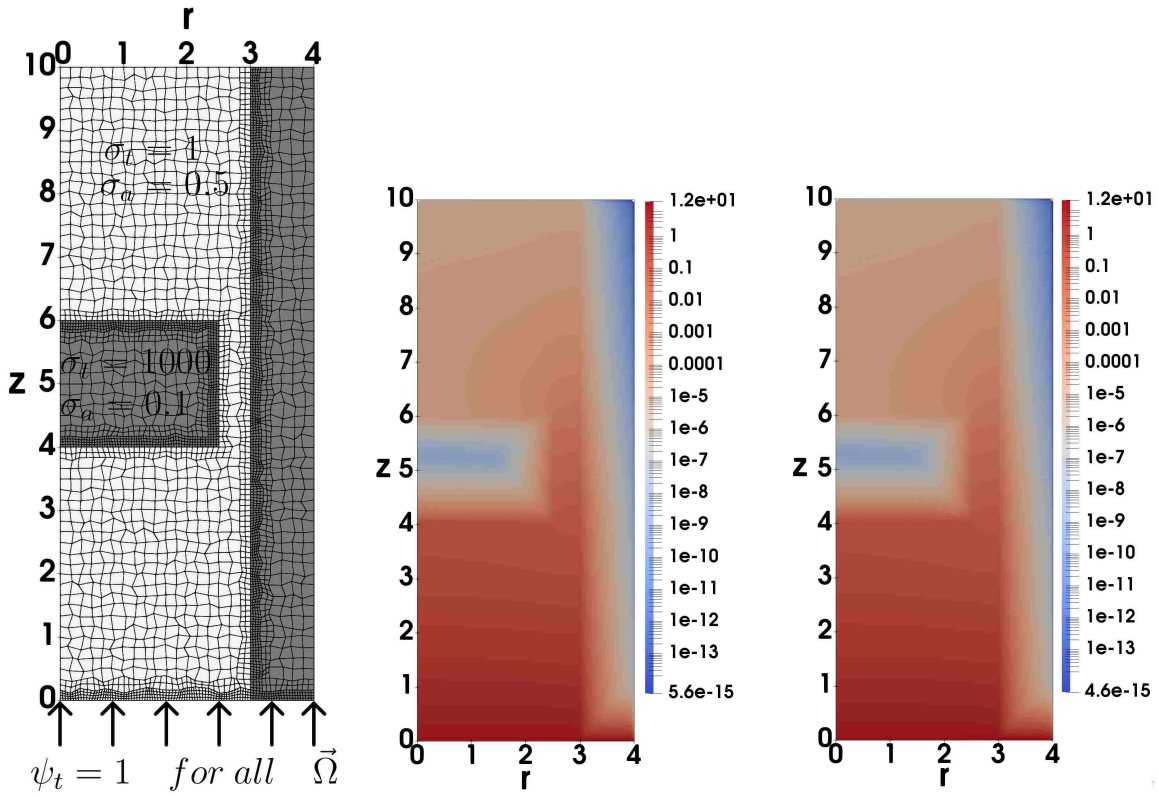

(a) T-Problem Definition

(b) Scalar Flux QD-VBMOSC

(c) Scalar Flux QD-SCB

Figure 4.28: T-Problem Setup and Solutions

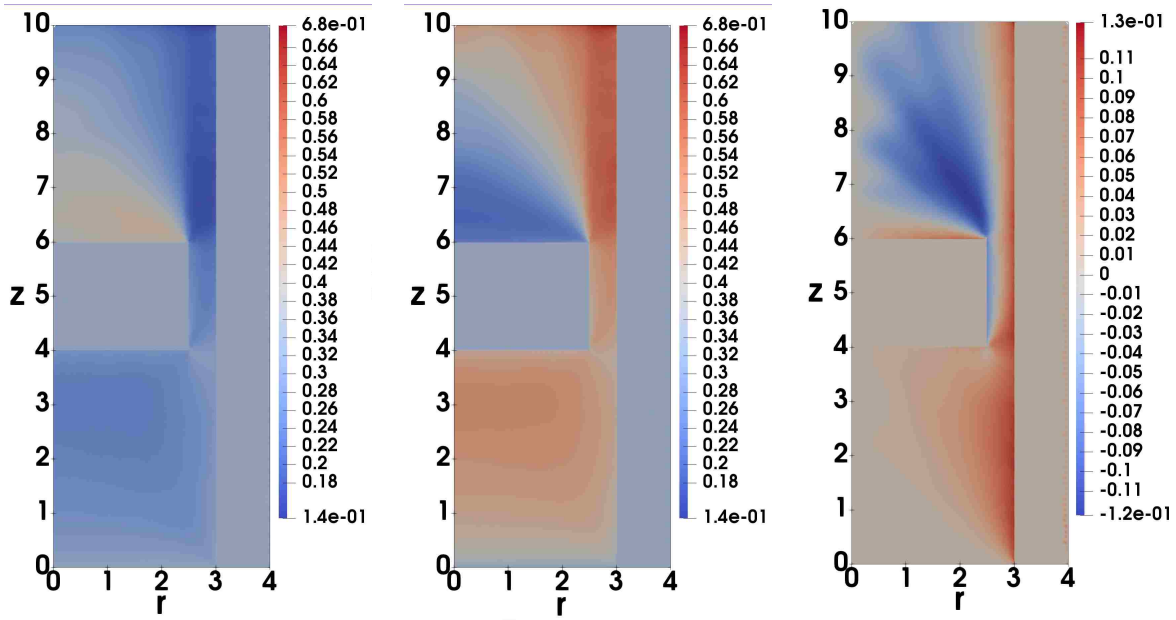

(a) E_{rr}

(b) E_{zz}

(c) E_{rz}

Figure 4.29: QD (Eddington) Factors for T-Problem with QD-SCB

To illustrate just how important it can be to choose a good acceleration/solution method for solving the transport equation on difficult problems Table 4.20 presents solution statistics for this problem using the methods discussed in this work. Table 4.20 gives the number of iterations taken to solve this problem, the wall clock time taken, and the measured iterative convergence rate of each method, ρ_∞. Note that VBMOSC's apparent advantage over SCB is due to VBMOSC's inability to model the problem within the highly scattering optically thick region since VBMOSC does not attain the diffusion limit. It is also important to point out that the reason the QD-SCB solve time is lower than QD-VBMOSC is due to the large computational workload associated with calculating the characteristic intersections with cell faces for VBMOSC.

Table 4.20: Solution Statistics for Different Methods Applied to The T-Problem

	VBMOSC	QD-VBMOSC	SCB	QD-SCB
# Its.	6133	21	153449	27
time (s)	1148.8	53.5	56015.1	24.7
ρ_∞	0.9961	0.31	0.99985	0.49

Chapter 5

Conclusions

In this work we developed a new discretization of the LOQD equations in 2D $r-z$ geometry on adaptive-like, arbitrary quadrilateral meshes, and used this new LOQD discretization to develop a QD method for use on meshes of this type. The LOQD discretization we developed is based on an advanced 2nd order discretization of the P_1 equations originally developed for arbitrary polyhedra in 3D Cartesian geometry [56]. Two extensions of the new LOQD equation discretization to adaptive-like grids were proposed, the continuity condition and pseudo-polygonal approaches. The continuity condition approach is one that has been used for LOQD equation discretizatoins in the past [27], where as the pseudo-polygonal approach is a new development. Numerical results showed that the new LOQD discretization converges with 2nd order behavior in space using both extensions to adaptive-like grids, and the developed QD method converges with 2nd order behavior when a 2nd order high-order discretization is used. The developed method exhibited stability even for difficult problems on the grids considered, and exhibited a large performance improvement over using simple SI. The new LOQD discretization was shown to work satisfactorily when used with multiple transport discretizations. It was also demonstrated that it is possible to boost the accuracy of a lower spatial convergence order transport discretization by coupling it with a higher convergence order LOQD discretization, as is the case with our LOQD discretization and the VBSC method used.

5.1 Future Work

An obvious next step for this research is to extend the LOQD discretization and associated QD method to arbitrary polygonal, adaptive-like grids. The method as of now when using the pseudo-polygonal coupling method is extremely close to this as it allows for an arbitrary number of faces per cell and the approximation of the gradient used was originally designed for such grids. Extending the method to treat arbitrary polygons is almost trivial and should require no additional theoretical work. Arbitrary polygonal meshes are becoming more popular due to the ability to better resolve the geometry of objects in a physical system. Thus extending to polygonal grids, though simple for this method, would constitute a significant advancement.

Another avenue of research would be to formulate the QD method using other transport discretizations with the new LOQD equation discretization. The interest here lies especially with using advanced discretizations of the transport equation [20, 21], especially those that have been shown to perform well for the type of grids we consider here [20]. It is also interesting to try a wide range of discretizations and study the effects of using different transport discretizations with this new LOQD equation discretization.

Application of this new LOQD equation discretization and the corresponding QD method based on it to practical problems in the area of radiative transfer would be very interesting. In order to treat practical radiative transfer problems the method would need to be extended to treat multigroup problems. As pointed out in the introduction of this work this extension is quite straight forward and should not pose any serious obstacles.

REFERENCES

[1] R. G. Lerner and G. L. Trigg, *Encyclopedia of Physics (2nd Edition)*. VHC Publishers, 1991.

[2] R. Sanchez, "Prospects in deterministic three-dimensional whole-core transport calculations," *Nuclear Engineering and Technology*, vol. 44, pp. 113–150, 2012.

[3] L. Dessart and D. J. Hillier, "Supernova radiative-transfer modelling : A new approach using non-local thermodynamic equilibrium and full time dependence," *Monthly Notices of the Royal Astronomical Society*, vol. 405, pp. 2141–2160, 2010.

[4] J. Arvo and D. Kirk, "Particle transport and image synthesis," in *SIGGRAPH '90 Proceedings of the 17th annual conference on Computer graphics and interactive techniques, Dallas, TX, USA*, pp. 63–66, 1990.

[5] L. A. DuBridge, ed., *Kinetic Theory of Gases*. McGraw-Hill Book Company, Inc., New York and London, 1938.

[6] E. E. Lewis and W. F. Miller, *Computational Methods of Neutron Transport*. American Nuclear Society, Inc., 1993.

[7] M. Planck, "On the theory of the energy distribution law of the normal spectrum," *Verhandlungen der Deutschen Physikalischen Gesellschaft*, vol. 2, p. 237, 1900.

[8] D. Y. Anistratov and V. Ya. Gol'din, "Multilevel quasidiffusion methods for solving multigroup neutron transport k-eigenvalue problems in 1D slab geometry," *Nuclear Science and Engineering*, vol. 37:2-4, pp. 111–132, 2011.

[9] V. Ya. Gol'din, "A quasi-diffusion method of solving the kinetic equation," *USSR Computational Mathematics and Mathematical Physics*, vol. 4, pp. 136–149, 1964.

[10] R. J. LeVeque, *Finite Difference Methods for Ordinary and Partial Differential Equations*. Society for Industrial and Applied Mathematics, 2007.

[11] A. D. Gadzhiev and O. S. Shirokovkaya, "Numerical solution of the two-dimensional transfer equation in curvilinear coordinates," *USSR Computational Mathematics and Mathematical Physics*, vol. 16, pp. 222–226, 1975.

[12] V. E. Troshchiev and V. A. Shumilin, "A difference scheme for solving the two-dimensional transport equation on irrecgular tetragonal nets," *U.S.S.R Computational Mathematics and Mathematical Physics*, vol. 26(1), pp. 141–148, 1986.

[13] R. E. Alcouffe, "A diffusion-acceleration S_n transport method for radiation transport on a general quadrilateral mesh," *Nuclear Science and Engineering*, vol. 105, pp. 191–197, 1990.

[14] T. S. Palmer, *Curvilinear Geometry Transport Discretizations In Thick Diffusive Regions*. (Doctoral Dissertation), University of Michigan, Ann Arbor, MI, USA, 1993.

[15] E. N. Aristova, V. Ya. Gol'din, and A. V. Kolpakov, "Multidimensional calculations of radiation transport by nonlinear quasi-diffusion method," in *Proceedings of The International Conference on Mathematics and Computational Methods Applied to Nuclear Science and Engineering, M&C 1999, Madrid, Spain*, pp. 667–676, 1999.

[16] A. V. Voronkov and E. P. Sychugova, "A second-order finite volume discretization of the time-dependent transport equation on arbitrary quadrilaterals in $r-z$ geometry," *Nuclear Science and Engineering*, vol. 148, pp. 186–194, 2004.

[17] E. N. Aristova, D. F. Baydin, and V. Ya. Gol'din, "Two variants of efficient method of the transport equation solving in $r-z$ geometry on the basis of transition to vladimirov's variables," *Mathematical Modelling*, vol. 18(6), pp. 43–52, 2006.

[18] J. E. Morel, A. Gonzalez-Aller, and J. S. Warsa, "A lumped linear-discontinuous spatial discretization scheme for triangular-mesh S_n calculation $r - z$ geometry," *Nuclear Science and Engineering*, vol. 155, pp. 168–178, 2007.

[19] E. N. Aristova, "Simulation of radiation transport in a channel based on the quasi-diffusion method," *Transport Theory and Statistical Physics*, vol. 37, pp. 483–503, 2008.

[20] T. S. Bailey, M. L. Adams, J. H. Chang, and J. S. Warsa, "A piecewise linear discontinuous finite element spatial discretization of the transport equation in 2D cylindrical geometry," in *Proceedings of The International Conference on Mathematics and Computational Methods Applied to Nuclear Science and Engineering, M&C 2009, Saratoga Springs, New York*, 2009.

[21] D. Y. Anistratov, "Step characteristic method for $r - z$ geometry in special coordinates," *Transactions of The American Nuclear Society*, vol. 103, pp. 351–353, 2010.

[22] M. L. Adams and E. W. Larsen, "Fast iterative methods for discrete-ordinates particle transport calculations," *Progress in Nuclear Energy*, vol. 40, pp. 3–159, 2002.

[23] A. Tamang and D. Y. Anistratov, "A multilevel projective method for solving the space-time multigroup neutron kinetics equations coupled with the heat transfer equation," *Nuclear Science and Engineering*, vol. 177, pp. 1–18, 2014.

[24] D. Mihalas, *Stellar Atmospheres*. W.H. Freeman & Co, 1978.

[25] J. S. Warsa, T. A. Wareing, and J. E. Morel, "Fully consistent diffusion synthetic acceleration of linear discontinuous S_n transport discretizations on unstructured tetrahedral meshes," *Nuclear Science and Engineering*, vol. 141, pp. 236–251, 2002.

[26] D. Y. Anistratov, "The generalized quasidiffusion method for solving adjoint transport problems with alternating solutions," *Transactions of American Nuclear Society*, vol. 83, pp. 348–350, 2000.

[27] W. A. Wieselquist, D. Y. Anistratov, and J. E. Morel, "A cell-local finite difference discretization of the low-order quasidiffusion equations for neutral particle transport on unstructured quadrilateral meshes," *Journal of Computational Physics*, vol. 273, pp. 343–357, 2014.

[28] J. P. Jones, D. Y. Anistratov, and J. E. Morel, "Discretization of low-order quasidiffusion equations on arbitrary quadrilaterals in 2D $r-z$ geometry," in *Proceedings of The International Conference on Mathematics and Computational Methods Applied to Nuclear Science and Engineering, M&C 2017, Jeju, Korea*, 2017.

[29] J. P. Jones, D. Y. Anistratov, and J. E. Morel, "The quasidiffusion method for transport problems on adaptive-like arbitrary quadrilateral meshes in 2D $r-z$ geometry," in *Proceedings of The International Conference on Mathematics and Computational Methods Applied to Nuclear Science and Engineering, M&C 2019, Portland, OR*, 2019.

[30] V. S. Vladimirov, "Numerical solution of the kinetic equation for a sphere," *Computational Mathematics*, vol. No. 3, pp. 3–33, 1958. (in Russian).

[31] V.Ya. Gol'din, N.N. Kalitkin, and T. V. Shishova, "Nonlinear difference scheme for hyperbolic equations," *USSR Computational Mathematics and Mathematical Physics*, vol. 5(5), p. 938–944, 1965.

[32] V.Ya. Gol'din, G.V. Danilova, and N.N. Kalitkin, "Numerical integration of several-dimensional transport equation," *Numerical methods of solving problems of mathematical physics*, pp. 190–193, 1966. (in Russian).

[33] D. F. Baydin, E. N. Aristova, and V. Ya. Gol'din, "Comparison of the efficiency of the transport equation calculation methods in characteristics variables," *Transport Theory and Statistical Physics*, vol. 37:2-4, pp. 286–306, 2008.

[34] M. L. Adams, "Subcell balance methods for radiative transfer on arbitrary grids," *Transport Theory and Statistical Physics*, vol. 26, pp. 395–431, 1997.

[35] P. G. Maginot, P. F. Nowak, and M. L. Adams, "A review of the upstream corner balance spatial discretization," in *Proceedings of The International Conference on Mathematics and Computational Methods Applied to Nuclear Science and Engineering, M&C 2017, Jeju, Korea*, 2017.

[36] E. W. Larsen, "The asymptotic diffusion limit of discretized transport problems," *Nuclear Science and Engineering*, vol. 112, pp. 336–346, 1992.

[37] M. L. Adams, T. A. Wareing, and W. F. Walters, "Characteristic methods in thick diffusive problems," *Nuclear Science and Engineering*, vol. 130, p. 18–46, 1998.

[38] M. L. Adams, "Discontinuous finite element transport solutions in thick diffusive problems," *Nuclear Science and Engineering*, vol. 137, pp. 298–333, 2001.

[39] J. E. Morel and G. R. Montry, "Analysis and elimination of the discrete ordinates flux dip," *Transport Theory and Statistical Physics*, vol. 13, pp. 615–633, 1984.

[40] E. W. Larsen, "Transport acceleration methods as two-level multigrid algorithms," in *Operator Theory: Advances and Applications*, vol. 51, pp. 34–47, Birkhauser, 1991.

[41] H. J. Kopp, "Synthetic method solution of the transport equation," *Nuclear Science and Engineering*, vol. 17, p. 65, 1963.

[42] Sh. S. Nikolaishvilli, "On solution of one-velocity transport equation based on yvon-mertens approxmiation," *Atomic Energy*, vol. 20, p. 344, 1966.

[43] K. S. Smith, "Nodal method storage reduction by non-linear iteration," *Transactions of The American Nuclear Society*, vol. 44, p. 265, 1983.

[44] K. S. Smith and J. D. Rhodes, III, "Full-core, 2-D, lwr core calculations with casmo-4e," in *PHYSOR 2002, Seoul, Korea*, 2002.

[45] M. L. Adams and E. W. Larsen, "Fast iterative methods for discrete-ordinates particle transport calculations," *Progress in Nuclear Energy*, vol. 40, pp. 3–159, 2002.

[46] R. E. Alcouffe, "A stable diffusion synthetic acceleration method for neutron transport iterations," *Transactions of The American Nuclear Society*, vol. 23, p. 203, 1976.

[47] D. Y. Anistratov, "Multilevel NDA methods for solving multigroup eigenvalue neutron transport problems," *Nuclear Science and Engineering*, vol. 174, pp. 150–162, 2013.

[48] K. S. Smith, L. Lulu, and B. Forget, "Techniques for stablizing coarse-mesh finite difference (CMFD) in methods of characteristics (MOC)," in *Proceedings of The International Conference on Mathematics and Computational Methods Applied to Nuclear Science and Engineering, M&C 2015, Nashville, TN*, 2015.

[49] L. Roberts and D. Y. Anistratov, "Nonlinear weighted flux methods for particle transport problems," *Transport Theory and Statistical Physics*, vol. 36, p. 589–608, 2007.

[50] V. Ya. Gol'din and B. N. Chetverushkin, "Methods of solving one-dimensional problems of radiation gas dynamics," *USSR Computational Mathematics and Mathematical Physics*, vol. 12, pp. 177–189, 1972.

[51] N. N. Aksenov and V. Ya. Gol'din, "Computing of two-dimensional steady equation of neutron tranport by quasi-diffusion method," *USSR Computational Mathematics and Mathematical Physics*, vol. 19, p. 1341, 1979.

[52] D. Y. Anistratov, E. N. Aristova, and V. Ya. Gol'din, "A nonlinear method for solving the problems of radiation transfer in medium," *Mathematical Modeling 8*, vol. No. 12, 3, 1996.

[53] V. Ya. Gol'din, D. A. Gol'dina, A. V. Kolpakov, and A. A. Shilkov, "Mathematical modeling of gas dynamic processes with high radiation energy densities," *Problems of Atomic Science and Engineering: Methods and Codes for Numerical Solution of Mathematical Physics Problems*, vol. No. 2, p. 59, 1986. (in Russian).

[54] V. E. Troshchiev, V.F. Yudintsev, and V.i. Fedyanin, "Acceleration of the convergence of iterations in solving the kinetic equation," *USSR Computational Mathematics and Mathematical Physics*, vol. 8,2, p. 298, 1968.

[55] W. A. Wieselquist and D. Y. Anistratov, "The quasidiffusion method for 2-D transport problems on AMR grids," *Transactions of The American Nuclear Society*, vol. 96, pp. 565–567, 2007.

[56] J. E. Morel, "A 3-D cell-centered diffusion discretization for arbitrary polyhedral meshes," tech. rep., Los Alamos National Laboratory, 2002. LANL Research Note, CCS-4:02-40(U).

[57] M. M. Miften and E. W. Larsen, "The quasi-diffusion method for solving transport problems in planar and spherical geometries," *Transport Theory and Statistical Physics*, vol. 22, pp. 165–186, 1993.

[58] V. Ya. Gol'din, A. V. Kolpakov, and A. V. Sokolov, "Methods for solving steady-state quasidiffusion system of equations," *Preprint No. 80, Keldysh Institute of Applied Mathematics*, 1978. (in Russian).

[59] D. Y. Anistratov and V. Ya. Gol'din, "Comparison of difference schemes for the quasi-diffusion method for solving the transport equation," *Problems of Atomic Science and Engineering: Methods and Codes for Numerical Solution of Mathematical Physics Problems*, vol. No. 2, pp. 17–23, 1986. (in Russian).

[60] D. Y. Anistratov and V. Ya. Gol'din, "Nonlinear methods for solving particle transport problems," *Transport Theory and Statistical Physics*, vol. 22, pp. 42–77, 1993.

[61] T. S. Palmer, "Discretizing the diffusion equation on unstructured polygonal meshes in two dimensions," *Annals of Nuclear Energy*, vol. 28, pp. 1851–1880, 2001.

[62] W. A. Wieselquist, *The Quasidiffusion Method for Transport Problems On Unstructured Meshes*. (Doctoral Dissertation), North Carolina State University, Raleigh, NC, USA, 2009.

[63] K. Lipnikov, J. Morel, and M. Shashkov, "Mimetic finite difference methods for diffusion equations on non-orthogonal non-conformal meshes," *Journal of Computational Physics*, vol. 199, p. 589–597, 2004.

[64] W. A. Wieselquist and D. Y. Anistratov, "A quasidiffusion method for unstructured quadrilateral meshes in 2d xy geometry," in *Proceedings of The International Con-*

ference on Mathematics and Computational Methods Applied to Nuclear Science and Engineering, M&C 2009, Saratoga Springs, NY, 2009.

[65] V. Ya. Gol'din, N. N. Kalitkin, and T. V. Shishova, "Non-linear difference schemes for hyperbolic equations," *USSR Computational Mathematics and Mathematical Physics*, vol. 5, pp. 229–239, 1968.

[66] A. Harten, "ENO schemes with subcell resolution," *Journal of Computational Physics*, vol. 83, pp. 148–184, 1987.

[67] V. Ya. Gol'din, "Characteristics difference scheme for non-stationary kinetic equation," *Soviet-Mathematics*, vol. 1 No-4, pp. 902–906, 1960.

[68] J. R. Askew, *A Characteristics Formulation of the Neutron Transport Equation in Complicated Geometries*. Winfrith Report M1108, 1960.

[69] J. E. Morel, R. M. Roberts, and M. J. Shashkov, "A local support-operators diffusion discretization scheme for quadrilateral $r - z$ meshes," *Journal of Computational Physics*, vol. 144, pp. 17–51, 1997.

[70] V. S. Ryaben'kii and S. V. Tsynkov, *Theoretical Introduction to Numerical Analysis*. Chapman&Hall/CRC Press Taylor & Francis Group, 2007.